TIPS PENTACENE CRYSTAL ALIGNMENT FOR IMPROVING PERFORMANCE OF SOLUTION PROCESSED ORGANIC THIN FILM TRANSISTORS

by

ZHENGRAN HE

DAWEN LI, COMMITTEE CHAIR

GREG SZULCZEWSKI
SUSHMA KOTRU
PATRICK KUNG
FEI HU

A DISSERTATION

Submitted in partial fulfillment of the requirements
for the degree of Doctor of Philosophy
in the Department of Electrical and Computer Engineering
in the Graduate School of
The University of Alabama

TUSCALOOSA, ALABAMA

2014

ABSTRACT

A newly-developed *p*-type organic semiconductor 6,13-bis (triisopropylsilylethynyl) pentacene (TIPS pentacene) demonstrates various advantages such as high mobility, air stability and solution processibility, but at the same time its application is restricted by major issues, such as crystal misorientation and performance variation of organic thin-film transistors (OTFTs). This dissertation demonstrates several different approaches to address these issues. As a result, both crystal orientation and areal coverage can be effectively improved, leading to an enhancement of average mobility and performance consistency of OTFTs.

Chapter 1 presents an introduction and background of this dissertation.

Chapter 2 explores the usage of inorganic silica nanoparticles to manipulate the morphology of TIPS pentacene thin films and the performance of solution-processed organic OTFTs. The resultant drop-cast films yield improved morphological uniformity at ~10% SiO_2 loading, which also leads to a 3-fold increase in average mobility and nearly 4-times reduction in the ratio of standard deviation of mobility (μ_{Stdev}) to average mobility (μ_{Avg}). The experimental results suggest that the SiO_2 nanoparticles mostly aggregate at TIPS pentacene grain boundaries, and that 10% nanoparticle concentration effectively reduces the undesirable crystal misorientation without considerably compromising TIPS pentacene crystallinity.

Chapter 3 discusses the utilization of air flow to effectively reduce the TIPS pentacene crystal anisotropy and enhance performance consistency in OTFTs. Under air-flow navigation

(AFN), TIPS pentacene forms thin films with improved crystal orientation and increased areal coverage, which subsequently lead to a four-fold increase of average hole mobility and one order of magnitude enhancement in performance consistency.

Chapter 4 investigates the critical roles of lateral and vertical phase separation in the performance of the next-generation organic and hybrid electronic devices. A novel method is demonstrated here to switch between lateral and vertical phase separation in semiconducting TIPS pentacene/ polymer blend films by simply varying the alkyl length of the polyacrylate polymer component. The phase separation modes depend on intermolecular interactions between small molecule TIPS pentacene and polymer additives. The blend film with a dominant vertical phase separation exhibits a significant enhancement in average mobility and performance consistency of organic OTFTs.

Chapter 5 demonstrates an effective approach to improve both charge transport and performance consistency in solution-processed OTFTs by blending TIPS pentacene with a series of small-molecule additives: 4-butylbenzoic acid (BBA), 4-hexylbenzoic acid (HBA), and 4-octylbenzoic acid (OBA). These three small molecules share a benzoic acid moiety, but have different length of hydrophobic tails. The self-assembled interfacial layer of small molecules on the gate oxide surface leads to uniform deposition of TIPS pentacene crystal seeds and facilitates TIPS pentacene to grow along the tilted orientation of substrate, which results in a film of enhanced crystal orientation and areal coverage. OTFTs based on TIPS pentacene/small molecule blends demonstrate greatly improved average hole mobility and performance consistency, which correlates with the length of hydrophobic tail of the small-molecule additives.

Chapter 6 summarizes the conclusions of this dissertation and the related future work.

DEDICATION

This dissertation is dedicated to everyone who has helped me and guided me through the trials and tribulations of creating this manuscript, and in particular, my family who stood by me throughout the time taken to complete this dissertation.

LIST OF ABBREVIATIONS AND SYMBOLS

C_i	Capacitance per unit area of the dielectric layer
ε	Permittivity
E_F	Fermi level
L_D	Debye length
k	Boltzmann's constant
ρ	Density of charge carriers (hole or electron)
q	Charge of charge carriers (hole or electron)
μ	Field-effect mobility

ACKNOWLEDGMENTS

I am pleased to take this chance to thank the many colleagues, friends, and professors who have helped me with my Ph. D. study and research at The University of Alabama. Otherwise, it would have been impossible for me to write this dissertation.

Firstly, I would like to express my great gratitude for my advisor, Dr. Dawen Li. Dr. Li has always been a knowledgeable mentor, great colleague and sincere friend who has been providing me with persistent help, great guidance and valuable advice. I am so glad to have him throughout my study and research and for sharing with me his research expertise and wisdom, making the pursuit of my Ph. D. degree such a great and unforgettable journey of my life.

Next, I would like to thank all of my committee members, Dr. Greg Szulczewski, Dr. Sushma Kotru, Dr. Patrick Kung and Dr. Fei Hu, for their great help and inspiring questions of both my academic study and dissertation writing.

Also, I would like to thank my colleagues for their help and suggestions for my research. I would like to thank Dr. Jihua Chen at Oak Ridge National Laboratory for his help on the transmission electron microscopy, and Mr. Xia Xu, Ms. Kyeiwaa Asare-Yeboah and Mr. Hao Su for their help and great discussion of my research. I thank financial support from National Science Foundation (NSF) and the scholarship from the MINT center.

Last but not least, I would like to thank my family who have always been supportive of me for every decision I make. Their great love, care and understanding is the most motivation with which I complete my Ph. D. study and research.

CONTENTS

LIST OF TABLES

LIST OF FIGURES

CHAPTER 1

INTRODUCTION

1.1 Overview of Organic Electronics

Organic electronics has received considerable attention in recent years due to great potential for manufacturing flexible, large-area and low-cost devices.[1-7] As a branch of materials science, organic electronics study various conductive and semi-conductive polymer and small molecules, and differs from conventional inorganic electronics in that the polymer and small molecules studied in organic electronics consist of carbon atoms.

1.2 Organic Semiconductors

Figure 1.1 introduces the energy level diagram of a typical metal, insulator and semiconductors. The conduction band of a metal is partially filled. At T=0 K, the valence band of both an insulator and an intrinsic semiconductor is fully filled. When temperature increases, electrons start to jump from the valence band to the conduction band via thermal excitation. Therefore, both valence band and conduction band can contribute to conduction for an insulator and an intrinsic semiconductor.

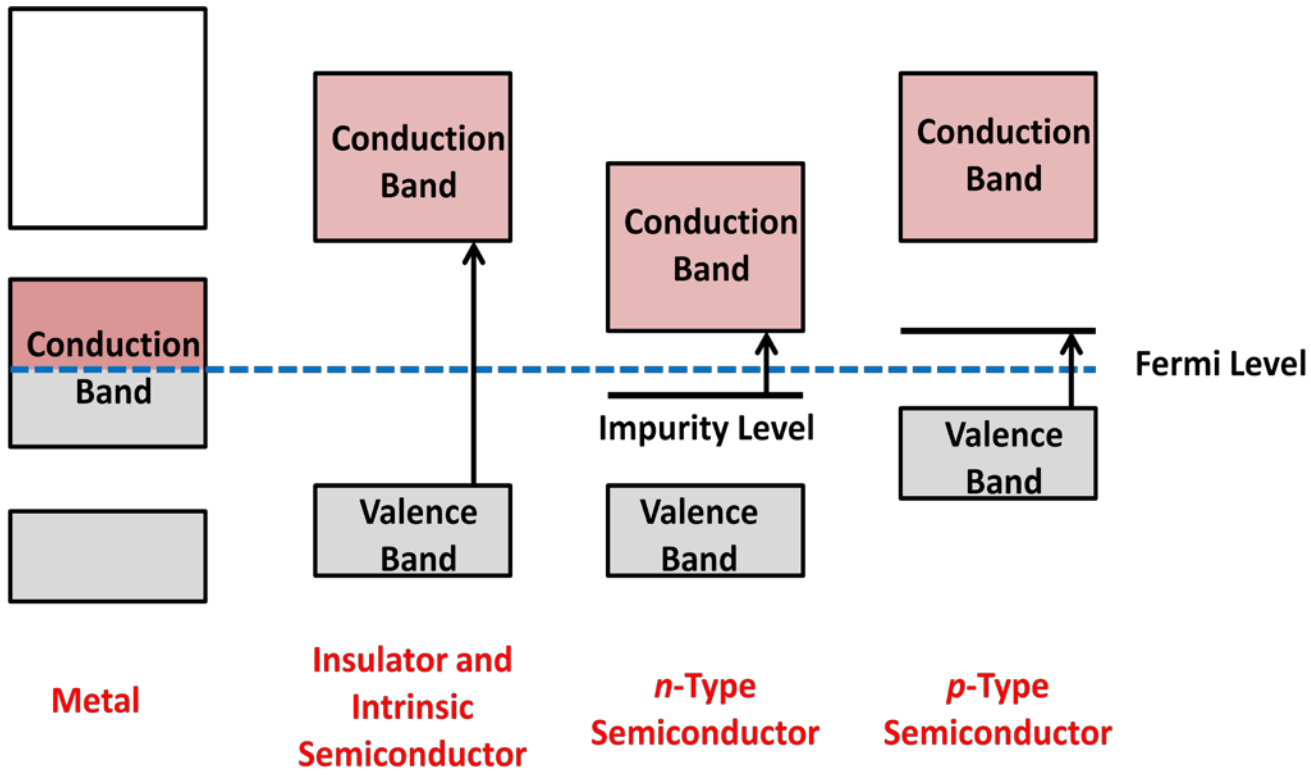

Figure 1.1. Energy diagram of a typical metal, insulator and semiconductor. The conduction band of a metal is partially filled. The valence band of an insulator and an intrinsic semiconductor is fully filled at T=0 K, and as temperature rises up, electrons can jump from the valence band to the conduction band via thermal excitation.

The electrical conductivity of a semiconductor is between that of metal and insulator, while doping a semiconductor can enhance its electrical conductivity. As shown in Figure 1.2, there are two types of doping: *n*-type and *p*-type. The doping of Boron, an element deficient of electrons compared to Si, facilitates hole transport and gives rise to conductivity, which is known as *p*-type doping. On the other hand, the doping of Phosphorous, an element with extra electrons, facilitates electron transport by giving up electrons to the lowest unoccupied orbital and also gives rise to conductivity. This is known as *n*-type doping. Since doping a semiconductor can

introduce localized energy levels into the energy band diagram, the energy that is needed to excite an electron/hole in the conduction/valence band is then reduced.

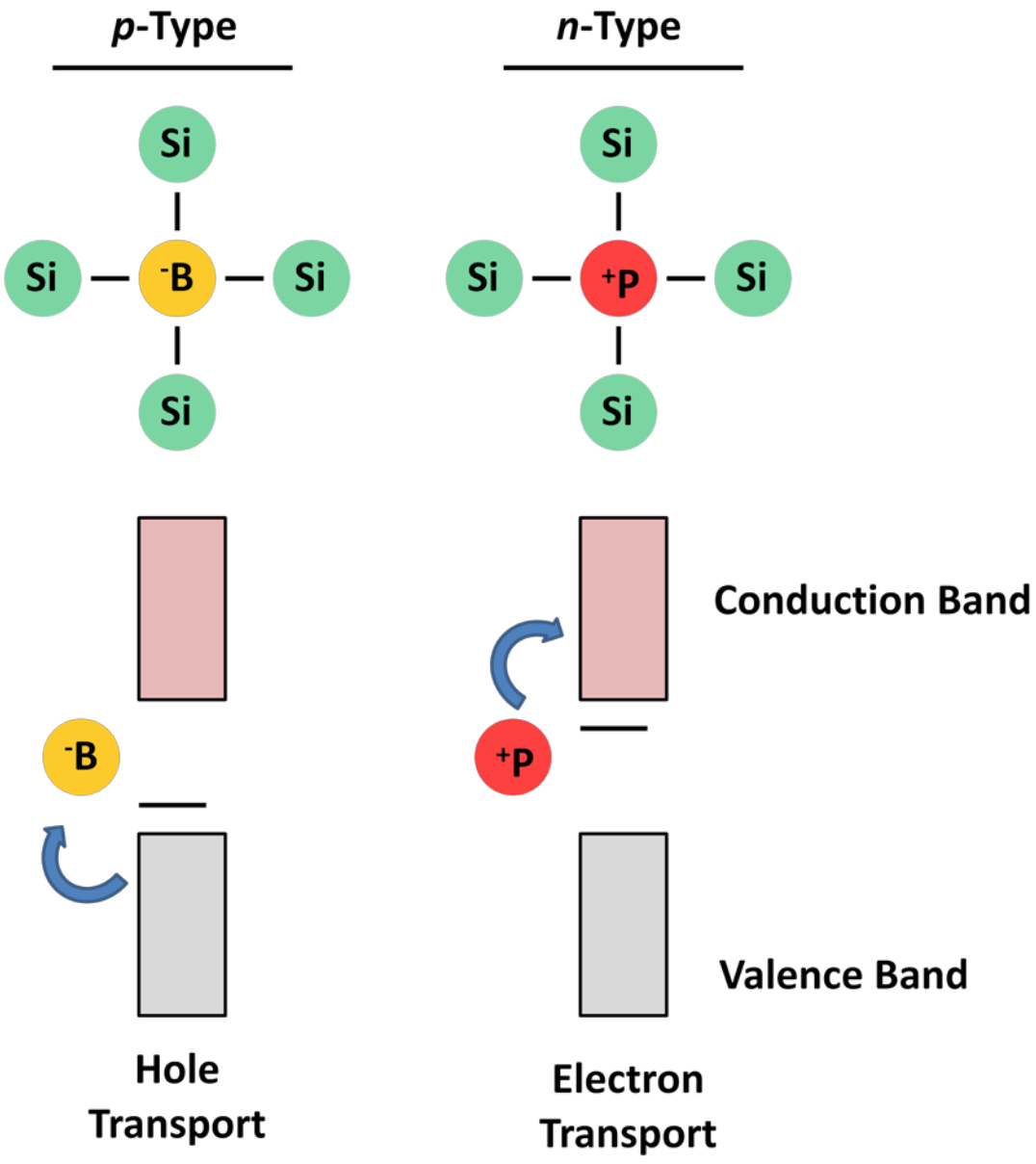

Figure 1.2. Typical *p*-type doping (left) and *n*-type doping (right). The doping of Boron, an element deficient of electrons, facilitates hole transport, while the doping of Phosphorous, an element with extra electrons, facilitates electron transport.

Conventional inorganic semiconductors are characterized by high mobility and excellent stability.[8] However, the processing of inorganic semiconductors for device fabrication usually requires high temperature and high vacuum.[9] Therefore, organic semiconductors have become increasingly attractive due to their solution processibility, which makes them promising for the next-generation display devices on flexible substrates.[10] Since no high temperature and high vacuum is required for organic semiconductors, manufacturing costs can be greatly reduced, allowing mass production. However, when compared to conventional inorganic counterparts whose carrier mobilities range from 0.1-10^4 cm^2/Vs, organic semiconductors still exhibit much lower mobilities.[11]

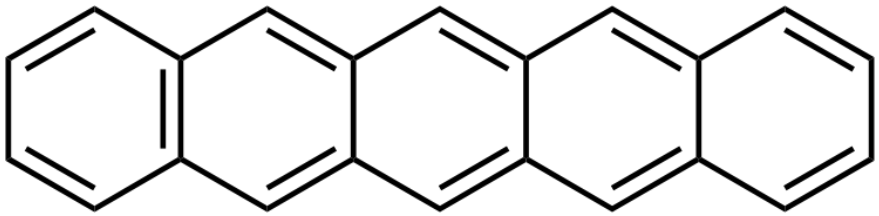

Figure 1.3. Molecular structure of pentacene. Pentacene is a polycyclic aromatic hydrocarbon with five linearly fused benzene rings.

For example, pentacene [12-20] is an organic semiconductor, as shown in Figure 1.2. The molecular structure of pentacene has a polycyclic aromatic hydrocarbon with five linearly fused benzene rings.[20] Pentacene thin films are usually made by vapor deposition because it has low solubility in common organic solvents. To obtain a high mobility from pentacene OTFTs, large grain size with remarkable molecular ordering is required, which can be achieved by vapor deposition at optimal evaporation rate and temperature.[21] The problem associated with this approach is that it is difficult to achieve good molecular ordering, and that vapor deposition requires high vacuum and high temperature. This has significantly increased the cost and has

become an obstacle to the low-cost manufacturing such as roll-to-roll printing. Therefore, it is important that a semiconductor can be processed in solution, which is one of the major criteria for selecting organic semiconductors.[22]

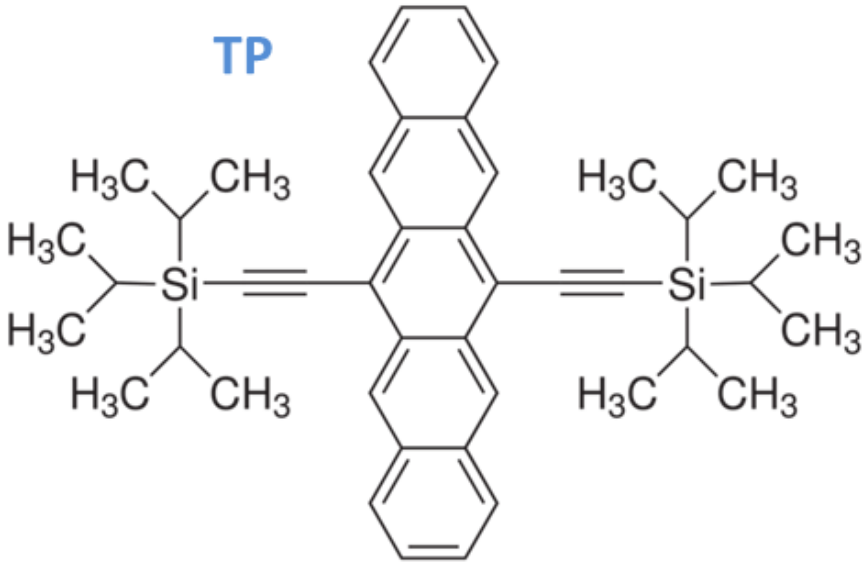

Figure 1.4. Molecular structure of 6,13-bis(triisopropylsilylethynyl) pentacene (TIPS pentacene). TIPS pentacene is a small molecule semiconductor which demonstrates high mobility due to strong molecular ordering and two-dimensional π-π stacking.

6,13-bis (triisopropylsilylethynyl) pentacene (TIPS pentacene) has received great attention due to its air stability, solution processibility, and high mobility.[23-34] TIPS pentacene, which is a derivative based on pentacene, is a newly-developed soluble small-molecule semiconductor and exhibits strong molecular ordering and two-dimensional π-π stacking as shown in the molecular structure of Figure 1.4, which leads to a higher mobility of organic OTFTs.[35] TIPS pentacene thin film can be formed by drop casting, and the resultant morphology depends on solution concentration, substrate surface energy and solvent evaporation rate.[36-38] With a high surface energy and a high solvent evaporation rate, TIPS pentacene thin films

exhibit small grains with a high density of grain boundaries, which restricts charge transport and lowers device performance. However, with a low surface energy and a controlled solvent evaporation rate, TIPS pentacene thin film shows large grains with much reduced grain boundaries, which facilitates charge transport and contributes to a high mobility.[35]

1.3 Organic Thin-Film Transistors (OTFTs)

1.3.1 Architectures of OTFTs

In OTFTs, charge transport is controlled in the conductive channel from source electrode to drain electrode by the voltage applied between the gate and source electrodes. Figure 1.1 shows the four configurations of (a) bottom-gate, top-contact OTFTs, (b) bottom-gate, bottom-contact OTFTs, (c) top-gate, top-contact OTFTs, and (d) top-gate, bottom-contact OTFTs. For bottom-gate, top-contact and top-gate, top-contact OTFTs, the semiconductor layer is firstly formed on the dielectric layer by using solution processing methods, such as spin coating, drop casting, and dip casting. Then the source and drain contact electrodes are formed on the semiconductor layer typically by thermally evaporating gold. On the contrary, for bottom-gate, bottom-contact and top-gate, bottom-contact OTFTs, source and drain electrodes are pre-patterned on the dielectric layer before semiconductor layer is formed.

In general, bottom-gate, top-contact OTFTs show better device performances, such as larger drain current and smaller contact resistance, than bottom-gate, bottom-contact OTFTs, because bottom-contact OTFTs typically exhibit a larger potential drop at the semiconductor and insulator interface.

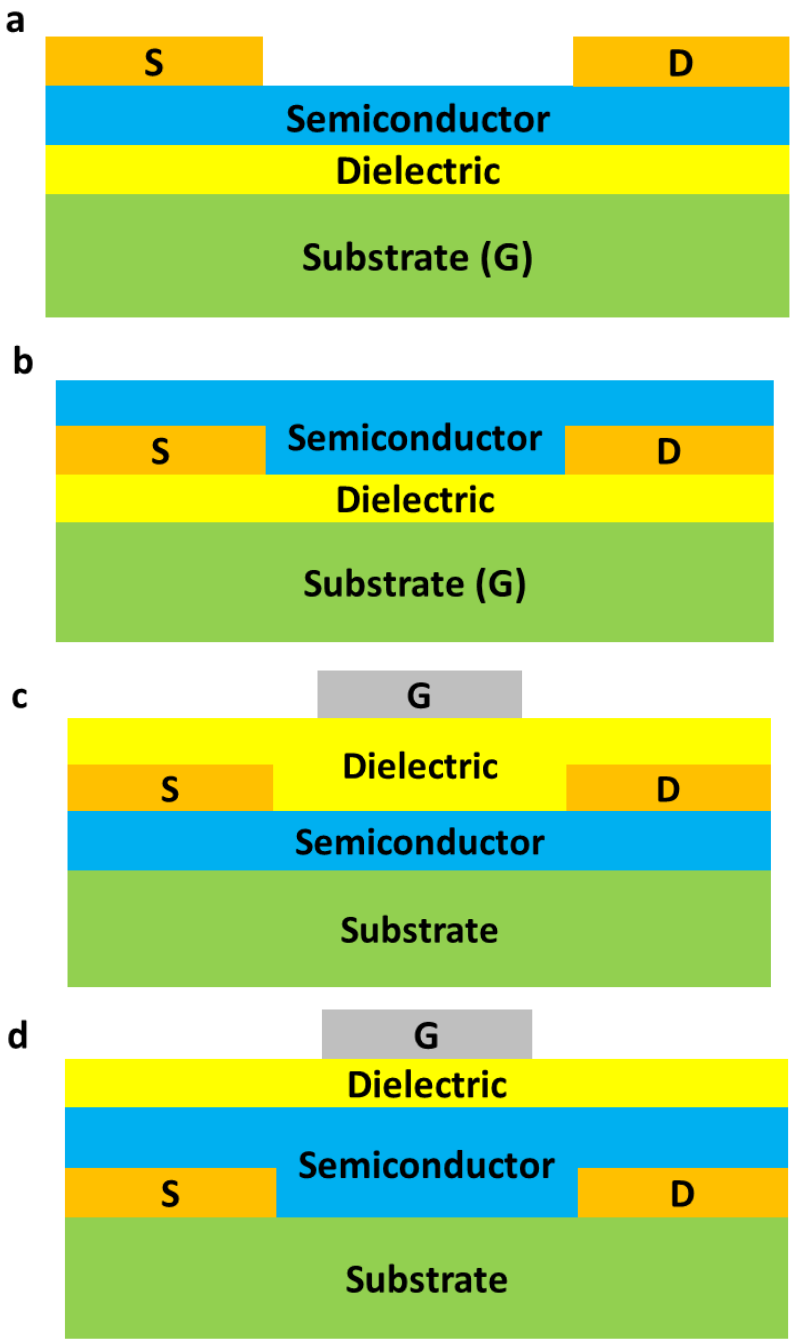

Figure 1.5. (a) bottom-gate, top-contact OTFT configuration, (b) bottom-gate, bottom-contact OTFT configuration, (c) top-gate, top-contact OTFT configuration, and (d) top-gate, bottom-contact OTFT configuration. The primary difference between top-contact and bottom-contact OTFT configurations is the sequence of forming the semiconductor layer and contact electrodes.

This larger potential drop is due to the following reasons. Firstly, the contact between the semiconductor layer and dielectric layer is poor. Secondly, there are larger the potential barriers at the interface.[39] Thirdly, the semiconductor layer is formed after the source and drain electrodes are patterned on the substrate, which leads to poor morphology in the regions around the electrodes.[40,41]

1.3.2 Operating Modes

Figure 1.6 shows a scheme of energy-level diagram of the interface between gold (Au) and the semiconductor TIPS pentacene layer.[42] The Fermi level is represented by E_F. HOMO refers to the highest occupied molecular orbital while LUMO refers to the lowest unoccupied molecular orbital. When the gate voltage is positive, it induces negative charges at the source electrode. However, the LUMO of TIPS pentacene is far from E_F, in which case the barrier for electrons to be injected into the semiconductor layer is large. On the other hand, when the gate voltage is negative, it induces positive charges at the source electrode. The HOMO of TIPS pentacene is close to E_F, so the energy barrier for hole injection is much smaller than that for electrons. As a result, a channel can be formed at the interface between the semiconductor layer and dielectric layer. When a second voltage is applied from the source to drain electrode, holes are also driven from source to drain electrode. In this case, it is much easier for hole injection to take place than electron injection, so TIPS pentacene is considered as *p*-type semiconductor. In fact, the definition of *p*-type or *n*-type semiconductor in the case of organic semiconductor is different from the case of doping semiconductors. The former considers whether LUMO or HOMO is closer to the Fermi level E_F whereas the latter considers whether the doping is from donors or acceptors.

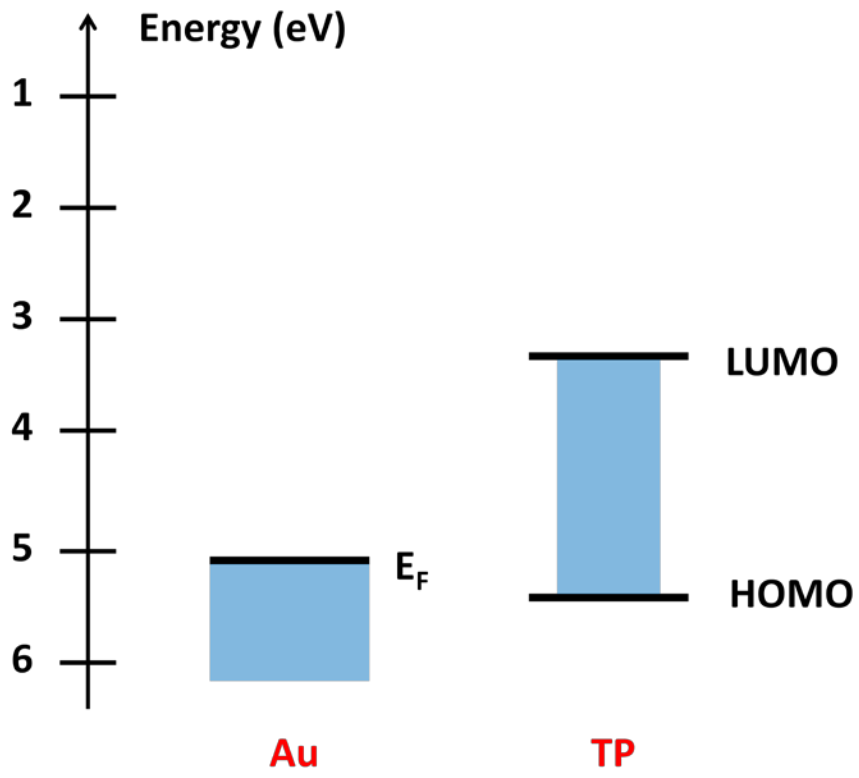

Figure 1.6. The energy scheme of the interface between gold (Au) and the semiconductor TIPS pentacene (TP) layer, where HOMO is the highest occupied molecular orbital while LUMO the lowest unoccupied molecular orbital. (adapted from reference 42)

When voltage is applied to the gate electrode, the voltage induces charge at two sides of the dielectric layer. The amount of induced charge is equal to the applied voltage. When successful charge injection takes place and forms a channel, the channel conductance is proportional to the applied voltage. At a low source-drain voltage, the current flow is proportional to both of these two voltages and is characterized by the "linear regime". When the source-drain voltage increases, the voltage drop gradually reduces to zero at the drain electrode. At this time a pinch off occurs in the channel, so the current is not controlled by the applied source-drain voltage anymore, which is characterized by "saturation regime".

1.3.3. Charge Distribution

Considering the thickness of the conducting channel, the distribution of charge carriers is characterized by a continuous decrease from the interface between the semiconductor layer and the dielectric layer to the bulk region of the semiconductor layer. In order to investigate the distribution of charge carriers, Piosson's equation is presented here.[43]

$$\frac{d^2V}{dx^2} = -\frac{\rho(x)}{\varepsilon_s}$$

where V is defined as the potential, x is along the direction vertical to the channel, ρ is the density of charge carriers, ε_s is permittivity of the semiconductor layer.

In the accumulation regime, an approximation of the solution can be presented as:

$$n(x) = \frac{\rho(x)}{q} = \frac{(C_i V_G)^2}{2kT\varepsilon_s}(1 + \frac{x}{\sqrt{2}L_D})^{-2}$$

where C_i is the capacitance per unit area of the dielectric layer, $n(x)$ is the density of charge carriers, q is the charge of charge carriers, L_D is the Debye length, which can be given by the following:

$$L_D = \frac{\sqrt{2}kT\varepsilon_s}{qC_iV_G}$$

where k is the Boltzmann's constant, and T is temperature.

The Debye length L_D can be considered to be an estimated value of the effective thickness of the channel, which can be close to the thickness of a monolayer but far less than the

actual thickness of the channel. Therefore, most of the charge carriers within the channel are considered to be located in the first few monolayers at the interface between the semiconductor layer and the dielectric layer.[44]

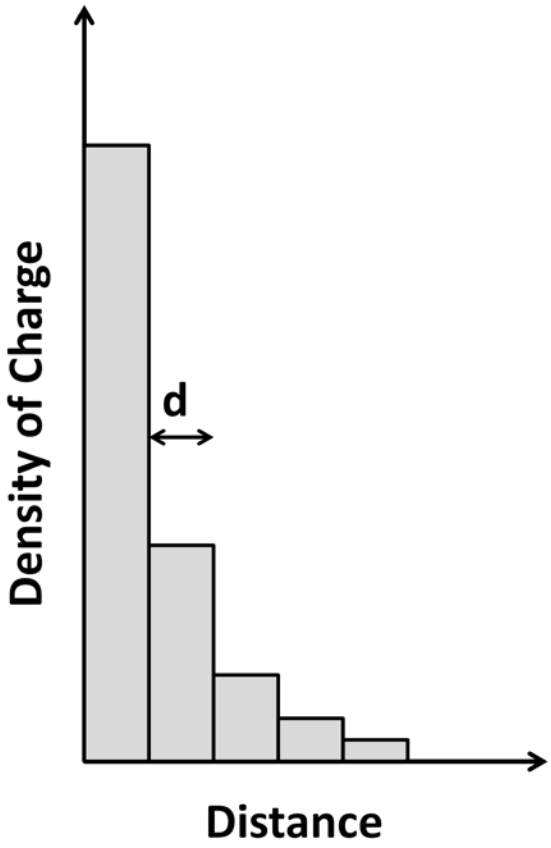

Figure 1.7. The distribution of charge carriers across the channel of OTFTs. The noncontinuous distribution is characterized by a staircase shape. "d" represents the width of each step, which equals to the width of a monolayer of molecules.

Now considering the equation that presents the approximated solution of the density of charge carriers, it can be seen that the density of charge carriers $n(x)$ decreases dramatically with the increase of x. By using quantum mechanical calculations of the transport phenomena, it can

be concluded that the distribution of charge within the semiconductor layer is noncontinuous, and that it can be represented by the staircase shape, as shown in Figure 1.7.

1.4 Current Issues

Despite the major advantages of TIPS pentacene as a newly-developed *p*-type semiconductor, such as solution processibility, high mobility and air stability,[45] there are several problems which have largely restricted the further application of TIPS pentacene for organic electronics. The TIPS pentacene crystals obtained from drop casting exhibit random orientation, big gaps and aggregation.[46] When OTFTs are fabricated based on such film morphology, the resultant devices exhibit severe performance variations. Furthermore, when such OTFTs are utilized to power a screen which is made of LEDs, this screen would suffer from brightness variation. Therefore, in order to address the related problems in the device performances, it is necessary to solve the problems of TIPS pentacene crystals, such as crystal misorientation and poor film uniformity.

1.5 Motivation

In order to address the problems of crystal misorientation and device performance variation as mentioned above, different approaches have been taken which can be basically divided into two categories. The first category of approaches is called "external force", which utilizes external force, such as air flow,[46] electrical field [47-51] or temperature gradient,[52] to align the misorientated TIPS pentacene crystals. The utilization of air flow to navigate the TIPS pentacene crystal growth will be discussed in Chapter 3. Electric field, which interacts with the dipole moment of the TIPS pentacene molecules, can be used to align the TIPS pentacene crystals because TIPS pentacene could respond to an external electrical field. As a result, the

TIPS pentacene molecules will be expected to be aligned to the direction of electrical field and will result into a film with improved crystal orientation and film uniformity.

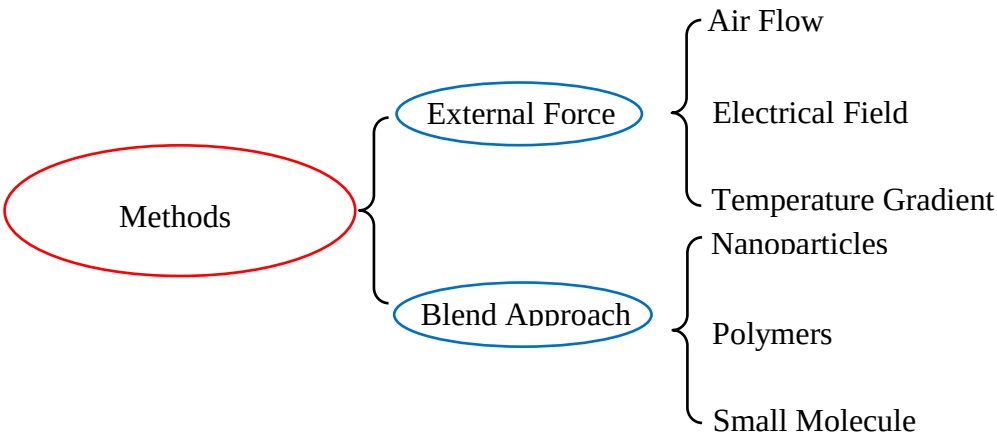

Figure 1.8. Two approaches to address the problems of crystal misorientation and device performance variation by using "external force" and "blend approach".

The second category takes advantages of a "blend method", such as adding various nanoparticles, polymers or semiconductors into TIPS pentacene. The resultant blend films demonstrate an improvement in both crystal orientation and film coverage. A lot of work has been done by various research groups to blend TIPS pentacene with polymers. For example, Ohe *et al*. blended TIPS pentacene with poly (alpha-methylstyrene) (PαMS) at 1:1 in weight ratio, and demonstrated that the resultant blend film exhibits a trilayer structure with vertical phase separation.[53] The bottom layer and top layer of the trilayer structure are rich of TIPS pentacene, while the middle layer is rich of PαMS. Also, their work indicated that the addition of PαMS results in an enhancement of performance consistency of their TIPS pentacene/ PαMS blend OTFTs. Furthermore, because of the addition of PαMS as an additional dielectric layer, the thermal stability of the blend OTFTs was improved when compared to pure TIPS pentacene OTFTs.[54]

Similarly, Hwang *et al*. blended TIPS pentacene with poly (triarylamine) (PTAA), and systematically examined the effect from the addition of PTAA.[32] Their results demonstrate that TIPS pentacene crystals phase-segregate from PTAA and form ordered domains. Increased XRD peak intensities found in the TIPS pentacene/PTAA blend film indicate enhanced crystallinity of the blend film. Because of the improvement of orderliness of TIPS pentacene domains and film crystallinity, the OTFTs fabricated based on the TIPS pentacene/PTAA blends demonstrated an enhancement of average mobilities. With the optimization of annealing conditions, the TIPS pentacene/PTAA blend OTFTs exhibit a highest mobility of 2.82 cm^2/Vs.[32]

CHAPTER 2

ENHANCED PERFORMANCE CONSISTENCY IN NANOPARTICLE/TIPS PENTACENE-BASED ORGANIC THIN FILM TRANSISTORS

2.1 Introduction

Solution-processed organic electronic devices are attractive because of their compatibility with solution-based low-temperature processing methods that could unlock the potential for low-cost, high-throughput fabrication over large areas on flexible substrates.[55-59] 6,13-bis (triisopropylsilylethynyl)-pentacene (TIPS pentacene) is a promising candidate for p-type organic thin-film transistor (OTFT) active layer because of its high mobility, air stability, and solution processibility.[12,35,60-63] However, TIPS pentacene crystalline films are highly anisotropic, which leads to significant variations in device performance.[8,64] In order to address this problem, polymer/TIPS pentacene blends have been used to improve film uniformity and reduce crystal misorientation. For example, Ohe *et al*. and Kang *et al*. blended poly(α-methylstyrene) (PαMS) with TIPS pentacene.[54,65] Enhanced performance reproducibility in PαMS/TIPS pentacene OTFTs was achieved due to vertical phase separation of the polymer and the small molecule organic semiconductor. Mobilities of 0.12 $cm^2 V^{-1} s^{-1}$ and 0.3 $cm^2 V^{-1} s^{-1}$, respectively, were reported [54,65] using a bottom-contact configuration. In addition, Smith *et al*. and Hamilton *et al*. blended an amorphous p-type polymer, poly(triaryl amine) (PTAA), with TIPS pentacene and successfully combined the good film- forming characteristics of PTAA and the high mobility of

TIPS pentacene in OTFT devices.[66,67] More detailed aspects of acene-polymer and other solution-processed semiconducting blends were thoroughly covered in a recent review by Smith, *et al*.[68]

In this chapter, the effect of nanoparticles, instead of polymer additives, on TIPS pentacene crystallization and OTFT performance, was investigated. Nanoparticles have been shown to reduce crystallinity and crystal sizes in poly(ethylene oxide)/ lithium salt systems,[69] but are barely explored in small molecule OTFT systems so far. SiO_2 nanoparticles rather than metal nanoparticles are used for morphological tuning because in ideal situations (i.e. without moisture absorption) insulating nanoparticles should not cause additional leakage current in the OTFT channel. Phase separation in blends of TIPS pentacene and additive materials is largely dominated by TIPS pentacene crystallization, instead of mixing free energy in liquid states,[54,65-68] which suggests that modifying TIPS pentacene crystallization with nanoparticle additives may have useful and important impact on TIPS pentacene based organic thin-film transistors.

X-ray diffraction and optical microscopy were used to investigate thin film morphology of nanoparticle/ TIPS pentacene blends, top-contact OTFTs to determine device performance, and TEM to image crystal edges. According to the X-ray diffraction and optical microscopy, 10% SiO_2 nanoparticles can appropriately reduce the TIPS pentacene crystal width and enhance crystal orientation without significantly compromising the crystallinity. This results in considerably improved average mobility and performance consistency of TIPS pentacene OTFTs. Finally, TEM images show a much darker and broader TIPS pentacene crystal edge after nanoparticle incorporation, which provides evidence for nanoparticle aggregation at TIPS pentacene grain boundaries. Overall, this work demonstrates that nanoparticle addition provides

a novel means to mediate the crystallization of solution processed small molecule organic semiconductor and may be used to effectively reduce the performance variation of solution-based organic thin-film transistors.

2.2 Experiment

2.2.1 Materials and Thin Film Formation

TIPS pentacene was synthesized according to an earlier publication.[12] SiO_2 nanoparticles (nominally 20 nm diameter, purchased from Sigma Aldrich) are highly hygroscopic because of their hydrophilic surfaces and extremely high surface- to-volume ratio. Before blending in solution, SiO_2 nanoparticles were baked in an oven at 160 °C for 2–3 days to drive out absorbed moisture. This step was found to be crucial, as TIPS pentacene solutions with moisturized nanoparticles will be more likely to dewet on oxide substrates. Dry SiO_2 nanoparticles were first dispersed in anhydrous toluene with ultra-sonication for 1 h, and then mixed with a pre-made TIPS pentacene solution (with anhydrous toluene) at different concentrations to yield solutions having specific nanoparticle loadings ranging from 0 to 20 wt%. A constant total solid concentration (~5 mg/ml) was maintained. SiO_2 nanoparticle/TIPS pentacene thin films are subsequently formed by drop casting in a solvent rich environment.[63] A small tilt angle of less than 5° was used to facilitate crystal orientation and keep the film thickness uniform over the substrate.

2.2.2 Device Fabrication and Characterization

A bottom-gate, top-contact configuration is used throughout this study. Heavily doped n-type Si substrates serve as the bottom gate contacts, and 250-nm-thick thermal oxide layers

function as gate insulators (specific capacitance:13.8 nF cm^{-2}). After drop-casting, a gold layer of 50 nm thickness was subsequently deposited through a shadow mask to form the source and drain contacts. The electrode deposition was performed in a thermal evaporator (Angstrom Engineering) at 10^{-7} Torr using a deposition rate of 0.5 Å s^{-1}. The electrical performance of OTFTs, including transistor transfer (I_{DS}–V_{GS}) and output (I_{DS}–V_{DS}) characteristics, was measured with a Keithley 4200 semiconductor parameter analyzer. All measurements were made at ambient conditions at room temperature. From the slope of the transfer characteristics $(I_{DS})^{1/2}$ – V_{GS}, field-effect mobility in the saturation regime (V_{DS} = –60 V) was extracted based on the traditional MOSFET equation:

$$I_{DS} = \mu C_i \frac{w}{2L}(V_{GS} - V_T)^2$$

where μ is the saturation mobility, C_i is the specific capacitance of gate insulator, L is the channel length, W is the channel width, and V_T is the threshold voltage.

2.2.3 Diffraction and Microscopy

Polarized optical micrographs of SiO2 nanoparticle/TIPS pentacene thin films were obtained with a Nikon OptiPhot2-POL polarized optical microscope. Grazing-incidence X-ray diffraction was performed with an X′Pert PRO MPD Diffractometer using Cu Kα radiation. TEM images were obtained using a Hitachi HF3300at 300 kV. Unlike films that served as the transistor active layers, TEM samples were prepared by drop casting from a much more dilute solution (0.1 wt% total solid content) onto amorphous carbon-coated copper grids to yield thin films that are suitable for imaging by transmission electron microscopy. A Zeiss Merlin SEM was used for cross-sectional imaging at 500–1000 V with the charge compensation mode to

avoid electron beam damage to the TIPS pentacene active layer. A tilt angle of 16.6° was used for edge imaging.

2.3 Results and discussion

A bottom-gate, top-contact, OTFT configuration is adopted throughout this work, with 250 nm thermal oxide gate insulator. Channel width and length are 2000 and 50 micrometers, respectively. Figure 2.1 shows typical output and transfer characteristics of OTFTs with 10% SiO_2 nanoparticles in TIPS pentacene. From the fitted line in the square root plot of transfer characteristics, the saturation mobility is determined to be 0.1 $cm^2 V^{-1} s^{-1}$, and threshold voltage (V_T) is approximately 8 V. From the plot in the logarithmic scale, on/off ratio is estimated to be 10^4–10^5. Transfer characteristics were measured 3 times in air and gave very consistent readings. The slight nonlinearity close to the origin of the output curves is caused by the intrinsic resistance of drop-cast TIPS pentacene active layer in a top contact, bottom gate OTFT configuration.[70]

Measured mobility variation of SiO_2 nanoparticle/TIPS pentacene OTFTs is compared with that of the devices based on pure TIPS pentacene, as shown in Figure 2.2. For devices with 0%, 2%, 5% and 10% SiO_2 nanoparticles, 10–20 devices were fabricated, while 6 devices were made for the OTFTs with 15% SiO_2 nanoparticles.

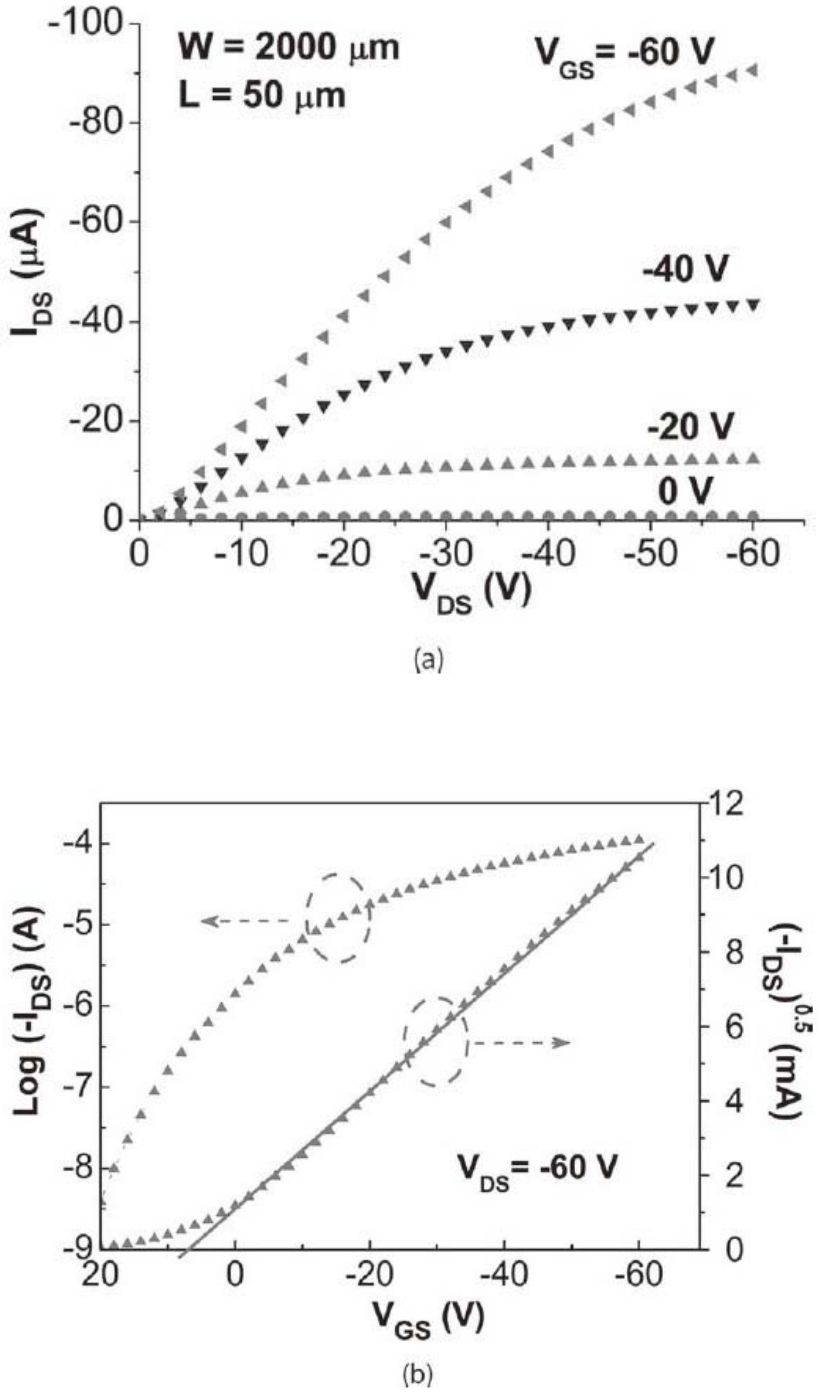

Figure 2.1. Typical output (left) and transfer characteristics (right) of SiO_2 nanoparticle/TIPS pentacene OTFTs. The shown device has a SiO_2 concentration of 10% by weight. The measured saturation mobility is 0.1 $cm^2\ V^{-1}\ s^{-1}$, with a threshold voltage of 8 V and on/off ratio above 10^4.

The measured mobility variation of 10% SiO_2 devices is significantly less than that measured for OTFTs made of pure TIPS pentacene, as shown in Figure 2.2 (a). OTFTs based on pure TIPS pentacene exhibit field-effect mobilities varying by six orders of magnitude (ranging from 1.6×10^{-1} to 3.1×10^{-6} $cm^2\ V^{-1}\ s^{-1}$), while the mobilities of TIPS pentacene OTFTs with 10% SiO2 nanoparticles are consistently between 2.1×10^{-1} and 6.5×10^{-2} $cm^2\ V^{-1}\ s^{-1}$.

The mobilities of pure TIPS pentacene obtained in this work are comparable to those measured in earlier work.[64,65] Park *et al*. reported hole mobilities of 0.65 ± 0.35 $cm^2\ V^{-1}\ s^{-1}$ in solution processed TIPS pentacene OTFT with a bottom-contact configuration and hexamethyldisilazane (HMDS) treatment on gate dielectrics, and their highest measured mobility (1.8 $cm^2\ V^{-1}\ s^{-1}$) [63] is one order of magnitude higher than the highest mobility measured (0.16 $cm^2\ V^{-1}\ s^{-1}$). Nevertheless, this OTFT configuration is more optimized for studying the effect of nanoparticle addition because a TIPS pentacene/SiO_2 nanoparticle solution severely dewets on HMDS treated substrate, resulting in poor film coverage. In Figure 2.2 (b), the measured average mobility and standard deviation of SiO_2 nanoparticle/TIPS pentacene OTFTs are plotted as a function of SiO_2 nanoparticle content. The average mobility increases as the concentration of SiO_2 nanoparticles initially increases from 0% to 2%, 5%, reaching a maximum at 10%. However, the average mobility drops when the concentration of SiO_2 nanoparticles is increased further to 15% as indicated in Figure 2.2 (b).

The ratio of standard deviation to measured average mobility, which may be a more proper indicator of OTFT performance consistency, is shown in Figure 2.2 (c). Among all devices studied, OTFTs with 10% SiO_2 nanoparticles show the lowest performance variation and the highest average mobility.

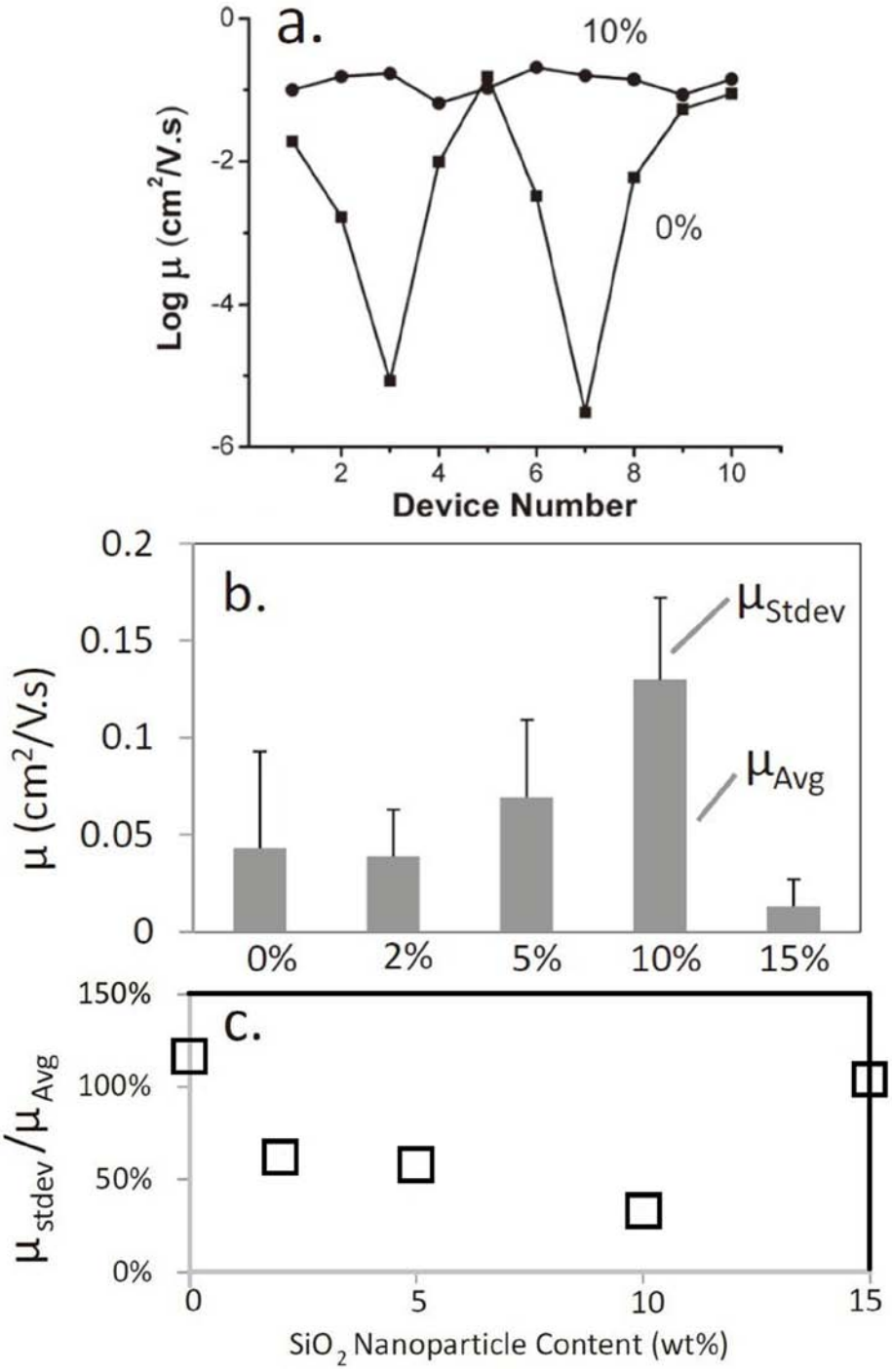

Figure 2.2. a) The mobility variation of 10% SiO_2 devices is significantly less than that of pure TIPS pentacene OTFTs. b) Measured standard deviation and average mobility as a function of SiO_2 content. The error bands stand for the standard deviation of measured mobilities (μ_{Stdev}), while the solid bars represent the measured average mobilities (μ_{Avg}). c) The ratio of standard deviation to measured average mobility as a function of SiO_2 content.

The ratios of measured mobility standard deviation (μ_{Stdev}) to average mobility (μ_{Avg}) for other nanoparticle concentrations (in the range of 0–15%) are up to 3 times higher than that of devices with 10% nanoparticles. At the same time, the average mobility of TIPS pentacene OTFTs is increased from 0.04 ± 0.04 $cm^2\ V^{-1}\ s^{-1}$ with 0% SiO_2 to 0.13 ± 0.04 $cm^2\ V^{-1}\ s^{-1}$ with 10% SiO_2. The average mobility measured for devices with 2%, 5%, and 15% nanoparticles is 0.04 ± 0.02 $cm^2\ V^{-1}\ s^{-1}$, 0.07 ± 0.04 $cm^2\ V^{-1}\ s^{-1}$, and 0.01 ± 0.01 $cm^2\ V^{-1}\ s^{-1}$, respectively. These mobilities are 2–10 times lower than that of devices with 10% nanoparticles. Based on the data, no strong dependence on nanoparticle concentration was observed for threshold voltages and on/ off ratios of devices with 0–15% SiO_2.

To further understand the measured OTFT mobility behavior, both polarized optical microscopy (Figure 2.3) and grazing-incidence X-ray diffraction (Figure 2.4) were used to study the crystal orientation and crystallinity of SiO_2 nanoparticles/TIPS pentacene thin films. As shown in Figure 2.3, the color variation of polarized light microscopy images results from both crystal orientation and thickness. The needle-shaped TIPS pentacene domains are highly crystalline with the acene-ring lying “edge-on” to the substrate.[45,71] The long axis of the needle-shaped crystalline domains is [210], while the short axis is $[1\bar{2}0]$.[35,72,73] As seen in Figure 2.3, the pure TIPS pentacene thin films are highly anisotropic with large variations in the grain width (the short axis of the needle-shaped crystals) and crystal orientation, which corresponds to measured mobilities varying widely from 1.6×10^{-1} to 3.1×10^{-6} $cm^2\ V^{-1}\ s^{-1}$.

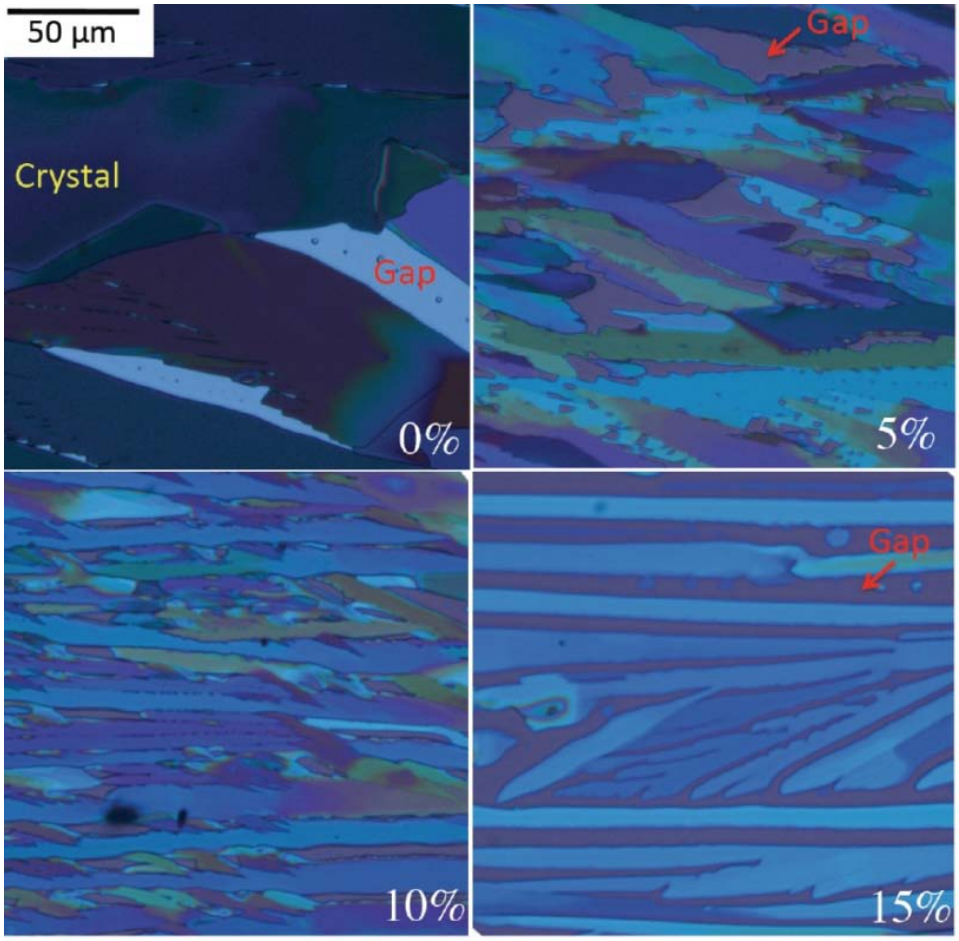

Figure 2.3. Polarized optical microscopy images of drop-cast TIPS pentacene films with SiO_2 concentrations of 0%, 5%, 10%, and 15%. All images share the same scale bar, which is shown at the top left.

When the concentration of SiO_2 nanoparticles is increased to 5–10%, TIPS pentacene crystals have a smaller average grain width and a more uniform grain size distribution. From 10 measurements on crystal size in optical microscopy, the grain width of pure TIPS pentacene films is 42 ± 24 µm, and with 10% nanoparticle, the value is reduced to 11 ± 4 µm. On the other hand, the TIPS pentacene crystal orientation is enhanced at the expense of reduced grain width at an intermediate SiO_2 loading (~10%), as indicated in Figure 2.3. These films had the highest average mobility and lowest performance variation (Figure 2.2 (b) and (c)). As the SiO_2

concentration is increased to 15%, nanoparticle aggregation becomes dominant, leading to circular-shaped small crystals and large gaps between TIPS pentacene “needles”. The grain width of needle-shaped domains is reduced to 8 ± 3 μm (based on 10 measurements).

Grazing-incidence X-ray diffraction results from TIPS pentacene films with different SiO_2 nanoparticle loadings are shown in Figure 2.4 (a). The curves consistently exhibit strong (00l) type reflections, which match results reported previously for TIPS pentacene films.[61] In Figure 2.4 (a), the curves corresponding to different nanoparticle concentrations are shifted vertically to enable comparison. It is noted that the crystallinity of TIPS pentacene films decreases as the SiO_2 nanoparticle content increases at SiO_2 nanoparticle loadings above 5%, as indicated by the intensity decrease of (00l) type reflections (Figure 2.4 (b)). Besides the intense (00l) reflections reported in literature,[61] it was also noted there are many fine peaks in films with 0–5% SiO_2 at 2θ of 5°–25° that are not of (00l) type (Figure 2.4 (a)). For example, the combined peak of (111) and (11$\bar{1}$) is visible in XRD results with 0–5% SiO_2. As the SiO_2 content increases to 10% and higher, this peak decreases significantly and then plateaus (Figure 2.4 (c)). For X-ray diffraction patterns of a TIPS pentacene single crystal through ac and bc planes, the combined peak of (111) and (11$\bar{1}$) will not be present according to the X-ray simulation; thus, to some extent, this combined peak can be used to represent the misorientation of TIPS pentacene films. With the information from both optical microscopy and X-ray diffraction, it can be conclude that a balance of film connectivity, high crystallinity, and crystal orientation is achieved in devices with 10% SiO_2. Films with higher nanoparticle concentration have poor film connectivity and low crystallinity, while lower SiO_2 content yields higher crystallinity but poor crystal orientation.

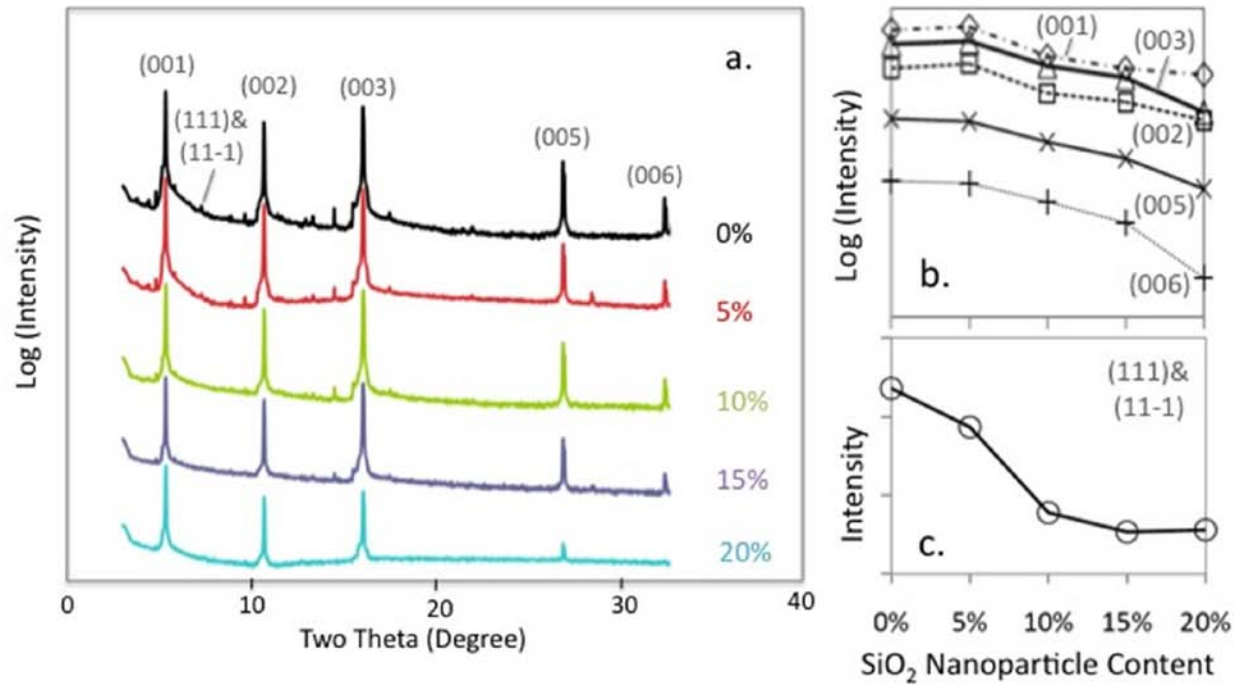

Figure 2.4. Grazing-incidence X-ray diffraction of TIPS pentacene films with different SiO_2 nanoparticle loading. a) The films exhibit consistent (00l) type reflections. b) The crystallinity of TIPS pentacene films decrease as the SiO_2 nanoparticle content increase beyond 5% as indicated by the reduced intensities of (00l) type reflections. c) The intensity of the combined peak of (111) and (111) plateaus after the nanoparticle concentration reaches 10%.

To investigate the microstructural arrangement in SiO_2 nanoparticle/TIPS pentacene films, bright field TEM images were taken for the blend film, pure TIPS pentacene film and the nanoparticles, respectively (Figure 2.5). Regions of darker color (i.e., smaller gray value in Figure 2.5 (d)) represent TIPS pentacene films or SiO_2 nanoparticles, while the lighter region (i.e., higher gray value in Figure 2.5 (d)) corresponds to amorphous-carbon supporting films. Although it was not possible to visualize individual nanoparticles in the blend because of their aggregation, TEM images did show a distinctively darker and broader edge for TIPS pentacene films with 10% SiO_2 nanoparticles (Figure 2.5 (a)) than that of the neat TIPS pentacene films

(Figure 2.5 (b)). Pure SiO_2 nanoparticles are shown in Figure 2.5 (c), and the diameters of these particles are 18 ± 4 nm based on 12 different measurements.

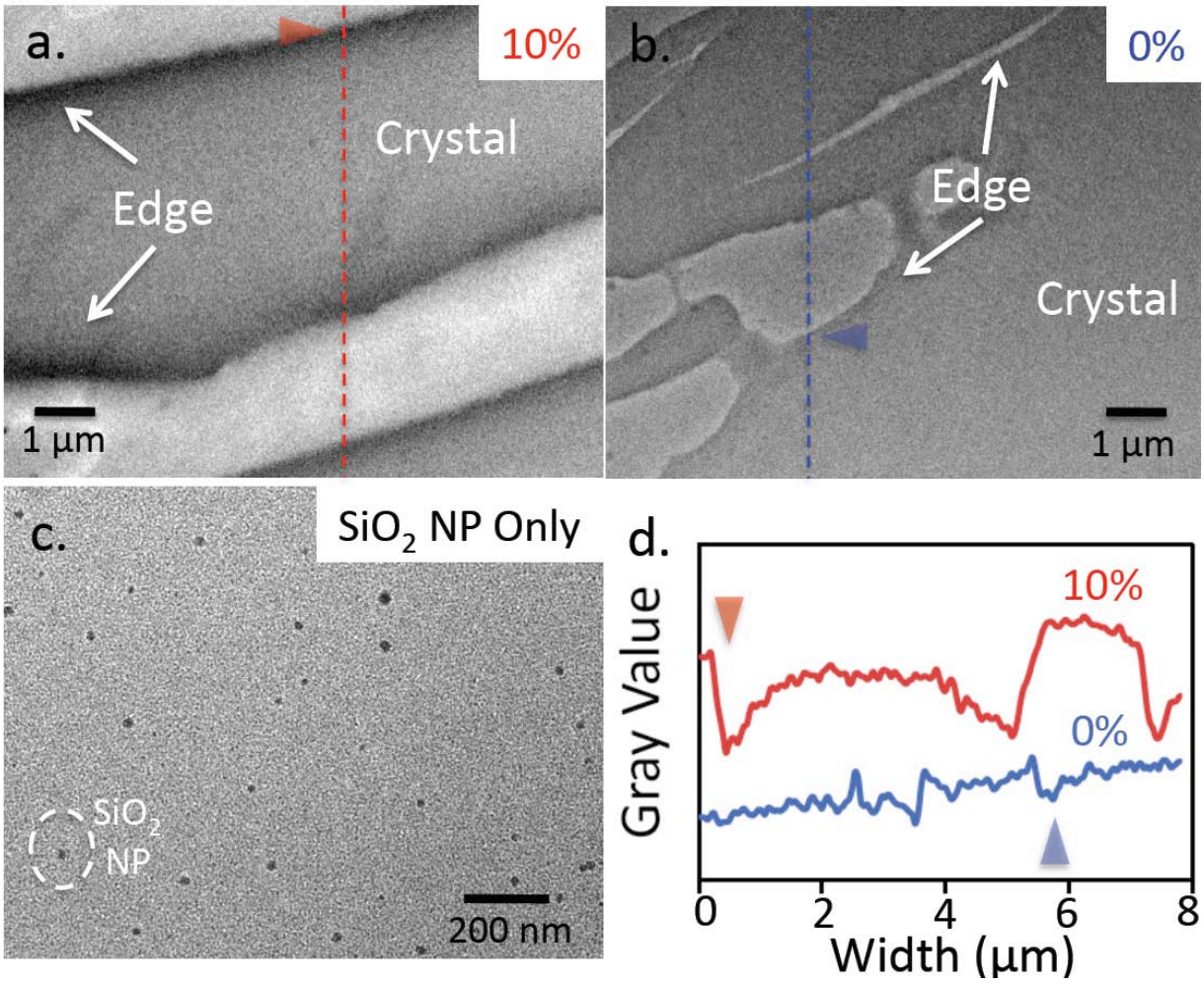

Figure 2.5. Bright-field TEM images show a distinctively darker and broader edge for TIPS pentacene films with a) 10% SiO_2 nanoparticles than that of b) the neat TIPS pentacene films. The freestanding SiO_2 nanoparticles are shown in (c). d) Two grayness curves are compared: a line corresponds to TIPS pentacene film with 10% nanoparticles (obtained from the dotted line shown in (a) and a line corresponds to the gray value obtained from pure TIPS pentacene film (at the dotted line shown in (b). Triangles shown in (a) and (b) mark the crystal edges, corresponding to the marked positions in the gray value curves (d).

It is noted that the darker edge of the blend film is not a result of defocus or crystal topography, as it appears consistently in different SiO_2/ TIPS pentacene crystals. The inner part of SiO_2/TIPS pentacene film is rather uniform in terms of electron contrast, while the gray value gradient of the film edge is very likely caused by aggregation of nanoparticles at grain boundaries, which is responsible for the changes observed in optical microscopy images (Figure 2.3). To quantitatively compare the film edges, a grayness plot is presented in Figure 2.5 (d). The two triangles in Figure 2.5 (a) and 2.5 (b) each mark a crystal (or film) edge, corresponding to the two marked edge positions in grayness curves (Figure 2.5 (d)). The width of the film edge with 10% nanoparticles is about 1.5 μm, while that of the pure TIPS pentacene film is only 0.2 μm. Because this edge width analysis is based on the gray value derived from the TEM image, it is not clear if the nanoparticles are located on top of the edge or inside TIPS pentacene crystals. A previous report confirmed that molecular orientation of TIPS pentacene on amorphous carbon substrate is identical to that on an oxidized silicon wafer.[8]

Since the semiconductor-insulator interface is most critical to thin-film transistor operation and vertical separation plays a significant role in TIPS pentacene/polymer binder systems,[51,62-65] low-voltage cross-sectional SEM was performed for TIPS pentacene blend film with 10% SiO_2 nanoparticles. A charge compensation mode was used at 0.5 kV to effectively avoid charging effects from TIPS pentacene. Round-shaped silicon dioxide nanoparticles with ~20 nm diameters are visible in typical low-voltage SEM images (Figure 2.6 (a)). The vertical distribution of SiO_2 nanoparticles in TIPS pentacene film is presented in Figure 2.6 (b). A total of 45 nanoparticles were sampled from different SEM images at different regions.

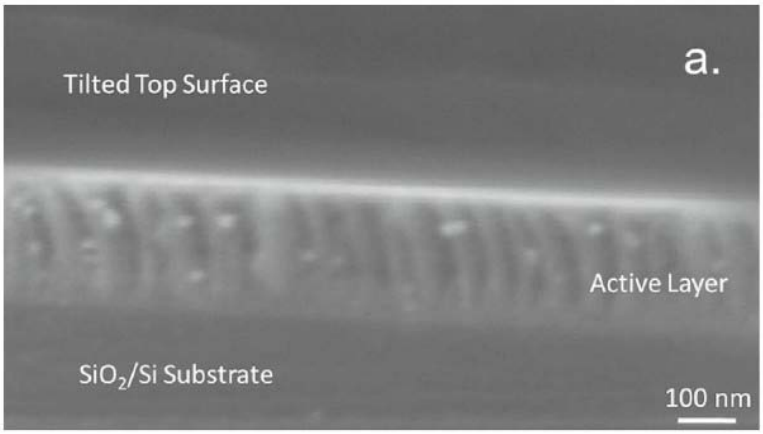

b.

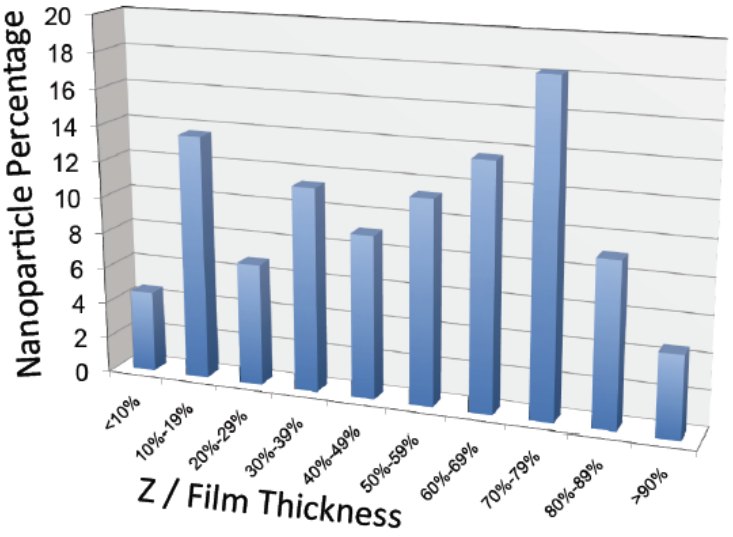

Figure 2.6. Vertical distribution of SiO_2 nanoparticles in TIPS pentacene active layer. a) A typical cross-section SEM image of TIPS pentacene with 10% SiO_2 nanoparticles loading. b) Vertical distribution of nanoparticles in TIPS pentacene blend with 10% SiO_2 nanoparticles. Z is the distance between the center of a nanoparticle and the semiconductor/dielectric interface. Only 4% SiO_2 nanoparticles are close to the TIPS pentacene/ SiO_2 insulator interface (Z/Film Thickness < 10%).

In Figure 2.6 (b), Z is defined as the distance from the center of a nanoparticle to the gate insulator surface. The plot of nanoparticle percentage as a function of relative vertical position

clearly demonstrates that the nanoparticles are mostly concentrated in the central region of the active layer (Z/Film Thickness = 20–80%). Since most nanoparticles are located away from the semiconductor/insulator interface, the addition of SiO_2 nanoparticles is not expected to significantly deteriorate charge transport in the channel.

Based on the diffraction and microscopy results, the TIPS pentacene crystalline films do not change their crystal structure or unit cell upon nanoparticle addition. Instead, the nanoparticles settle at the grain boundaries of TIPS pentacene crystals, effectively modifying film anisotropy as sketched in Figure 2.7. With the reduced grain width at 10% SiO_2, it is easier for the TIPS pentacene crystals to grow and organize along a uniform direction. This in turn leads to more consistent OTFT performance; however, too high of a nanoparticle concentration seems to reduce the TIPS pentacene crystallinity and grain size, which leads to poorer OTFT performance.

The nanoparticles used in this work are highly hydrophilic in nature as they have many hydroxyl groups on nanoparticle surface. This may not be ideal for OTFT application because of the possibilities of moisture absorption and enthalpically unfavored interactions with TIPS pentacene. Further work could be done to modify the nanoparticle surfaces with polymers and organic ligands with different hydrophobicity. By making the surfaces less hygroscopic and tuning the polarity of nanoparticle surfaces, it may be possible to better mediate thin film morphologies and crystallization of solution-processable small molecule organic semiconductors for OTFT applications.

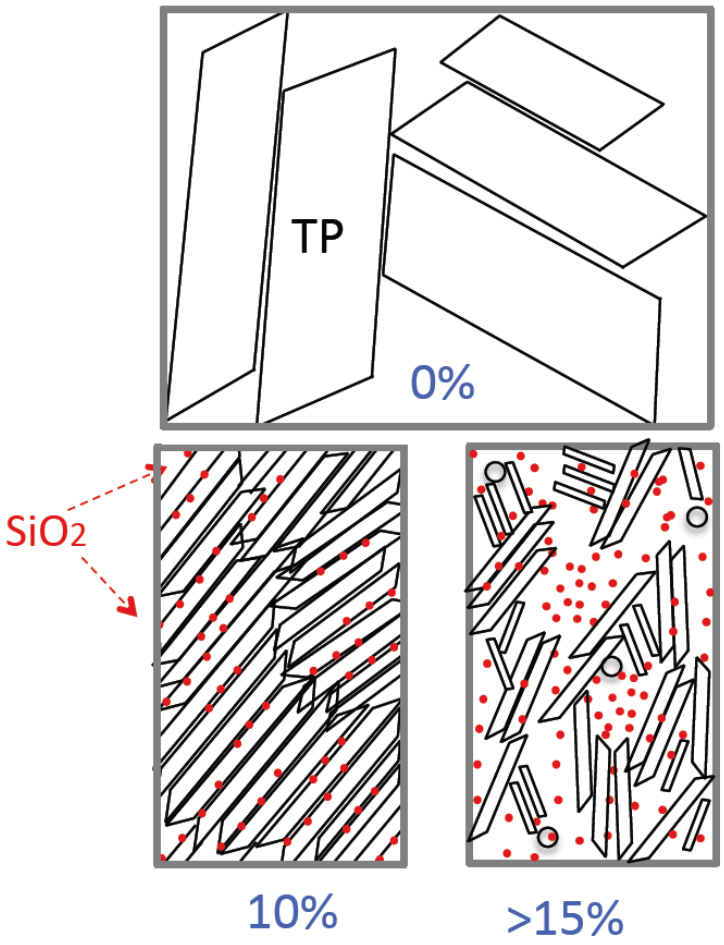

Figure 2.7. Sketches representing TIPS pentacene films with different SiO_2 nanoparticle concentration. “TP” stands for TIPS pentacene crystals.

2.4. Conclusions

The OTFTs based on SiO_2 nanoparticles/TIPS pentacene show enhanced performance consistency marked by increases in average mobility and reduction of mobility standard deviation(μ_{Stdev}) to average mobility (μ_{Avg}) ratio in comparison to OTFTs made from neat TIPS pentacene. At 10% SiO_2 concentration, the measured hole mobility is 0.13 ± 0.04 $cm^2\ V^{-1}\ s^{-1}$ while the corresponding OTFTs made from neat TIPS pentacene have a mobility of 0.04 ± 0.04 $cm^2\ V^{-1}\ s^{-1}$. TEM images reveal that the edges of TIPS pentacene crystals with 10% SiO_2 are

significantly darker and about 8 times wider than that of pure TIPS pentacene films, which is likely caused by nanoparticle aggregation at TIPS pentacene grain boundaries. Both polarized optical microscopy images and X-ray diffraction results demonstrate that, with 10% SiO_2 nanoparticles, improved crystal orientation is achieved while maintaining relatively high level of TIPS pentacene crystallinity.

CHAPTER 3

AIR-FLOW NAVIGATED CRYSTAL GROWTH FOR TIPS PENTACENE-BASED ORGANIC THIN-FILM TRANSISTORS

3.1. Introduction

In recent years, significant progress has been made in the development of organic thin-film transistors (OTFTs). Due to their ease of fabrication, high performance and cost-effectiveness, solution-processed OTFTs have great potential for applications in large-area flexible integrated systems.[55-59,66] Among solution-processable organic semiconductors, 6,13-bis(triisopropylsilylethynyl) pentacene (TIPS pentacene) is a very promising material because of its high hole carrier mobility and environmental stability. [12,35,60-62,74-77] However, its tendency to form randomly oriented needle-shaped crystals when crystallized from solution leads to significant performance variations in OTFT performance.[8,10]

Drop casting TIPS pentacene (solute) in toluene (solvent) is a widely used method to form polycrystalline TIPS pentacene thin films. When a droplet of solution is in contact with a substrate, its contact lines are pinned and thus restrict the volume change of the liquid content, which is known as the “pinning effect”.[78-81] Consequently, the volume change at the droplet edge is smaller than that in the center. On the other hand, solvent evaporation at the edge is faster than the center of the droplet because of an increased available angle of evaporation at the edge.[82,83] The difference in evaporation rate and volume change between the edge and the center of the

droplet causes a radial flow, which supplies the solvent and carries the solute from the center to the edge. The increased density of solute at the edge eventually deposits, forming the so-called "coffee ring", [75-81] which adversely affects crystallization and thin-film morphology thereby leading to poor performance of OTFTs. To prevent the "coffee ring" patterns, the pinning effect and excessive center-to-edge solute diffusion should be minimized. In addition, to keep the needle-shaped crystal growth in a consistent orientation, the solution drying direction must be aligned as well. In this paper, external air flow is applied in an effort to facilitate contact line moving and counteract excessive solute diffusion from the center to the edge of the droplet and keep the solution drying direction identical to that of the air flow.

The gas flow approach to control the TIPS pentacene crystallization and morphology has been studied before. For example, Chen *et al*. used an air flow in vertical configuration (air flow vertical to the substrate plane) to control solvent evaporation and be able to manipulate crystal domain sizes.[35] Also, Kim *et al.* showed a correlation between the injected gas flow direction and the OTFT performance.[84] In this chapter, the effects of horizontal air flow were systematically investigated not only on improving the TIPS pentacene crystal orientation, but also on enhancing the film areal coverage over the whole substrate, which work together to achieve an eleven-fold enhancement in performance consistency of OTFTs. The performance consistency here is defined as the ratio of average mobility to the standard deviation of the field-effect mobilities, which is an indication of the mobility uniformity for the OTFT devices over the whole substrate. Optical microscopy and X-ray diffraction were employed to investigate the morphology of TIPS pentacene thin films at different air flow speeds. This work demonstrates that the employment of external air flow provides a simple, yet effective approach to control solution-processed TIPS pentacene crystal growth, thereby improving the average hole mobility and performance

consistency of OTFTs.

3.2. Experiment

3.2.1. Materials and Thin Film Formation

TIPS pentacene was used as purchased (Sigma Aldrich) without further purification. TIPS pentacene powder was first dissolved in toluene with a concentration of 5 mg/ml. Subsequently, TIPS pentacene thin films were formed by drop casting in a solvent rich environment.[72] The experiment was carried out in a plastic chamber to prevent the effect of the air circulation in the chemical hood. For air-flow navigated TIPS pentacene growth, external air flow from a nozzle was turned on simultaneously upon drop casting to facilitate crystal orientation over the whole substrate. Because TIPS pentacene is known for its excellent air stability,[60] here dry air with ~20% humidity was simply used for the flow navigation experiments, instead of using an inert gas such as argon or nitrogen. Flow rate was measured for air flow inside the plastic tube by using Dwyer VF Visi-Float Flowmeter VFB-65-BV. Since the influence of air flow on the TIPS pentacene growth depends on the distance between air nozzle and substrate and other environmental conditions, the corresponding effects at different air flow rates are based on the in-house experimental setup. Optical micrographs of TIPS pentacene thin films were taken using an optical microscope with a camera built in a Signatone PSM 1000 probe station. Thin film crystallinity and coverage was characterized using Philips X'Pert X-ray Diffraction.

3.2.2. Device Fabrication and Characterization

Bottom-gate, top-contact OTFT configuration was adopted in device fabrication. Heavily doped n-type silicon substrate serves as bottom gate, and 250 nm thermal oxide as gate insulator.

After TIPS pentacene growth on the substrate, Au source/drain contacts were thermally deposited through shadow mask with channel length of 100 microns and channel width of 1000 microns. The electrical performance of OTFTs was characterized by current-voltage measurement using an Agilent B1500A semiconductor parameter analyzer. In order to ensure the extracted parameters from the transfer characteristic were consistent, all devices were measured for five times. All measurements were done in the ambient environment at room temperature. From the slope of the transfer characteristic $(I_{DS})^{1/2}$-V_{GS}, field-effect mobility in the saturation regime was extracted.

3.3. Results and discussion

Figure 3.1 illustrates the concept of the air-flow navigation for TIPS pentacene crystal growth. As compressed dry air flows against and over a drop-cast TIPS pentacene droplet (dashed line) on the SiO_2/Si substrate, it pushes the front area and contact line forward, minimizing the pinning effect. Also air flow counteracts solute diffusion from center to edge by pushing back the solute away from the edge, preventing solute deposition.[84] As the front contact line moves forward, the solvent evaporates along the air flow path, leading to an orientated crystal growth in the same direction as air flows. As a result, air flow effectively navigates the TIPS pentacene crystallization and reduces the crystal anisotropy over the whole substrate.

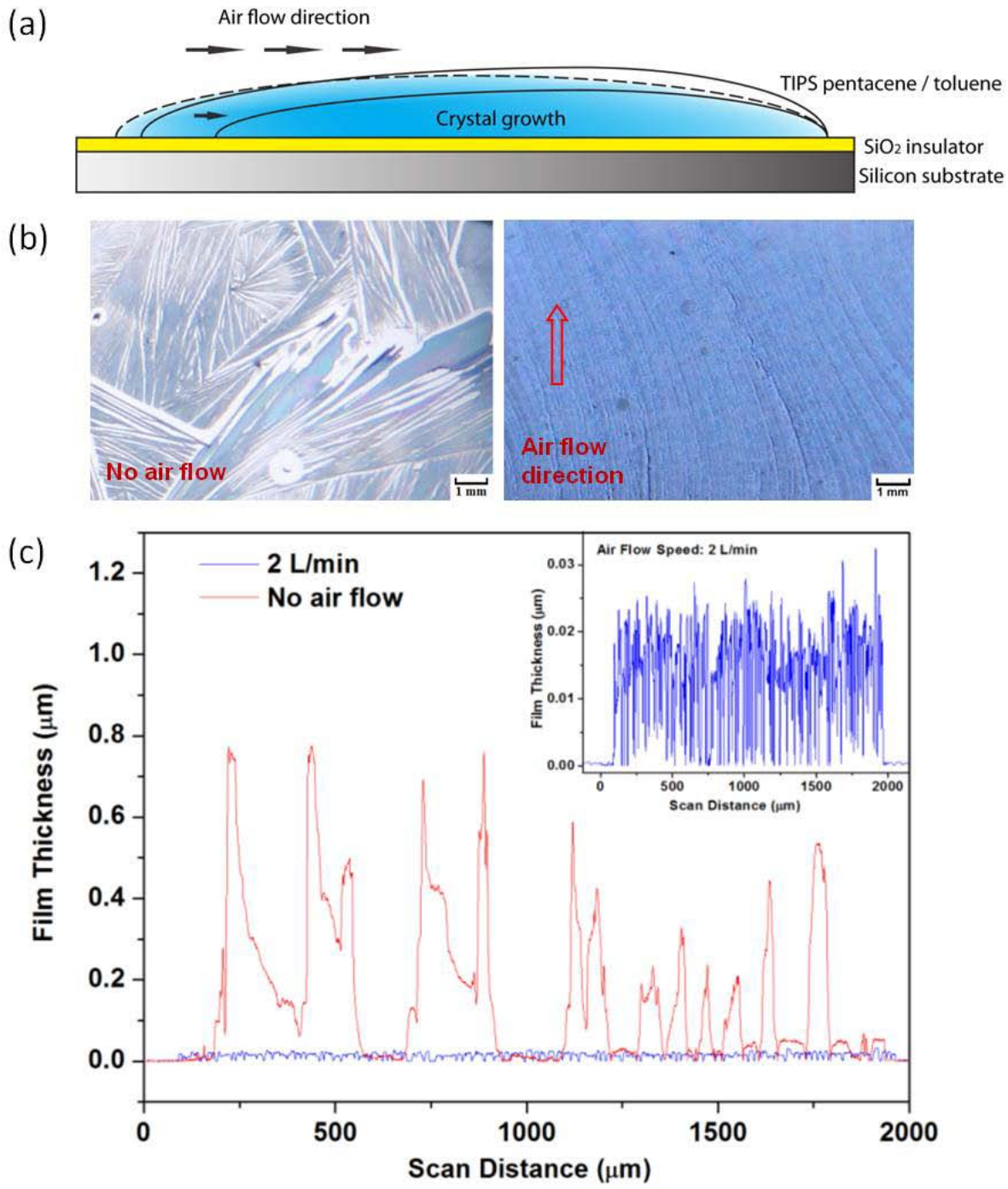

Figure 3.1. (a) Schematic drawing of the crystal growth with air-flow navigation. (b) Comparison of crystal orientation and areal coverage over the whole substrate without and with air flow at a flow rate of 2 L/min, which represents an optimized TIPS pentacene film morphology. (c) Film topography without AFN shows large crystal thickness variation, while films with AFN exhibit reduced average thickness with improved uniformity.

Figure 3.1(b) compares the air flow guided crystal growth at the optimal flow rate with the simple drop-casting crystallization without AFN. If no air flow is applied, the TIPS pentacene thin film exhibits large needle-shaped crystals with random orientation and huge gaps in between. When a proper air flow is applied, TIPS pentacene crystals become well orientated with enhanced areal coverage. The polycrystalline TIPS pentacene thin film obtained at optimum flow rate of 2 L/min yields optimal crystallization in terms of crystal orientation and coverage. Note in Figure 3.1(b) that the crystal orientation does not exactly match the air flow direction. This may be partially attributed to the fact that in the experimental setup, some compressed air bounces back from the chamber side wall, causing air disturbances on the substrate edge and affecting crystal growth orientation.

The results also suggest that the air flow is not only able to improve morphology, but also affect film topography. As shown in Figure 3.1(c), without air-flow navigation, the crystal film thickness varies significantly from 30 nm to 770 nm. In contrast, when air flow is applied to navigate crystallization, the TIPS pentacene film demonstrates significantly reduced maximum thickness and less thickness variation. At the flow speed of 2.0 L/min, the thin-film thickness ranges from 13 nm to 35 nm with an average of 20 nm over the whole substrate. The improved uniformity in thickness contributes to an even distribution of nucleation and crystallization events on the substrates because the air flow counteracts to the solute diffusion from the center to the edge, resulting in uniform deposition of crystal seeds.

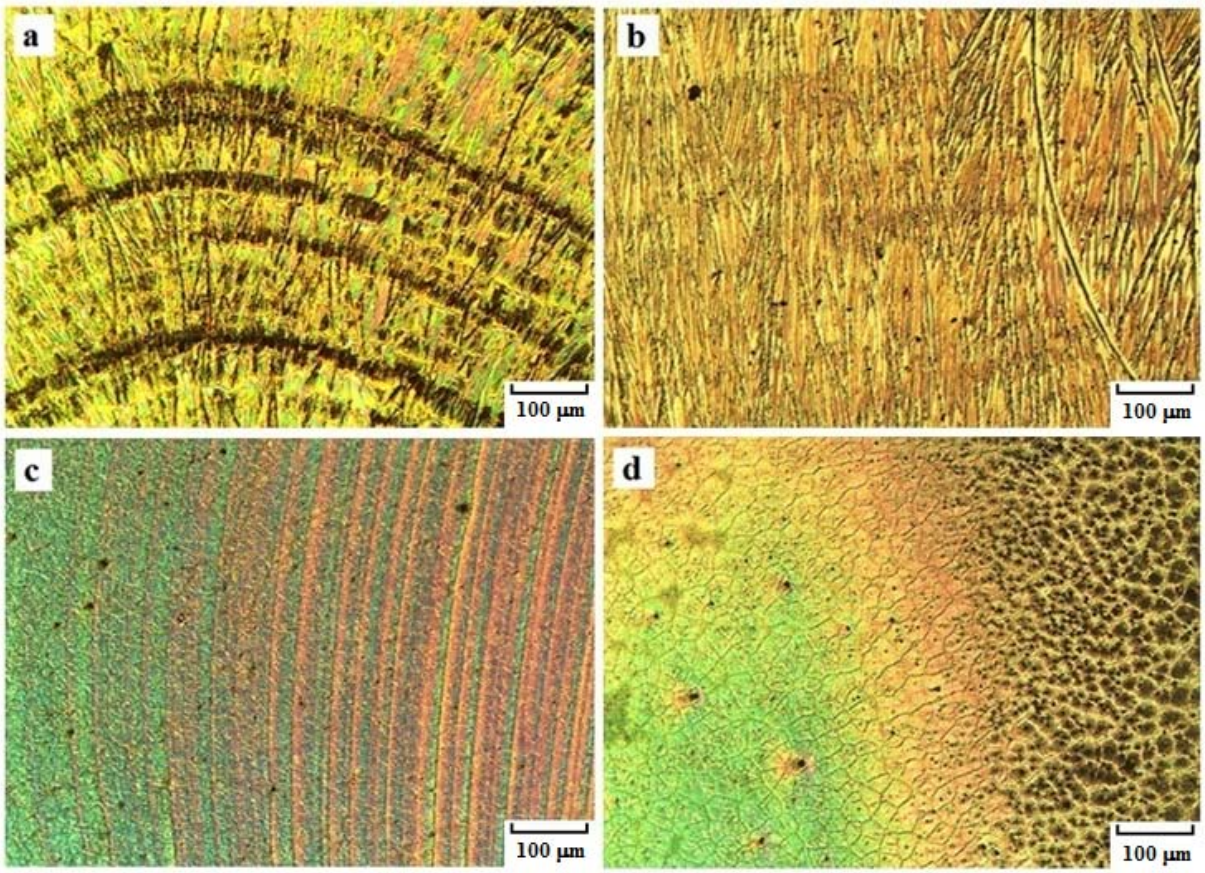

Figure 3.2. Optical images of TIPS pentacene thin films with air-flow navigation. Air-flow direction is from the bottom to the top in each optical image. Panels (a), (b), (c), and (d) correspond to the air flow speed of 1 L/min, 2 L/min, 3 L/min, and 4 L/min, respectively.

The optical images in Figure 3.2 show morphology variations of TIPS pentacene films at different air flow speeds: (a) 1 L/min, (b) 2 L/min, (c) 3 L/min, and (d) 4 L/min, respectively. At a low air flow speed of 1 L/min, the "coffee ring" crystal patterns still persist, with largely improved crystal orientation as compared to the drop-cast TIPS pentacene film. When the air flow rate increases to 2 L/min, the air flow is able to suppress the "coffee ring" effect, leading to the best TIPS pentacene crystal orientation and needle-crystal growth as shown in Figure 3.2(b). The TIPS pentacene crystal domains are long needle-shaped [45,71] with the long axis along the [210] direction as well as short axis of [$1\bar{2}0$] orientation.[35,63,72,73] As the air-flow speed is further

increased to 3 L/min, the toluene solvent evaporates rapidly, resulting in the initiation of some round-shaped crystal domains that are smaller in size within the crystal needles as shown in Figure 3.2(c). Those crystal domains do not fully crystallize because of the reduced crystallization time. Such a phenomenon becomes more significant when the air flow speed is increased up to 4 L/min: the external air flow quickly evaporates toluene and TIPS pentacene is almost directly deposited on the substrate, presenting extremely small crystals with very little orientation as shown in Figure 3.2(d).

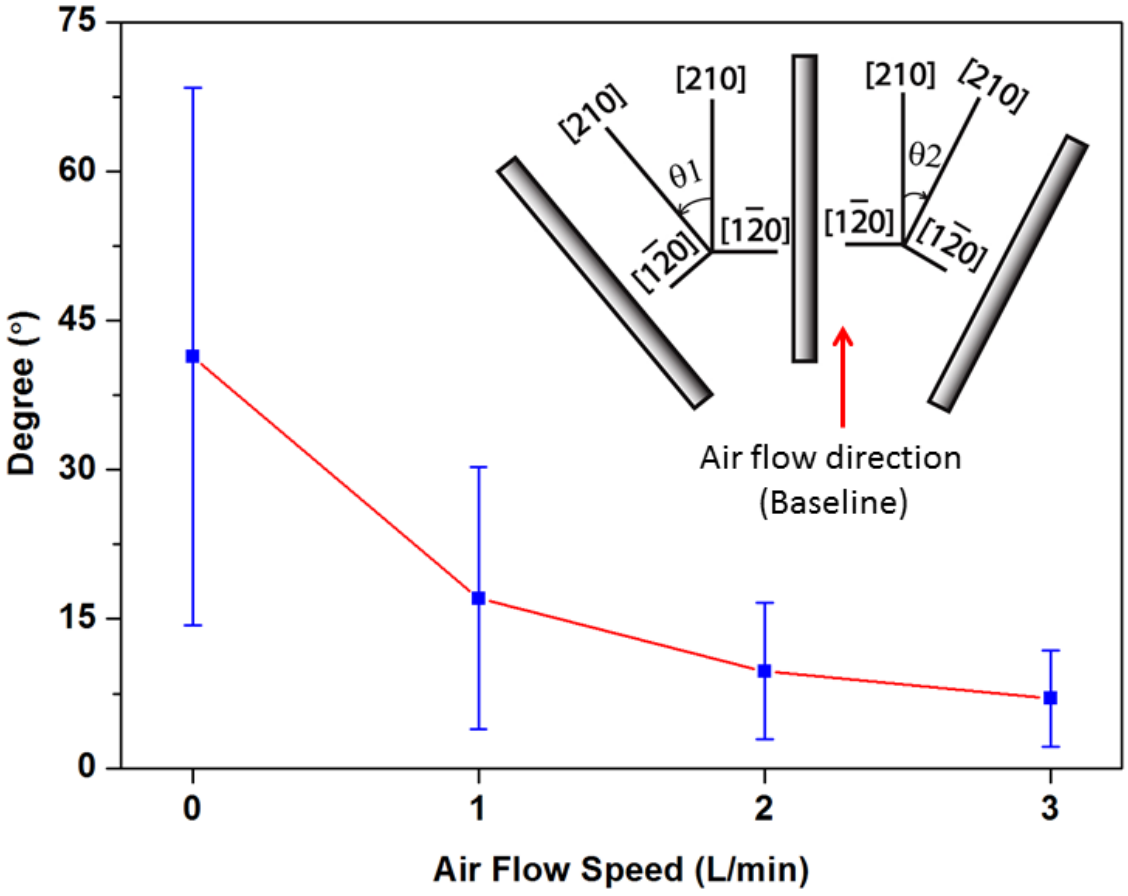

Figure 3.3. Average misorientation angles in air-flow navigated TIPS pentacene films as a function of air flow speeds.

The crystal anisotropy of TIPS pentacene thin film is quantified by the misorientation angles of crystal needles. The misorientation angle (θ) is defined as the angle between crystal long axis and air flow direction (as shown in inset of Figure 3.3). The average θ and standard deviation of θ at different air flow speeds is plotted in Figure 3.3. Without air flow, average misorientation angle is 41.4º±27.1º (based on six measurements) showing significant thin-film anisotropy. When air flow was applied at speeds of 1 L/min, 2 L/min, and 3 L/min, average values of the angle θ drop to 17.1º ±13.2º , 9.7º ±6.9º, and 7.0º ±4.8º, respectively. It is noted that at air flow speeds of both 2 L/min and 3 L/min, average misorientation angles are below 10º, which indicates a 4-6 times reduction in the values of θ as compared to the original drop-cast film. As air flow rate reaches 4 L/min, the long needle-shaped crystals become round-shaped domains as shown in Figure 3.2(d). This is the reason why there are no misorientation angles reported at this flow rate.

As observed in Figure 3.2, air flow not only effectively navigates the TIPS pentacene crystal growth, but also affects areal coverage as well as individual crystal domain width. Grain width, W_G, is defined as domain dimension along the short axis [$1\bar{2}0$] of the crystal needles. The TIPS pentacene grain width and coverage as a function of air flow speed were quantitatively analyzed and shown in Figure 3.4(a) and 3.4(b), respectively. Without air-flow navigation, the TIPS pentacene film demonstrates largely anisotropic crystal morphology with an average width W_G of 91±20 μm. (The average grain width at a specific flow speed is calculated based on ten crystal measurements.) As the air flow speed increases, the grain width decreases due to the fact that air flow facilitates toluene evaporation thereby decreasing the crystallization time.

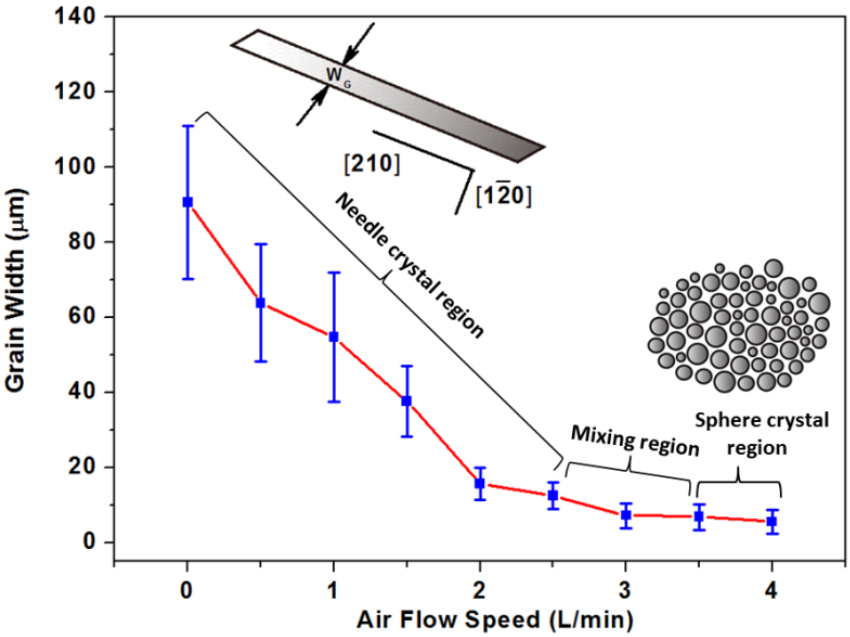

(a)

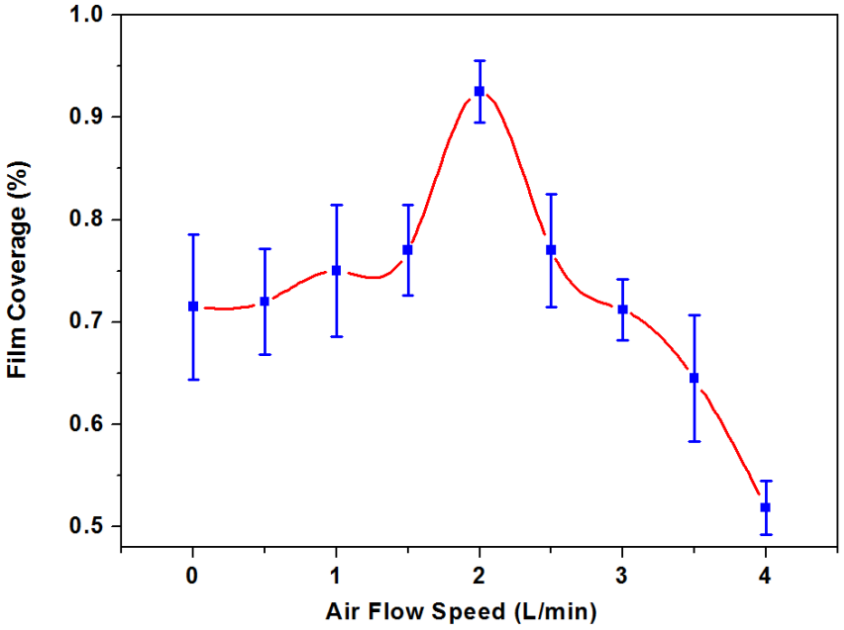

(b)

Figure 3.4. (a) Plot of average grain width versus flow rate. The TIPS pentacene grain width decreases as air flow speed increases due to enhanced solvent evaporation. (b) Plot of film areal coverage versus air flow speed. The highest film coverage occurs at optimal flow rate of 2 L/min, which corresponds to an optimized TIPS pentacene thin-film morphology. The error bars represent the standard deviation of 10 measurements for both (a) and (b).

As shown in Figure 3.4(a), at the flow speed of 2.0 L/min, the average grain width is 17±4 μm. At the maximum flow speed of 4.0 L/min, the average grain width, which refers to diameter of round-shaped crystals in this case, further reduced to 5±3 μm. This demonstrates that the improvement of crystal orientation with AFN is at the expense of the reduced TIPS pentacene crystal grain sizes. Figure 3.4(b) shows variations of film coverage with the air flow speed. Here the film coverage is defined by area ratio of the covered film to the whole area from the optical micrographs. Good film coverage (>90%) was obtained at the air flow speed ranging from 1.5 L/min to 2.5 L/min. When the flow rate is too small (<1.5 L/min), the air flow is not strong enough to be effective in aligning the crystals, and large gaps between crystals exist. On the other hand, at a high flow speed (>2.5 L/min), the air flow leads to rapid evaporation of the toluene, resulting in small crystal sizes and poor film coverage (<60%). At the optimal air flow speed of 2.0 L/min, the thin-film morphology exhibits uniform and long needle-shaped crystals with least gaps in between, reaching the highest film coverage.

To further study the effect of air flow rate, X-ray diffraction experiment was carried out on air-flow navigated TIPS pentacene films. As shown in Figure 3.5(a), the XRD results consistently exhibit strong (*00l)* type reflections, which match results reported previously for TIPS pentacene films.[61] (Note that XRD spectra are vertically shifted in order to clearly demonstrate the differences in intensity.) For a better comparison, the intensity values of (*00l*) type reflections were extracted from Figure 3.5(a) and plotted as a function of air flow speed in Figure 3.5(b).

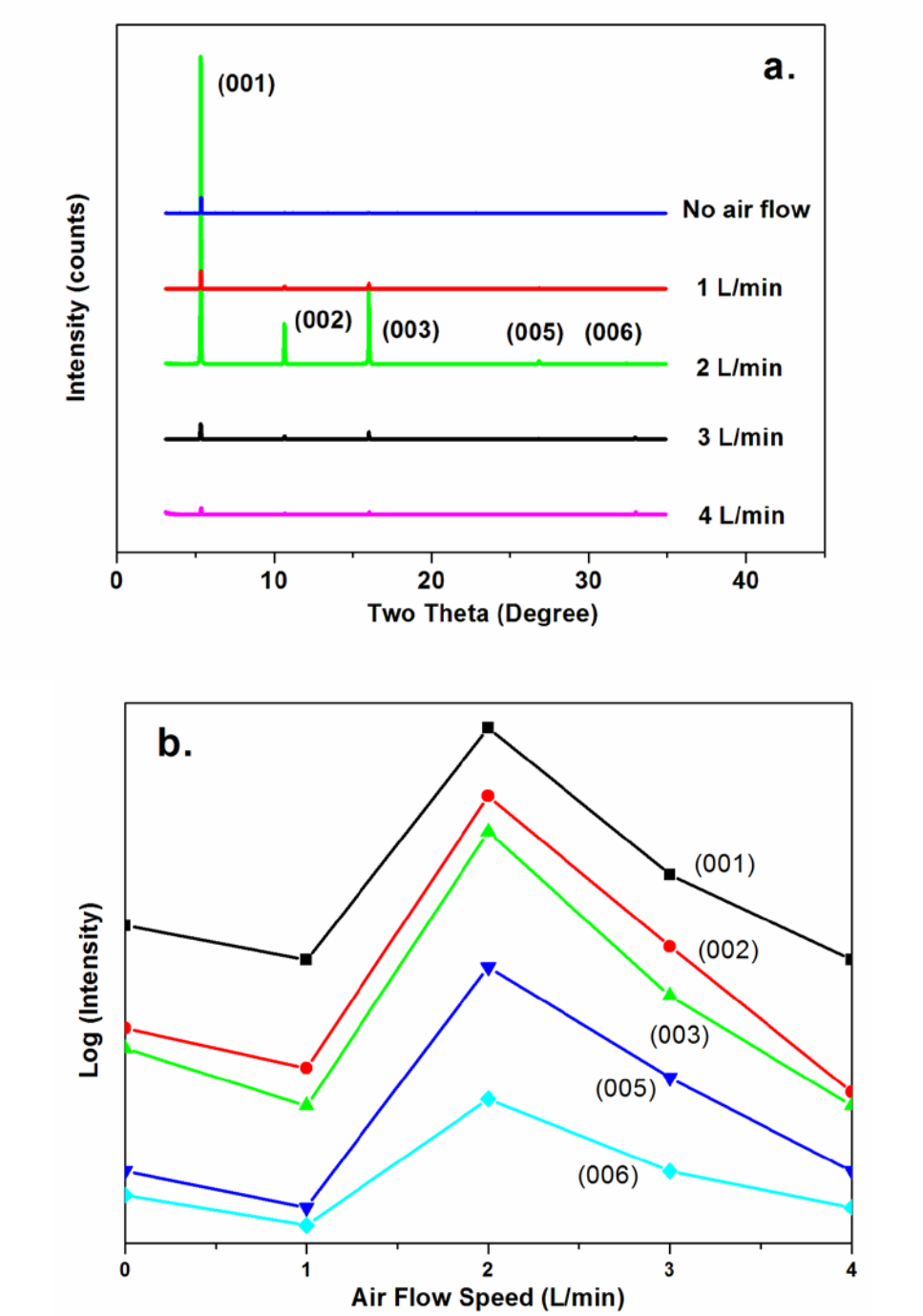

Figure 3.5. (a) X-ray diffraction results for TIPS Pentacene thin films obtained at different flow speeds. (b) Intensities of (*00l*) type reflections versus air flow speed. The high peak intensity at the flow speed of 2 L/min indicates an optimal combination of film coverage, crystallinity, and crystal orientation.

For the cases with air flow speed of 0-1 L/min, the intensities of the reflection peaks are low, which can be reasonably explained by the poor film coverage. When the flow speed increases to 2 L/min, the highest intensities of (*00l*) type reflections are achieved, corresponding to the highest film coverage in these films. As the air flow speed further increases beyond 3 L/min, the peak intensities are significantly reduced, accompanied with their reduced film coverage and crystal shape transition from needles to circular domains.

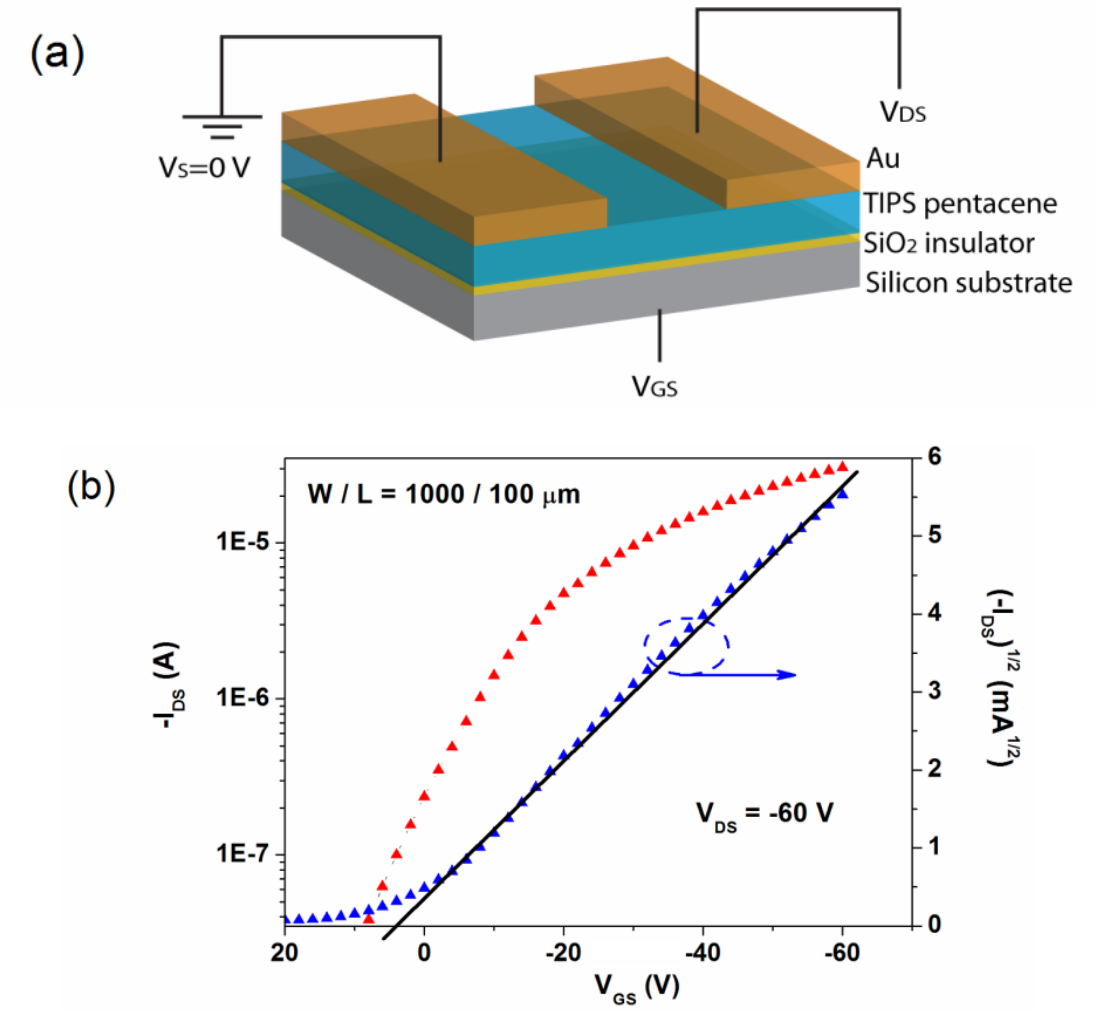

Figure 3.6. (a) Schematic drawing of the bottom-gate, top-contact OTFT structure, (b) a typical transfer characteristic of OTFTs with AFN at an optimal air flow speed of 2 L/min.

After optimization of TIPS pentacene thin film morphology with air-flow navigation, OTFTs were fabricated using TIPS pentacene films obtained at flow speed of 2 L/min. A bottom-gate, top-contact OTFT configuration was used and shown schematically in Figure 3.6 (a). Since TIPS pentacene crystals are well oriented with optimal air-flow navigation, source/drain contacts are placed along the crystal growth direction to yield the best charge transport in the OTFT channel. Figure 3.6 (b) shows a typical transfer characteristic of OTFTs at an air flow speed of 2 L/min. The field-effect mobility in the saturation region and threshold voltage (V_T), determined from the fitted line in the square root plot of transfer characteristic, are 0.12 cm^2/Vs and 4V, respectively. The current on/off ratio obtained from the lograthmic plot is above $5x10^3$. Note that hole mobility was extracted based on overall channel width rather than an individual needle crystal and there was no surface treatment of the oxide substrates before TIPS pentacene growth.

Finally, the performance consistency of TIPS pentacene based OTFTs in term of mobility variations was studied. Figure 3.7(a) shows that OTFTs with AFN exhibit much less variation in the hole mobility than those without AFN. Field-effect mobilities of OTFTs without AFN vary by three orders of magnitude (ranging from 8.4×10^{-2} to $9.8\times10^{-5}cm^2$/Vs), while those with AFN at the optimum flow rate of 2 L/min stay consistently between 1.2×10^{-1} and 9.5×10^{-2} cm^2/Vs, indicating a much enhanced consistency of OTFT performance. The improved OTFT performance consistency is considered to result from both improved crystal orientation and enhanced thin film coverage.

In addition, the average mobility and standard deviation are plotted in Figure 3.7(b). Without AFN the average mobilities are 0.03±0.03 cm^2/Vs (the standard deviation was calculated from 6 different devices.) The average mobilities are 0.11±0.01cm^2/Vs at the optimal air flow rate of 2 L/min, which is nearly a four-fold enhancement in average hole mobilities.

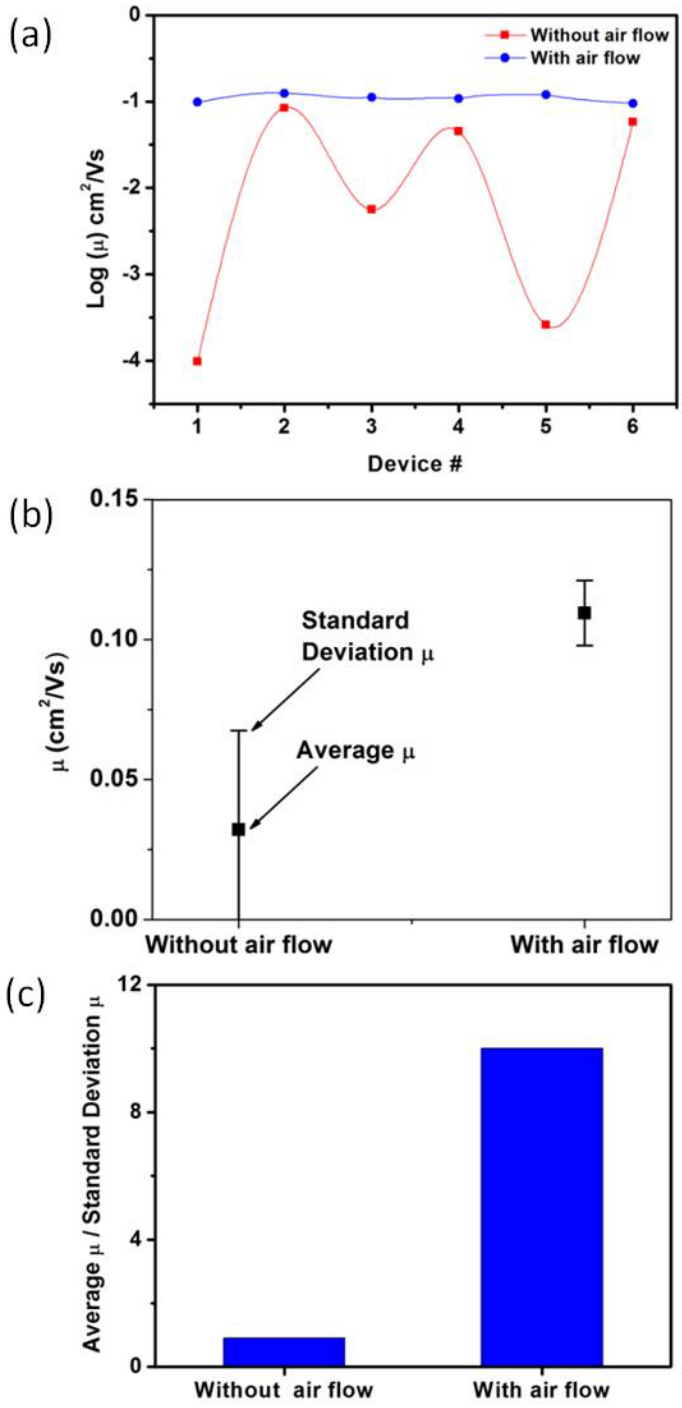

Figure 3.7. (a) Comparison of OTFT performance between devices without and with air flow at a flow speed of 2 L/min. (b) The average OTFT hole mobility with air flow demonstrates nearly four-fold enhancement as compared to the one without air flow. (c) The ratio of average mobility to standard deviation of field-effect mobilities (μ_{Ave}/μ_{Stdev}) for devices without and with air flow at a flow speed of 2 L/min.

Figure 3.7(c) shows the ratio of average mobility (μ_{Ave}) to the standard deviation of the field-effect mobilities (μ_{Stdev}), which serves as an indicator of OTFT performance consistency. OTFTs without AFN show μ_{Ave}/μ_{Stdev} of 0.9 while those with an optimized AFN show μ_{Ave}/μ_{Stdev} of 10, which exhibits an eleven-fold increase in performance consistency.

3.4. Conclusions

In summary, air flow is able to effectively guide TIPS pentacene growth and simultaneously enhance overall areal coverage on a substrate, which was clearly demonstrated by optical microscopy and X-ray diffraction results. With air-flow navigation, the factors that normally lead to “coffee rings” are minimized. It is demonstrated that the air-flow navigated TIPS pentacene film morphology strongly correlates with the air flow speed applied. A balance of crystal orientation, crystallinity, and film connectivity is achieved at an optimal flow speed of 2.0 L/min. OTFTs based on TIPS pentacene with a proper air-flow navigation show four times increase in average mobility and an eleven-fold enhancement of performance consistency.

CHAPTER 4

SWITCHING PHASE SEPARATION MODE BY VARYING THE HYDROPHOBICITY OF POLYMER ADDITIVES IN SOLUTION-PROCESSED SEMICONDUCTING SMALL-MOLECULE/POLYMER BLENDS

4.1 Introduction

Solution-processed organic thin-film transistors (OTFTs) are promising for the next-generation large-area electronics on flexible substrates.[55,58,59] Semiconducting small molecule/polymer blends, as newly-developed, promising active layer systems in OTFTs, take advantages of the high charge-carrier mobility of the semiconducting small molecules, the excellent film formation capability and mechanical properties from polymers, as well as the intriguing phase separation behaviors between the small molecules and polymers.[54,85] Although phase separation behaviors were shown to strongly correlate with charge transport in these systems, no simple and straightforward method to switch between lateral and vertical phase separation modes has been previously reported. Therefore, the exact effect of phase separation modes on crystal alignment and charge transport remains largely underexplored. For example, Harmilton *et al.* blended 6,13-bis(triisopropylsilylethynyl) pentacene (TIPSE pentacene) or 2,8-difluoro-5, 11-bis(triethylsilylethynl)anthradithiophene (diF-TES ADT) with inert and semiconducting polymers, which resulted in improved performance uniformity and simultaneously maintained the peak device performance.[67] Cho and coworkers reported that the vertical phase separation in TES ADT/ poly(methylmethacrylate) (PMMA) blends has the

potential of an all-solution route to fabricate flexible organic transistors.[86,87] Most recently, Yoon and coworkers, explored the phase separation of diF-TES ADT blends with polymers including poly(*alpha*-methylstyrene), PMMA, and syndiotactic polystyrene.[88] Conventional wisdom is that the crystallization of small molecule organic semiconductor dictates the phase separation and self-assembly of polymer-small molecule organic semiconductor blends. However, the effects of specific intermolecular interactions on the phase separation and charge transport of semiconducting small molecule-polymer blends are not well revealed yet.

In this work, the importance of hydrophobic forces was demonstrated in phase separation mode, crystal orientation, as well as charge transport of the small molecule organic semiconductor-polymer blends. It was shown that by simply varying the length of the hydrophobic side groups in a series of polyacrylate additives, the switching between lateral and vertical phase separation can be easily achieved in solution-crystallized semiconducting small molecule/polymer blend films. Herein, TIPS pentacene [89-91] was chosen as a model small molecule to blend with poly(ethyl acrylate) (PEA), poly(butylacrylate) (PBA), and poly(2-ethylhexyl acrylate) (P2EHA), respectively, to demonstrate different phase separation modes. The results show that the vertical phase separation leads to well aligned 2-D crystal growth and a large improvement of average mobility and performance consistency.

4.2 Experimental

4.2.1 Materials

TIPS pentacene and acrylate polymers including PBA, PEA, and P2EHA, were purchased from Sigma Aldrich and used without further purification. The three polymers have weight-average molecular weight M_W of 120 k, 100 k, and 110 k, respectively, with a similar

polydispersity index of ~3. TIPS pentacene powder and acrylate polymers were dissolved in toluene with a concentration of 5 mg/mL before being mixed at desired weight ratios. Subsequently, TIPS pentacene/acrylate polymer thin films were formed by drop casting the mixture solution in a solvent rich environment.

4.2.2 Device Fabrication

Bottom-gate, bottom-contact OTFT configuration was utilized to test charge transport in the TIPS pentacene/polyacrylate blends. The bottom-gate, bottom-contact OTFT substrates were fabricated by using standard photolithography, thermal evaporation, followed by lift-off, as shown in Figure 4.1.[44] Silicon wafers with a silicon dioxide layer with the thickness of 100nm were cleaned by using Acetone, IPA and DI water to remove the organic and inorganic contaminations. Then, the silicon wafer was heated on a hot oven at 120°C for 60 seconds to drive off moistures. A thin layer of hexamethyldisilazane (HMDS) was formed on the substrate by spin coating, which then chemically reacted with the silicon dioxide layer to form a highly water repellent tri-methylated silicon-dioxide layer and helped facilitate the adhesion of photoresist. Then, photoresist was dispensed onto the substrate and forms a thin film while the substrate was spun at 300 rpm for 5 seconds followed by 1000 rpm for 60 seconds. In order to drive off the excess photoresist, the wafer was baked on a hot oven at 100°C for 60 seconds. Subsequently, standard photolithography was carried out by using Quintel 7000 Contact/Proximity Photolithography Aligner, in which broad band UV was used to perform microscale lithographic exposures, which caused a chemical reaction of the exposed photoresist and allowed it to be removed by developer. Then the exposed substrate was baked on a hot oven at 80°C for 30 seconds before being developed. After development, the substrate was etched by using plasma etching. Next, a gold layer with a thickness of 100 nm was deposited to form the

source and drain electrodes via thermal evaporation. Finally, the photoresist was removed by a process called “lift-off”, in which the substrate was ultrasonicated in acetone and the photoresist was washed out along with gold covering it.

Before drop casting the TIPS pentacene/polyacrylate blends in toluene to form active layer of OTFTs, both HMDS and PFBT treatments are carried out. HMDS vapor deposition is utilized to convert a hydrophilic SiO_2 surface into a hydrophobic surface. As shown in Figure 4.2, HMDS is heated out at 140°C, which is above its boiling point, and HMDS molecules react with the hydrophilic –OH groups on the SiO_2 surface, which then forms water and evaporates. As the hydrophilic –OH groups are removed, SiO_2 surface now becomes hydrophobic. The whole substrate is rinsed by using IPA. Besides, HMDS vapor deposition can form self-assembled monolayers (SAMs) at the interface, which alters the interface surface energy, molecular ordering and device performance of OTFTs. As a result, the interactions between semiconductor layer and substrate layer at the interface will be weakened, which makes it much easier for the first few semiconductor layers to grow.

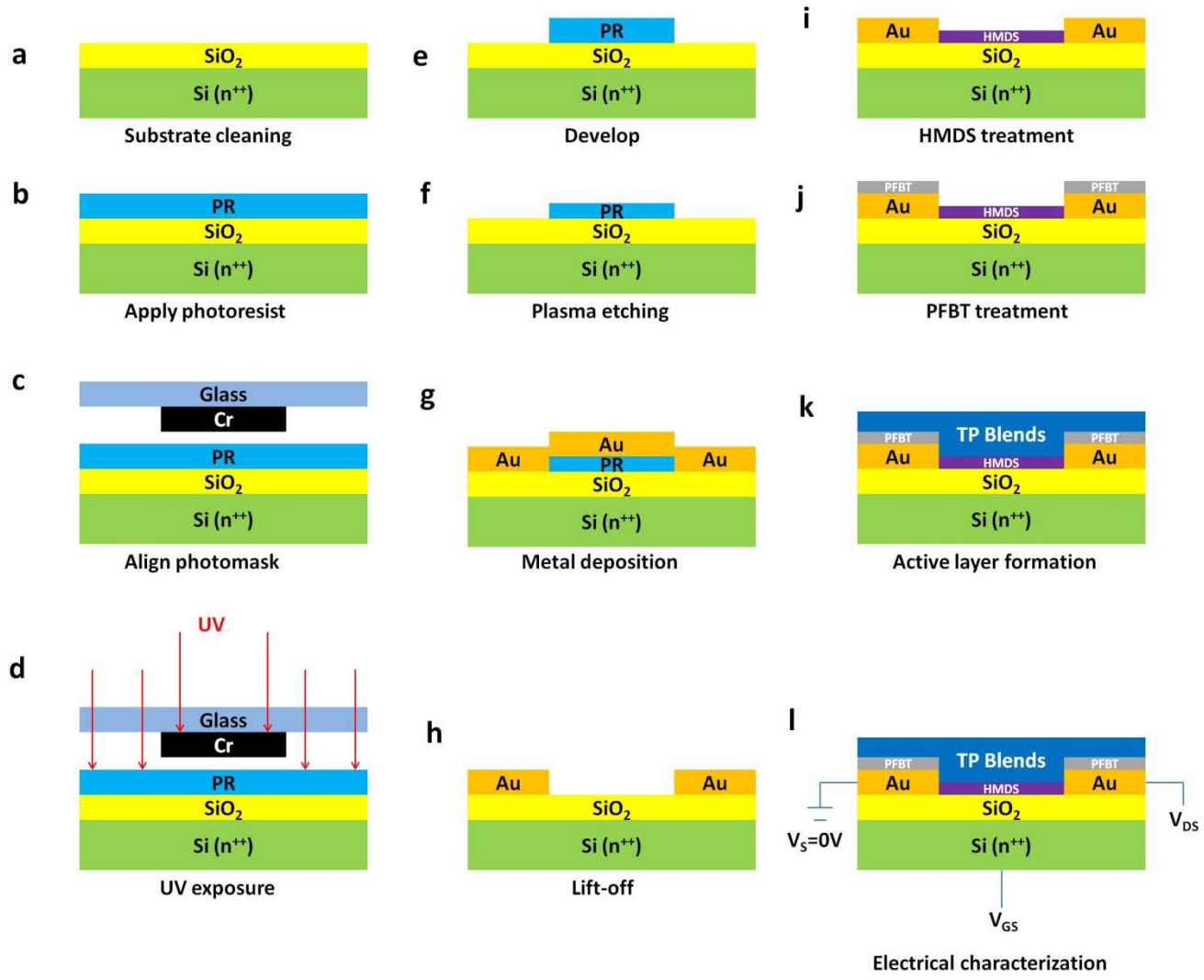

Figure 4.1. Bottom-gate, bottom-contact OTFT fabrication procedure (a) substrate cleaning by using Acetone, IPA and DI water, (b) apply photoresist onto substrate by spin coating, (c) align photomask, (d) UV exposure: patterns uncovered by Cr layer of the photomask are exposed, (e) develop to remove exposed regions of photoresist, (f) plasma etching to remove the residue layer of photoresist, (g) metal deposition of gold to form source and drain contact electrodes, (h) lift-off, (i) HMDS vapor deposition onto silicon dioxide layer, (j) PFBT treatment of source and drain contact electrodes, (k) active layer formation by drop casting under controlled solvent evaporation, and (l) electrical characterization to test charge transport.

After HMDS vapor deposition, the substrate was immersed in the pentafluorobenzene thiol (PFBT)/toluene solution for 2 hours and then rinsed by toluene. PFBT treatment aims to tune the surface energy of the gold contact electrodes and therefore enhance the device performances of OTFTs. After HMDS vapor deposition and PFBT surface treatment, active layer will be formed by drop casting TIPS pentacene, TIPS pentacene/PEA, TIPS pentacene/PBA, TIPS pentacene/P2EHA blend in toluene at 5 mg/mL.

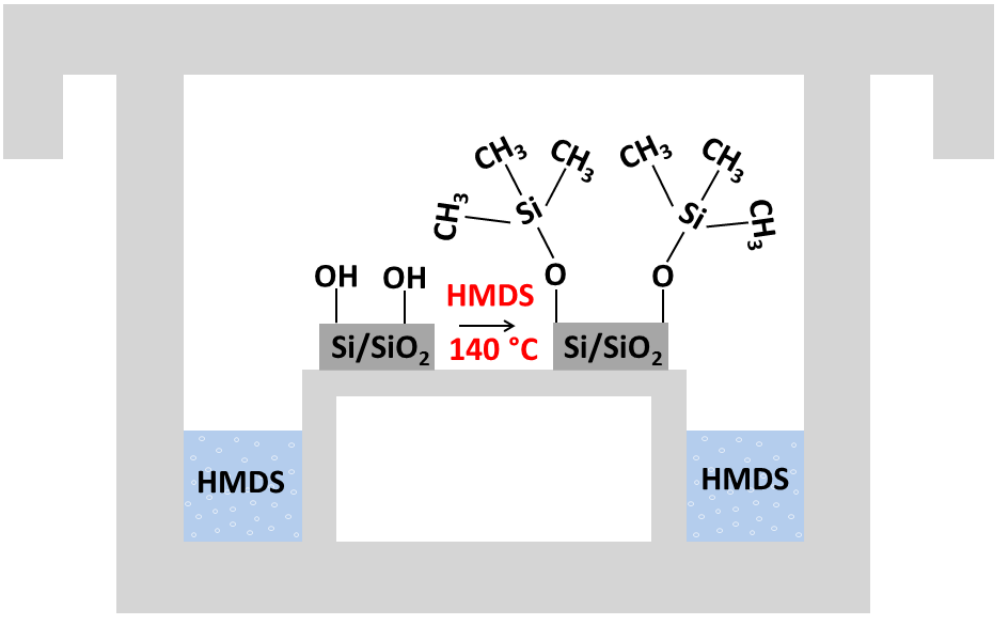

Figure 4.2. HMDS vapor deposition for surface treatment. HMDS is heated above its boiling point, and its vapor deposits onto the SiO_2 surface. HMDS vapor reacts with and then removes –OH groups on the SiO_2 surface, and thus turns a hydrophilic SiO_2 surface to a hydrophobic SiO_2 surface.

4.2.3 Characterization

Electrical characterization of OTFTs was carried out in ambient environment at room temperature using an Agilent B1500A semiconductor parameter analyzer. Field-effect hole mobility in the saturation regime (V_{DS}=-20 V) was extracted from the slope of the transfer

characteristic $(I_{DS})^{1/2}$-V_{GS}, and all devices were measured five times to ensure the consistency of the extracted field-effect hole mobility. Contact angle measurements were performed with a Kruss DSA30 system using 3μL deionized water and sessile fitting for each measurement. Thin film crystallinity and coverage were characterized by using Philips X'Pert X-ray Diffractometer. Energy filtered TEM was performed with a Zeiss Libra 120 at 120kV on drop cast films on amorphous carbon coated copper grids at 120kV. Samples on silicon substrates for cross-section SEM were immersed in liquid nitrogen, allowed to equilibrate, and cleaved before performing cross-section SEM experiments at 1.7kV with a charge compensation mode in a Zeiss Merlin. In the charge compensation mode of SEM, a dry nitrogen gas is brought nearby the sample area under examination to minimize charge accumulation on the poorly conductive sample which had no conductive coating.

4.3 Results and Discussion

Figure 4.3 (a) shows the molecule structures of TIPS pentacene and the three polyacrylates: PEA, PBA, and P2EHA. These three polyacrylates have similar weight-average molecular weight and polydispersity index (M_W of 100-120k and PDI of 3), while their hydrophobic side groups differ in the alkyl length: two carbon atoms for PEA, four for PBA, and eight for P2EHA. A simulated molecular view of TIPS pentacene molecules in its needle-shaped crystal is presented in Figure 4.3 (b).[46,76,92] The red arrow indicates the long axis of the needle shaped TIPS pentacene crystals, and the light blue rods stand for the acene units of TIPS pentacene.

Thin films of pristine TIPS pentacene and TIPS pentacene/polymer blends were slowly crystallized in a solvent-rich environment with an optimized weight ratio of 1:1 from dilute toluene solutions (5 mg total solids per ml). The optical micrographs in Figure 4.3 (c-f) show that

the pure TIPS pentacene thin film has large crystals with random orientations and poor substrate coverage, while the addition of polyacrylate polymers improves both film coverage and TIPS pentacene crystal alignment at different extents. TIPS pentacene/P2EHA blend film exhibits the most uniform crystal orientation and highest film coverage, while TIPS pentacene/PEA demonstrates the least crystal alignment and coverage enhancement under the same blending and solution crystallization conditions. Therefore, it can be inferred that the effect of polyacrylate polymer additives on the TIPS pentacene thin film morphology can be correlated to the length of the polymer hydrophobicity side group.

To further demonstrate the effect of P2EHA additive on the thin film structures of TIPS pentacene/P2EHA films, TIPS pentacene was blended with varied P2EHA content of 0%, 5%, 30%, 50%, and 67%. The resultant morphologies are shown in the optical micrographs of Figure 4.3. TIPS pentacene/P2EHA film with 0-30% P2EHA content exhibits poor coverage and random crystal orientation, as shown in Figure 4.4 (a)-(c). When P2EHA content increases to 50% (TIPS pentacene:P2EHA = 1:1 weight ratio), TIPS pentacene/P2EHA film shows a remarkable improvement of crystal orientation and film coverage, as shown in Figure 4.4 (d). However, when P2EHA content further increases to 67%, TIPS pentacene/P2EHA film undergoes transition towards a structure with more polymer-like domains shown in Figure 4.4 (e). Finally, when P2EHA content increases to 100%, the resultant film exhibits the typical morphology of polymers with great uniformity, as shown in Figure 4.4(f).

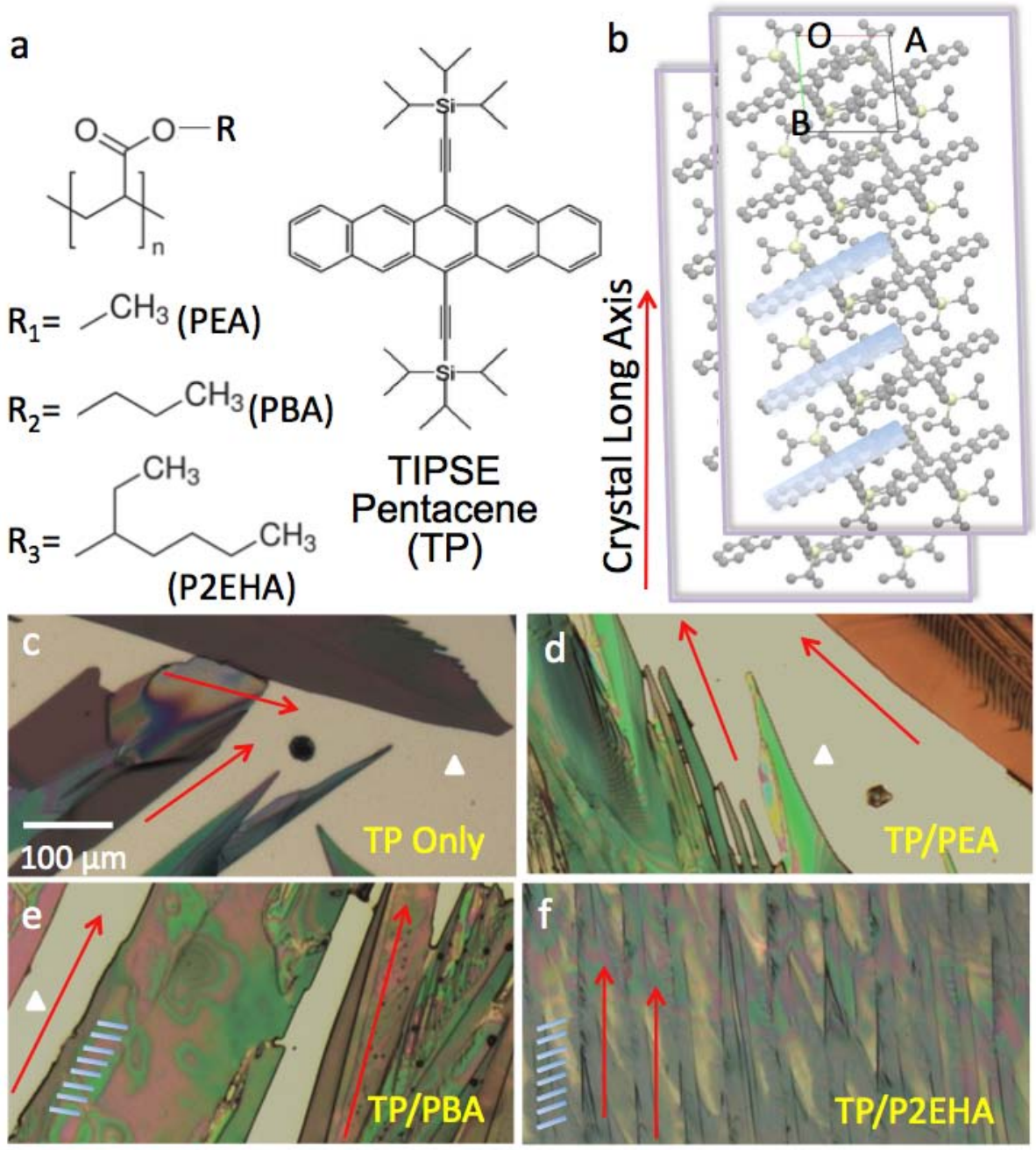

Figure 4.3. (a) Molecule structures of TIPS pentacene, PEA, PBA, and P2EHA. (b) A simulated molecular view of needle-shaped TIPS pentacene crystals on substrate. (c-f) Optical micrographs of pure TIPS pentacene film and the three TIPS pentacene/polyacrylate blend films (weight ratio of 1:1). The red arrows in (b-f) indicate the long axis of the needle shaped TIPS pentacene crystals, and the tilted light blue rods represent the directions of TIPS pentacene backbones. The triangles mark the uncovered substrate areas. All optical images share the same scale bar of 100 micron in (c).

As observed in the optical micrographs shown in Figure 4.3 and Figure 4.4, all three polymer additives affect TIPS pentacene grain width and film coverage. The change of grain width and film coverage was quantitatively analyzed and plotted as a function of active layer type, as shown in Figure 4.5 (a) and 4.5 (b), respectively. Grain width, denoted as "W_G", is defined as the crystal domain dimension along the short axis [$1\bar{2}0$] of the TIPS pentacene needles. Without the addition of polymer additives, pure TIPS pentacene film exhibits crystals with random orientation and large variations in grain width. The average grain width W_G is around 90.6±20.4 μm (based on ten crystal measurements). With the addition of polymer additives, the average TIPS pentacene grain width W_G was reduced to 82.4±17.7 μm for TIPS pentacene/PEA, to 75.7±8.1 μm for TIPS pentacene/PBA, and further to 69.2±7.4 μm for TIPS pentacene/P2EHA film, respectively, as shown in Figure 4.5 (a).

In addition, the effect of polymer additives on film coverage is shown in Figure 4.5 (b). Film coverage is defined as the ratio of the area covered by film to the whole substrate area. Pure TIPS pentacene films exhibit poor film coverage ~51%, which is due to large gaps between TIPS pentacene crystals. In contrast, TIPS pentacene/PEA, TIPS pentacene/PBA, and TIPS pentacene/P2EHA films demonstrate film have surface coverage ~53%, ~78%, and ~95%, respectively, which suggests that all three polymer additives increase film coverage at the expense of grain width. The device performance and performance consistency of the TIPS pentacene/polyacrylate based OTFTs is largely dependent upon the film coverage and grain width

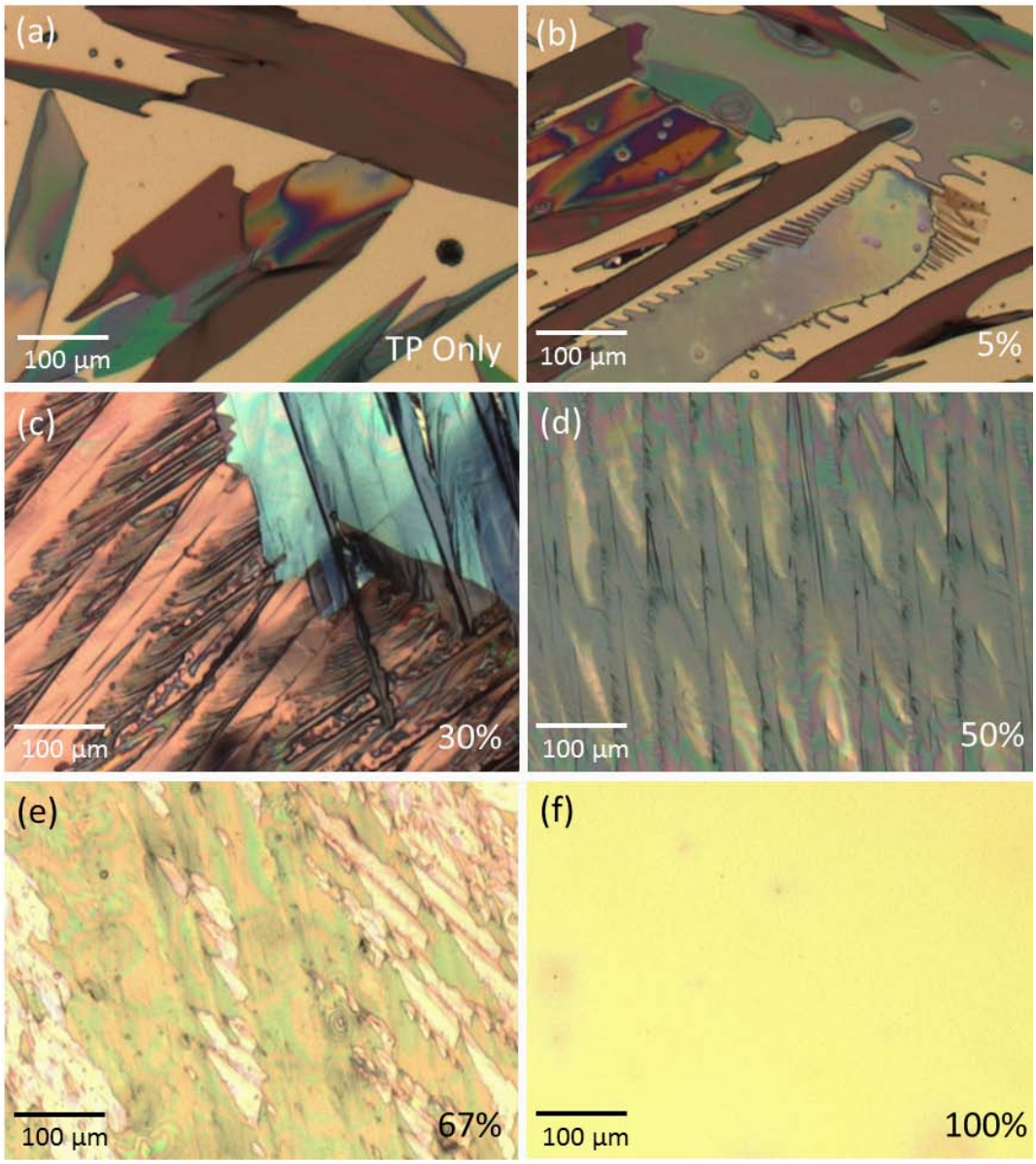

Figure 4.4. Optical micrographs of (a) pure TIPS pentacene film, and TIPS pentacene/P2EHA blend films with varied P2EHA content at (b) 5%, (c) 30%, (d) 50%, (e) 67, and (f) pure P2EHA film. At a lower content of loading (0-30%), the TIPS pentacene/P2EHA film still exhibits crystal misorientation and poor film coverage. When the content of P2EHA reaches 50% (TIPS pentacene:P2EHA = 1:1 weight ratio), TIPS pentacene/P2EHA film shows a remarkable improvement of crystal orientation and film coverage. However, when the P2EHA content further increases above 50%, the TIPS pentacene/P2EHA film shows a polymer-like morphology with reduced crystallinity.

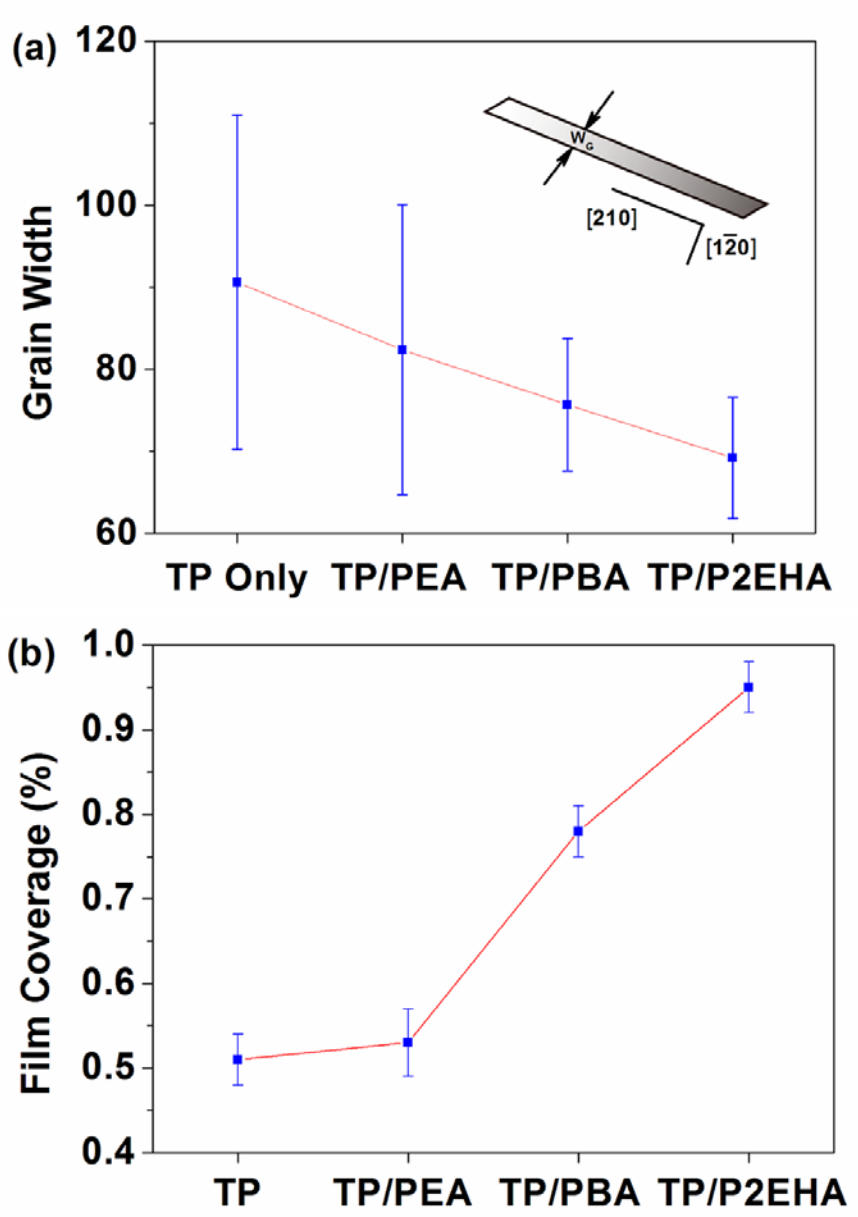

Figure 4.5. Plot of (a) average TIPS pentacene grain width and (b) TIPS pentacene crystal coverage as a function of active layer type. TIPS pentacene/PEA, TIPS pentacene/PBA, and TIPS pentacene/P2EHA film at 1:1 weight ratio. The error bars represent the standard deviation of 10 measurements for calculating grain width and film coverage. As the hydrophobicity side group of the polyacrylate polymers increases, the film coverage increases at the expense of grain width.

In particular, TIPS pentacene/P2EHA film has the smallest average grain width and largest film coverage among the three polymer additives, which is expected to contribute to a significant improvement of the average mobilities as well as enhancement of performance consistency of TIPS pentacene/P2EHA OTFTs, when compared to the pure TIPS pentacene OTFTs. In contrast, TIPS pentacene/PEA film has the largest average grain width and smallest film coverage among the three polymer additives, so the TIPS pentacene/PEA OTFTs are expected to demonstrate only limited improvement in average mobilities as well performance consistency when compared to pure TIPS pentacene OTFTs.

To examine the influence of crystal alignment on charge transport in the TIPS pentacene/polyacrylate films, bottom-gate, bottom-contact OTFTs were fabricated. Gold electrodes were patterned on heavily doped *n*-type silicon substrate by using standard photolithography followed by metal deposition and lift-off. The silicon substrate with a 100 nm thermal oxide was surface treated with hexamethyldisilazane (HMDS) followed by gold contacts treatment using pentafluorobenzenethiol (PFBT).[78,93] HMDS self-assembled monolayer was formed on the gate dielectric by vapor deposition at 140 °C, and rinsing by isopropanol. PFBT treatment on the source/drain contacts was carried out by immersing the substrates in a 10mM PFBT/toluene solution for 2 hours, and rinsing them with toluene.

Electrical characterization of OTFTs was carried out in ambient environment at room temperature using an Agilent B1500A semiconductor parameter analyzer. Typical output and transfer characteristics of TIPS pentacene/P2EHA based OTFTs are shown in Figure 4.6 (a) and (b). The extracted field-effect mobility and threshold voltage (V_T) are 0.33 $cm^2V^{-1}s^{-1}$ and 6V, respectively, and the on-/off- current ratio obtained from the logarithmic plot of transfer characteristics is 9.6×10^3.

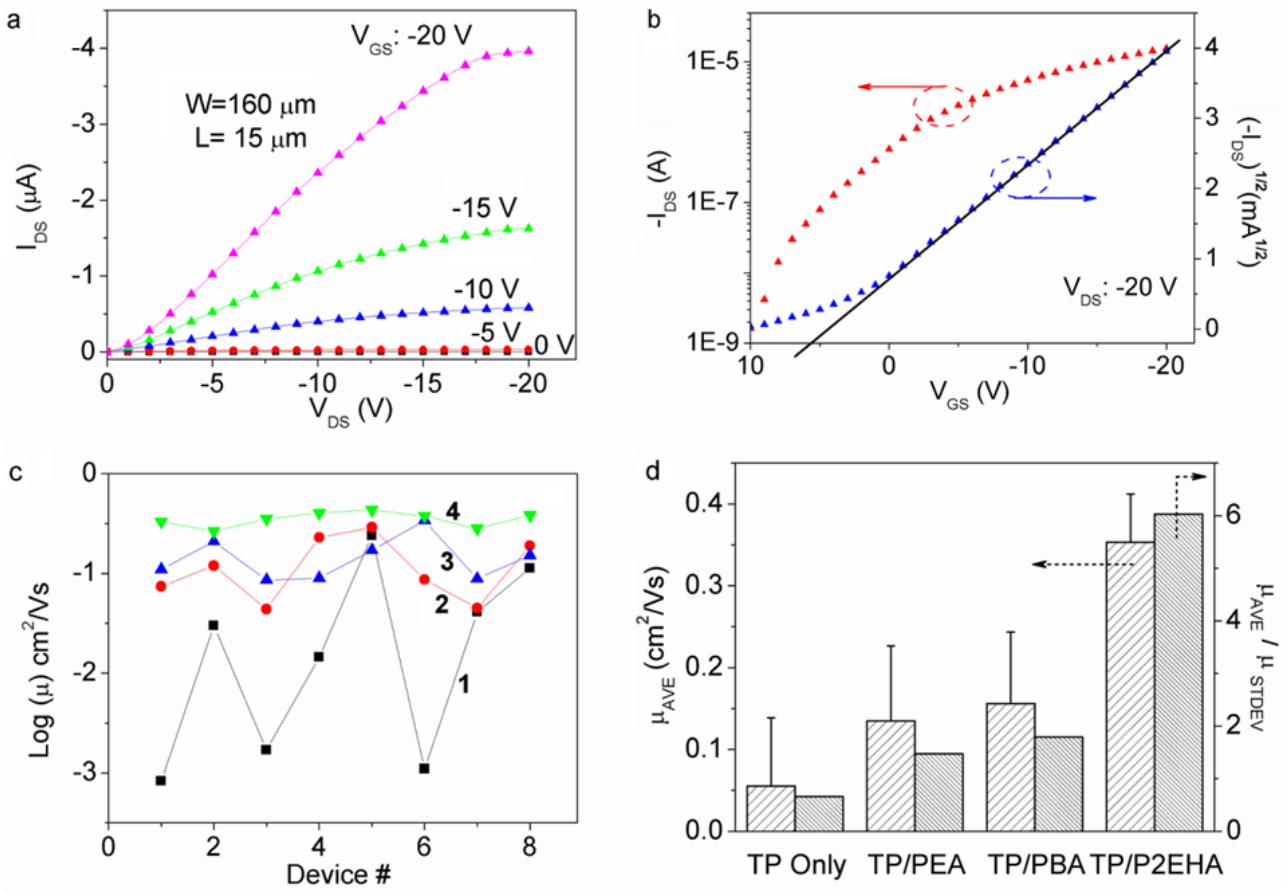

Figure 4.6. Typical (a) output and (b) transfer characteristics of TIPS pentacene/P2EHA blend based OTFTs. From the transfer characteristics, the extracted field-effect mobility and threshold voltage (V_T) are 0.33 $cm^2V^{-1}s^{-1}$ and 6V, respectively, and the on-/off- current ratio obtained from the logarithmic plot of transfer characteristics is 9.6×10^3. Curves 1- 4 in (c) represent devices based on pure TIPS pentacene, TIPS pentacene/PEA, TIPS pentacene/PBA, and TIPS pentacene/P2EHA, respectively. (d) Comparison of average hole mobility and performance consistency (represented by the value of μ_{Ave}/μ_{Stdev}). In general, the addition of polyacrylate polymers enhances both average mobilities and performance consistency of the OTFTs.

Figure 4.2 (c) clearly shows that the addition of acrylate polymers in general reduces mobility variation. The field-effect mobilities of pure TIPS pentacene based OTFTs vary by four orders of magnitude (2.4×10^{-1}~8.3×10^{-4} cm^2 $V^{-1}s^{-1}$), while TIPS pentacene/PEA, TIPS pentacene/PBA, and TIPS pentacene/P2EHA based OTFTs demonstrate hole mobilities of

0.04~0.29 $cm^2 V^{-1}s^{-1}$, 0.09~0.34 $cm^2V^{-1}s^{-1}$, and 0.26~0.43 $cm^2 V^{-1}s^{-1}$, respectively. Figure 4.6 (d) provides a comparison of average mobility (with standard deviation) before and after the addition of acrylate polymers. Average mobility and the associated standard deviation are based on eight measurements for each type of active layer. Pure TIPS pentacene based devices show an average hole mobility of 0.06 $cm^2 V^{-1}s^{-1}$, and the addition of PEA, PBA, and P2EHA enhances the average hole mobility to 0.14, 0.16, and 0.35 $cm^2 V^{-1}s^{-1}$, respectively. Notably, the addition of P2EHA into TIPS pentacene leads to a six-fold enhancement in average hole mobility as compared to pure TIPS pentacene devices. Furthermore, the ratio of average mobility (μ_{Ave}) to the standard deviation of measured mobility (μ_{Stdev}) is used to represent the performance consistency of OTFTs.[10] The devices based on TIPS pentacene/PEA and TIPS pentacene/PBA blends have μ_{Ave}/μ_{Stdev} values increased by 2- and 3-fold, respectively, while TIPS pentacene/P2EHA based devices demonstrated a nine-fold enhancement in performance consistency (or μ_{Ave}/μ_{Stdev}). The results obtained above are consistent with the expectation of enhanced average mobilities and performance consistency based on the average grain width and film coverage plot, as shown in Figure 4.5.

The crystallization of pure TIPS pentacene, TIPS pentacene/PEA, TIPS pentacene/PBA, and TIPS pentacene/P2EHA film was studied by using X-ray diffraction. The peak intensities of different blend films were plotted with a vertical shift for a better comparison, as shown in Figure 4.7 (a). The XRD spectra of TIPS pentacene, TIPS pentacene/PEA, TIPS pentacene/PBA, and TIPS pentacene/P2EHA films all exhibit dominating (*00l)* type reflections, indicating the same edge-on orientation and unit cell structure for all of these films. To better demonstrate the enhancement of peak intensities by the addition of acrylate polymer, each peak intensity in Figure 4.7 (a) is plotted as a function of active layer type, as shown in Figure 4.7 (b). TIPS

pentacene/PEA, TIPS pentacene/PBA, and TIPS pentacene/P2EHA films all demonstrate higher peak intensities for all (*00l)* type reflections than pure TIPS pentacene film, and particularly, TIPS pentacene/P2EHA film shows the highest peak among all the blend films. A reasonable explanation for such results is that the addition of acrylate polymers not only improves crystal orientation but also enhances film coverage, which consequently leads to enhanced peak intensities of the XRD spectra.

In order to understand the reason of the significantly enhanced crystal alignment and OTFT performance in TIPS pentacene/polyacrylate (especially TIPS pentacene/P2EHA) polymer blend films, energy filtered transmission electron microscopy (EF-TEM) was carried out. A Zeiss Libra 120 at accelerating voltage of 120kV was used to image the solution-crystallized films in planar view. Each TIPS pentacene/polymer blend was imaged at 0±5eV and 20±5eV, respectively, as shown in Figure 4.8. The 0 eV (elastic) image reveals features based on electron density contrast, including mass-thickness (composition) contrast and topographical thickness variation. Higher electron density results in darker regions in 0 eV TEM images because of less transmitted electron signals. The 20eV image specifically highlights the low-eV plasmon contribution from the aromatic organic functional group, in which the brighter areas refer to higher *p*-type TIPS pentacene semiconductor content.[94,95] Furthermore, thickness maps were generated by taking the intensity ratio of an elastic and unfiltered image, giving a thickness variation based on pixel-by-pixel values of t/λ, where t is the thickness in nm and λ is the mean free pathway of the electron (an unknown constant in this case). The brighter region in a thickness map corresponds to a higher value of t/λ.

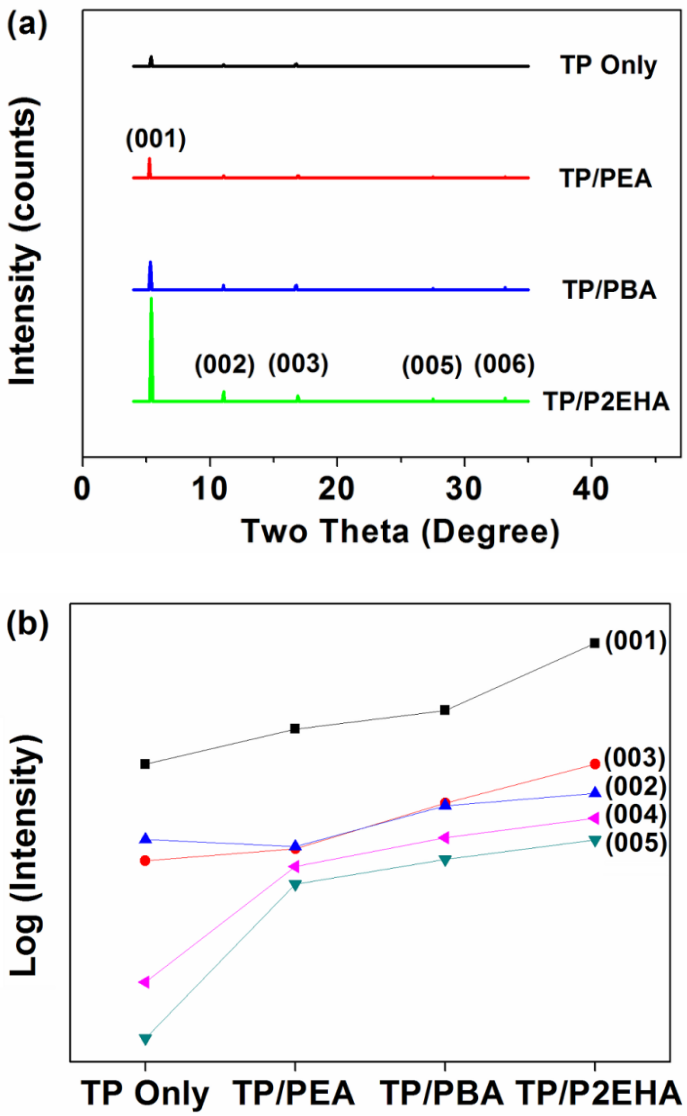

Figure 4.7 (a) X-ray diffraction results for TIPS pentacene only, TIPS pentacene/PEA, TIPS pentacene/PBA, and TIPS pentacene/P2EHA blend films. (b) Peak intensities of (*00l)* type reflections for TIPS pentacene only, TIPS pentacene/PEA, TIPS pentacene/PBA, and TIPS pentacene/P2EHA blend films. TIPS pentacene/P2EHA film demonstrates the highest peak intensity, which indicates an enhancement of TIPS pentacene crystal coverage and crystal orientation due to vertical phase separation.

In Figure 4.8, the TIPS pentacene-rich regions are generally darker in elastic (0 eV) image because of the crystallinity of TIPS pentacene and the correspondingly higher electron density, while they are brighter in the 20eV image because of the low-eV plasmon contribution

from TIPS pentacene. The 20eV image and thickness map nicely decouples the different features in the elastic image, which are evidently caused by both composition contrast and thickness variation.

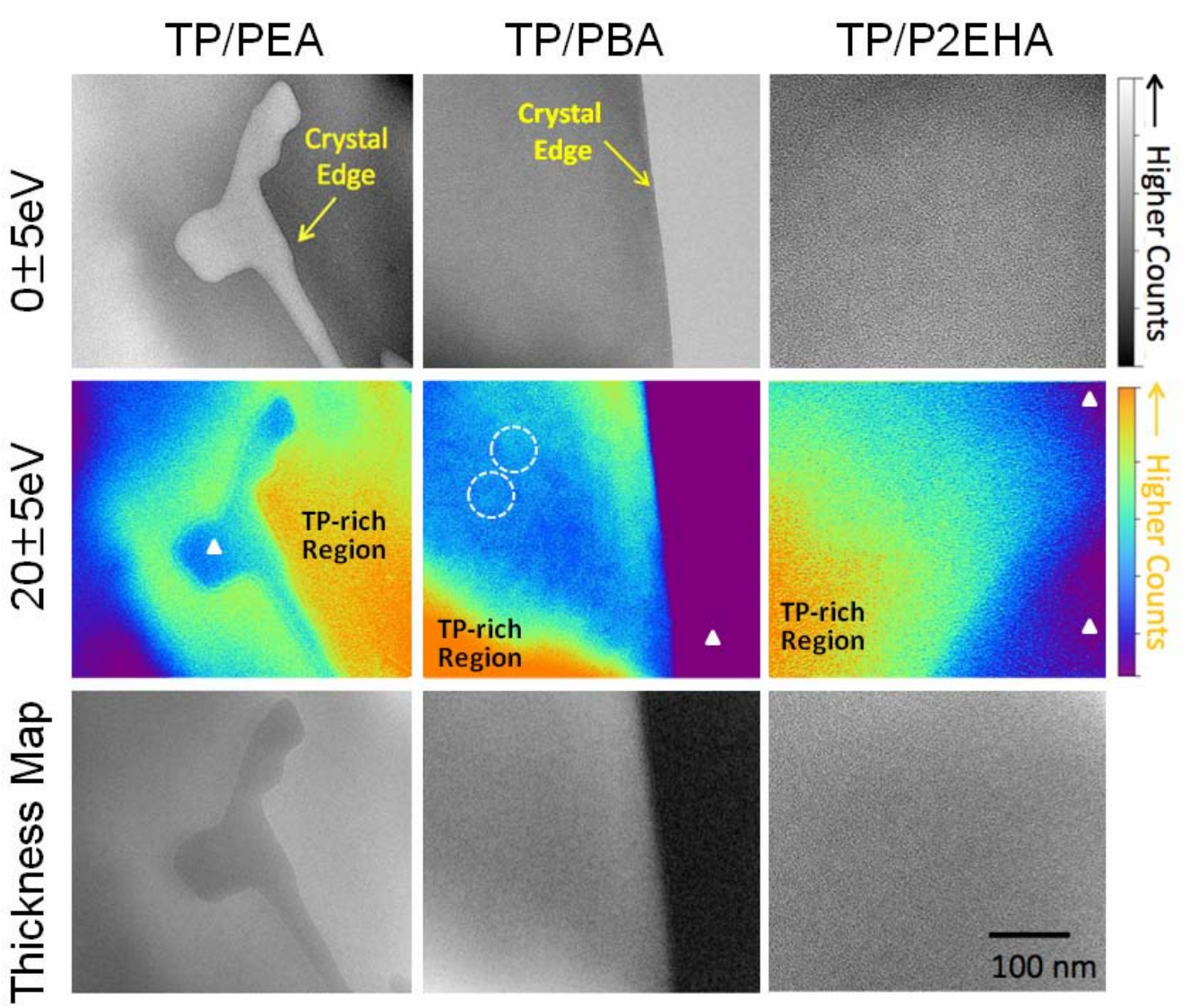

Figure 4.8. Energy filtered TEM images (planar view) of TIPS pentacene blends with PEA, PBA, and P2EHA polymer. For each blend film of TIPS pentacene/PEA, TIPS pentacene/PBA, and TIPS pentacene/P2EHA, images at 0±5eV (elastic) and 20±5eV, and corresponding thickness maps are presented. All images share the same scale bar at bottom right (100 nm). In general, the TIPS pentacene-rich region is darker in elastic image, and brighter in the 20eV image. TIPS pentacene-deficient regions are marked with white triangles.

For the TIPS pentacene/P2EHA blend, the featureless appearances in elastic image and thickness map, together with broad edges in 20 eV image, imply vertical phase separation and intimate interpenetration between TIPS pentacene- and P2EHA-rich regions. On the other hand, for both TIPS pentacene/PBA and TIPS pentacene/PEA films, sharp crystal edges are often observed. TIPS pentacene/PEA shows identical features between 0 eV, 20 eV image and thickness map, which agrees with a dominating lateral phase separation mode. In the 20 eV image of TIPS pentacene/PBA film, white circles highlight some of the features (20-50 nm in size) absent in the corresponding elastic image and thickness map, suggesting that there are some minor vertical but major lateral phase separations between TIPS pentacene and PBA.

Cross-sectional SEM experiments are carried out on cryo-fractured films in a charge compensation mode (i.e. with localized nitrogen flushing). Relatively low accelerating voltage of 1.7 kV is used to minimize charging effect. Samples were immersed in liquid nitrogen, allowed to equilibrate, and cleaved before performing cross-section SEM experiments in a Zeiss Merlin. As shown in cross-sectional SEM view (Figure 4.9 (a) and (b)), TIPS pentacene/PBA and TIPS pentacene/P2EHA exhibit monolayer and trilayer structures, respectively.

In addition to the EF-TEM and cross-sectional SEM study, contact angle measurements were conducted to provide additional insight into the nature of phase separation in the TIPS pentacene/polyacrylate systems. Static water contact angle measurements were performed using a Kruss DSA30 system. The contact angles of deionized water are summarized in Table 4.1. The average contact angle value and standard deviation were estimated based on up to 15 measurements for each film type with sessile fittings.

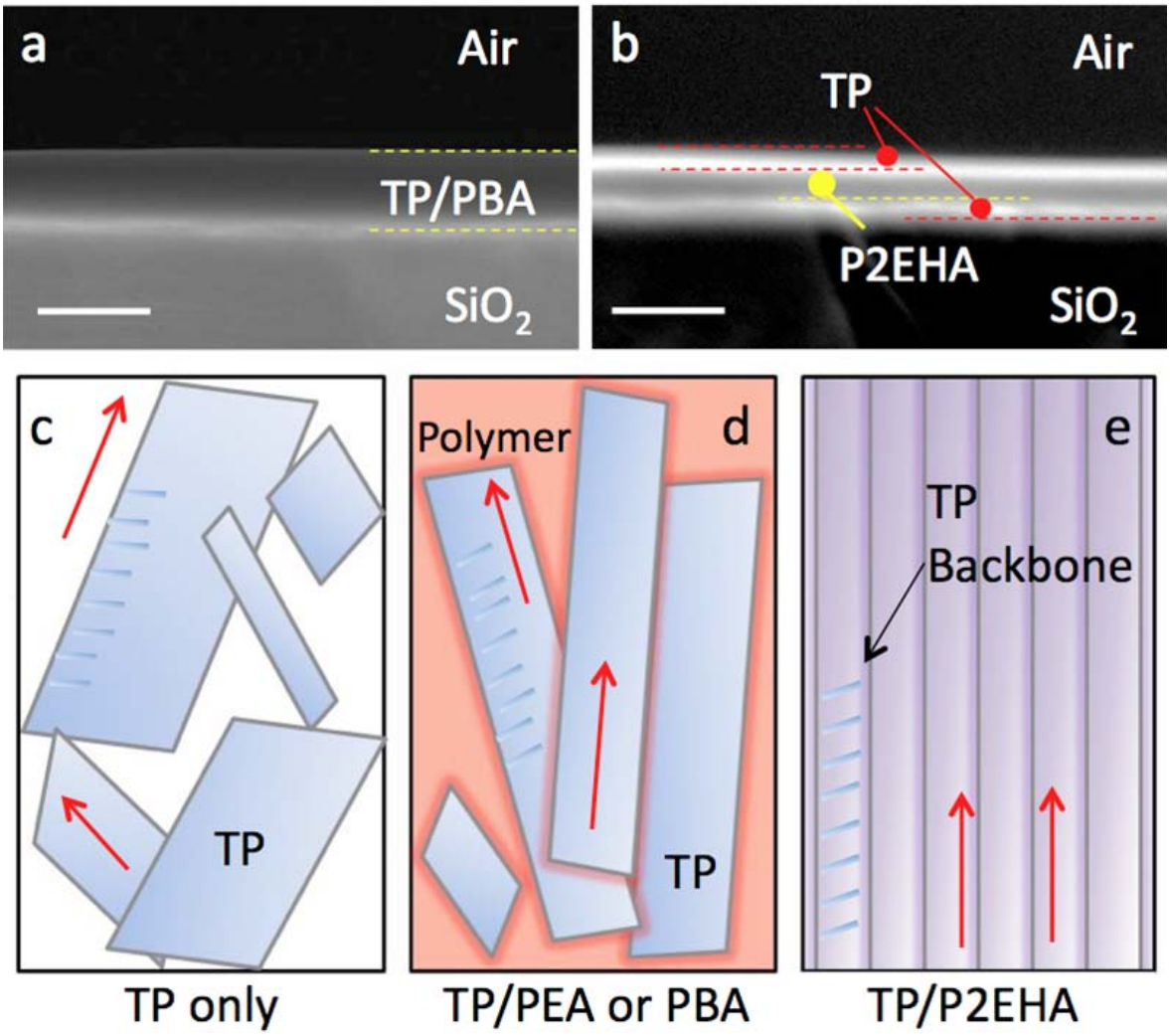

Figure 4.9. Cross-sectional SEM images of (a) TIPS pentacene/PBA with a monolayer structure and (b) TIPS pentacene/P2EHA film with a trilayer configuration. The scale bars are 200 nm. (c)-(e) illustrate the effect of phase separation on crystal alignment. TIPS pentacene/PEA film has a dominating lateral phase separation, providing limited crystal confinement. TIPS pentacene/P2EHA demonstrates mainly vertical phase separation, providing excellent 2-D confinement for crystal growth. TIPS pentacene/PBA has some minor vertical but mainly major lateral phase separations, providing intermediate crystal alignment. The red arrows stand for the long axis of the needle shaped TIPS pentacene crystals, and the light blue rods represent the TIPS pentacene backbones.

	Average (^{o})	Standard Deviation (^{o})
PEA only	78.1	1.3
PBA only	102.5	1.5
P2EHA only	108.0	1.8
TP only *(on selected, well- covered regions)*	99.6	3.6
TP only *(on typical, poorly covered region)*	84.5	5.6
TP/PEA	96.9	11.9
TP/PBA	104.7	3.0
TP/P2EHA	101.6	1.6

Table 4.1. Water contact angle measurements on TIPS pentacene and TIPS pentacene/polymer blend films. The average and standard deviation values are based on up to 15 measurements for each surface.

The pure PEA, PBA and P2EHA surfaces have an average water contact angle of 78.1±1.3 ^{o}, 102.5±1.5 ^{o}, and 108.0±1.8 ^{o}, respectively, showing progressively increasing hydrophobicity as expected. To ensure accuracy and minimize the influence from the substrate, contact angles of pure TIPS pentacene films were measured on both typical TIPS pentacene film (poorly covered) and selected, highly covered area of TIPS pentacene film. The poorly covered TIPS pentacene film has a water contact angle of 84.5±5.6 ^{o}, while its well-covered areas exhibit a contact angle of 99.6±3.6 ^{o}. TIPS pentacene/P2EHA film has a water contact angle of 101.6±1.6 ^{o}, which is reasonably close to the value from well covered TIPS pentacene film (99.6±3.6 ^{o}). This provides direct evidence that the TIPS pentacene layer is on the top of the observed TIPS pentacene/P2EHA trilayer structure. Considering the top and bottom layer in the cross-sectional SEM (Figure 4.9 (b)) share similar contrast, this leads to the conclusion that both top and bottom layer of the trilayer structure are TIPS pentacene-rich. This proposed trilayer layout of TIPS pentacene/P2EHA film agrees well with the vertical phase separation structure of TIPS pentacene/poly(*alpha*-methylstyrene) film reported in literature.[65] In contrast, the TIPS pentacene/PEA blend film has a large fluctuation in water contact angles with an average of

96.9±11.9 °, which supports the conclusion that it has a lateral phase separation mode with TIPS pentacene and PEA components side by side. The lower side of the measured contact angles of TIPS pentacene/PEA is likely caused by the relatively small contact angle of PEA (78.1±1.3 °), while the higher side results from the higher contact angle of TIPS pentacene (99.6±3.6 ° for the well covered regions). The TIPS pentacene/PBA film has an intermediate contact angle (104.7±3.0 °), which can be attributed to a mixture of lateral and vertical phase separation modes coexists and the fact that TIPS pentacene and PBA have similar water contact angles.

Finally, the schematic in Figure 4.9 (c)-(e) is employed to illustrate how the phase separation affects crystal alignment. TIPS pentacene/PEA film has a dominating lateral phase separation, which only leads to limited crystal growth confinement, while TIPS pentacene/PBA film has minor vertical but major lateral phase separation, providing intermediate crystal confinement. TIPS pentacene/P2EHA film, with a confirmed trilayer structure in vertical phase separation mode, provides excellent 2-D confinement for TIPS pentacene crystal growth and thus the best OTFT performance.[54]

For a binary blend of solute and solvent, the Gibbs free energy of mixing (*ΔG)* has the following expression based on Flory-Huggins theory, [96]

$$\frac{\Delta G}{RT} = \sum_{i=1}^{2} n_i \ln \phi_i + n_1 \phi_2 \chi \qquad (1)$$

where n_i is the number of moles for each component, ϕ_i is the corresponding volume fraction, and χ is the interaction parameter between the two components. In Equation 1, the first term on the right side is the combinatorial entropy change, while the second term is largely considered as contact dissimilarity. Similarly, in a three-component blend system (i.e. TIPS pentacene, polymer and solvent in this case), the free energy of mixing is expressed as: [97]

$$\frac{\Delta G}{RT} = \sum_{i=1}^{3} n_i \ln \phi_i + \Gamma(T, \phi, N) \quad (2)$$

$$\Gamma(T, \phi, N) = n_1\phi_2 g_{12} + n_1\phi_3 g_{13} + n_2\phi_3 g_{23} + n_1\phi_2\phi_3 g_{123} \quad (3)$$

where $\sum_{i=1}^{3} n_i \ln \phi_i$ is the combinatorial entropy term, $\Gamma(T, \phi, N)$ accounts for both non-combinatorial entropy of mixing and enthalpy changes, g_{ij} (i and j=1, 2, or 3) is the composition-dependent binary interaction parameter, and g_{123} is the ternary interaction parameter. In a polymer containing ternary blend, Γ is also a function of the degree of polymerization (N).

From a thermodynamic point of view, Equations 2 and 3 provide a basis to understand the interplay between the different components in a ternary system (TIPS pentacene, polymer and solvent). It is expected that the long alkyl side chains of P2EHA slightly reduce the effect of the combinatorial entropy ($\sum_{i=1}^{3} n_i \ln \phi_i$) because of their slightly larger size as compared to the side groups of PEA and PBA.[96,97] At the same time, they also contribute to a significantly decreased $\Gamma(T, \phi, N)$ (likely through a large enthalpy change) in TIPS pentacene/P2EHA solution because of their largely increased hydrophobicity, driving the system towards phase separation ($\Delta G<0$) in the early stage of solvent evaporation to form the top layer of TIPS pentacene. Crystallization plays important kinetic roles in phase separation, which is attributed to the fact that TIPS pentacene forms the top layer. The residual blend solution has a P2EHA region in the middle layer due to precipitation. Finally, as the rest of the solvent evaporates, the residual TIPS pentacene component forms the bottom layer in Figure 4.9 (b). This vertical phase separation and sequential layer formation resulted from slow solution crystallization of TIPS pentacene/P2EHA effectively confine the highly anisotropic TIPS pentacene crystals into a well-aligned 2-D growth

pattern. In contrast, the polarity of PEA is expected to correspond to a large $\Gamma(T, \phi, N)$, which contributes to a positive ΔG and delays the phase separation until the majority of solvent evaporates out. This forces PEA to precipitate with the semiconducting small molecules side-by-side, and only provides limited confinement effect and charge transport enhancement.

In summary, by systematically varying the hydrophobicity (alkyl length) of the polymer additive in a model semiconducting small molecule/polymer blend, switching between the lateral and vertical phase separation is demonstrated for the first time. The blend system with vertical phase separation exhibits well-aligned TIPS pentacene crystals, leading to a significant enhancement in average mobility and performance consistency of organic thin-film transistors (OTFTs). The results from this work shed light on the important but underexplored interplay among phase separation mode, crystal alignment, and charge transport of solution crystallized, semiconducting small molecule/polymer blends.

CHAPTER 5

IMPROVING PERFORMANCE OF TIPS PENTACENE-BASED ORGANIC THIN FILM TRANSISTORS WITH SMALL-MOLECULE ADDITIVES

5.1. Introduction

As a solution-processable organic semiconductor with high mobility and air stability, 6,13-bis(triisopropylsilylethynyl)pentacene (TIPS pentacene) provides a great promise for large-area, low-cost fabrication of organic thin-film transistors (OTFTs) on flexible substrates.[12,58,59,76,98] Normally hexamethyldisilazane (HMDS) [99,100] or octadecylsilane (OTS) [22,70] treatments are employed to improve the performance of OTFTs. These surface treatments enhance π-π stacking of organic molecules and also remove silanol groups (Si-O-H) that act as charge trapping states on the hydrophilic SiO_2/Si surface,[101] thereby improving the charge transport. However, in the fabrication of TIPS pentacene based OTFTs, when the gate dielectric surface is made hydrophobic by surface treatments, dewetting of the TIPS pentacene solution on the substrate occurs and reduces film coverage and the fraction of working OTFTs.[102] Some researchers employed polymer additives to improve the performance of TIPS pentacene based OTFTs, and the device-to-device performance variation was largely suppressed, due to the good film-formation property of the polymers.[54,65,67] Nevertheless, when TIPS pentacene is blended with such polymers, the resultant films typically exhibit vertical segregation with TIPS pentacene serving as an active layer and polymers acting as an additional dielectric layer.

Consequently, due to the fact that the polymers are blended with TIPS pentacene at 1:1 weight ratio, the polymer dielectric layer is expected to be thick enough to unfavorably reduce the overall capacitance, thereby decreasing the saturation current.

In this study, we add a small amount (0.25% weight ratio) of small-molecule additives into the TIPS pentacene solution to address the performance variation issue of TIPS pentacene based OTFTs, and investigate the effect of the alkyl side chains on the crystallization of the TIPS pentacene/small-molecule blend systems. The small molecules we used, including 4-butylbenzoic acid (BBA), 4-hexylbenzoic acid (HBA), and 4-octylbenzoic acid (OBA), have similar molecular structures with the same hydrophilic head but different length of hydrophobic tail. These small molecules were chosen as additives for TIPS pentacene solution mainly for three reasons. First, the formation of the small-molecule self-assembled interfacial layer eliminates the problem of dewetting as in the case of HMDS or OTS treatment. Due to the interaction between their hydrophilic head and the silanol groups on the hydrophilic SiO_2 substrate, the small-molecule additives form very thin interfacial layers via self-assembly.[103,104] Second, the incorporation of small molecules enhances TIPS pentacene film coverage. As the hydrophilic head of small molecules facilitates self-assembly on the hydrophilic substrate, their hydrophobic tail simultaneously interacts with the alkyl groups of TIPS pentacene,[105] which contributes to uniform deposition of TIPS pentacene seeds and improved TIPS pentacene π-π stacking [106] on the hydrophobic interfacial layer. The uniformly distributed seeds serve as nucleation sites for crystallization and facilitate TIPS pentacene to grow along the tilted direction of the substrate, leading to the formation of a TIPS pentacene film with improved crystal orientation and enhanced areal coverage. Third, the capacitance from the insulating layer is anticipated to remain the same because the thickness of the small-molecule self-assembled layer

is anticipated to be very thin due to a small amount of small molecule loading. The results show that the TIPS pentacene/small-molecule blend films exhibit an improved crystal orientation and film coverage, which lead to an enhancement in OTFT average mobility and performance consistency. In particular, OTFTs based on the optimal TIPS pentacene/OBA blend film demonstrate approximately a five-fold enhancement in average mobility and eight-fold improvement in performance consistency when compared to pure TIPS pentacene OTFTs.

5.2. Experiment

5.2.1. Materials and Thin Film Formation

TIPS pentacene and the small-molecule additives including BBA, HBA, and OBA were purchased from Sigma Aldrich and used without further purification. These three small molecules have molecular weights of 178, 206, and 234 g/mol, respectively. TIPS pentacene powder and small molecules were dissolved in toluene at a concentration of 5 mg/mL, respectively, before being mixed at different weight ratios. Subsequently, the mixture solution was drop cast onto a heavily doped n-type silicon substrate with a 300 nm thermal oxide. The substrate is slightly tilted (3~5 degrees) to facilitate TIP pentacene crystal growth in a solvent rich environment.[107] Then gold was deposited onto the grown films as source and drain contacts via thermal evaporation. The fabricated bottom-gate, top-contact (TC) OTFTs were used to test charge transport in pure TIPS pentacene film and TIPS pentacene/small-molecule blend films.

5.2.2. Device Fabrication and Characterization

Charge transport in OTFTs was characterized using an Agilent B1500A semiconductor parameter analyzer under ambient conditions at room temperature. Field-effect hole mobility in

the saturation regime (V_{DS}= -60 V) was extracted from the slope of the transfer characteristic $(I_{DS})^{1/2}$-V_{GS}, and all devices were measured five times to ensure the consistency of the extracted field-effect mobilities. X-ray diffraction spectra of the thin films were measured with a Philips X'Pert X-ray diffractometer.

X-ray reflectivity (XRR) experiment was carried out to investigate the distribution of the small-molecule additives along the direction normal to the substrate surface. XRR data were measured using PanAnalytical MRD Pro instrument. The voltage and current for the X-ray generation was 45kV and 40mA, respectively. The step size was 0.01° and the time at each step was 10 seconds. The measured reflectivity (R) vs. α_i curves were converted to RQ_z^4 vs. Q_z, where Q_z is equivalent to $4\pi\sin(\alpha_i/\lambda)$ with α_i and λ equal to the incidence angle and wavelength of X-ray beam, respectively. To prepare the films, TIPS pentacene (10 mg/ml) was blended with BBA, HBA, or OBA at 97:3 weight ratio in toluene. The blend solutions were stored overnight before being spin-cast onto silicon substrate at the spin rate of 1500 rpm for 1 minute.

5.3. Results and Discussion

The small-molecule additives have the same hydrophilic head but different length of hydrophobic tail (represented by "R" in Figure 5.1). Specifically, BBA has the shortest hydrophobic tail with four carbon atoms, OBA has the longest hydrophobic tail with eight carbon atoms, and HBA lies in between with six carbon atoms. HBA was used as a prototype to investigate how different weight ratios of small molecules may affect the TIPS pentacene thin film morphology. HBA was blended with TIPS pentacene at various weight ratios: 0.1%, 0.25%, and 5%, corresponding to 0.31%, 0.78%, and 15.6% molar fraction, respectively. Polarized optical micrographs of the pristine TIPS pentacene film and TIPS pentacene/HBA blend films at

different weight ratios are shown in Figure 5.2(a)-(d). The pristine TIPS pentacene film exhibits large crystal needles with misorientation and large gaps in between.[10,35] The addition of HBA at 0.1% weight ratio slightly reduces the crystal gaps, but crystal misorientation still dominates (Figure 5.2(b)). The increase of HBA weight ratio to 0.25% leads to the smallest crystal gaps and the least crystal misorientation (Figure 5.2(c)). However, as the content of HBA further increases to ~5%, it eventually causes the aggregations of TIPS pentacene, as shown in Figure 5.2(d). Thus, it can be inferred that the loading of small-molecule additives at the weight ratio of 0.25% leads to the optimal thin film morphology in terms of crystal alignment and film coverage.

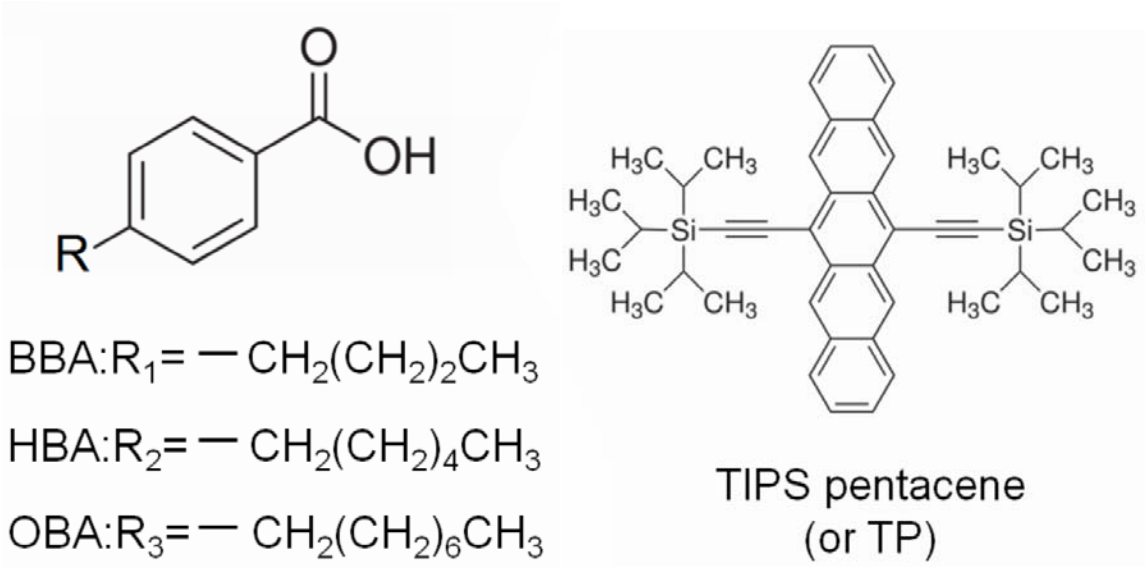

Figure 5.1. Molecular structures of TIPS pentacene, BBA, HBA and OBA. The hydrophobic tail of small-molecule BBA, HBA and OBA has four, six and eight carbon atoms, respectively.

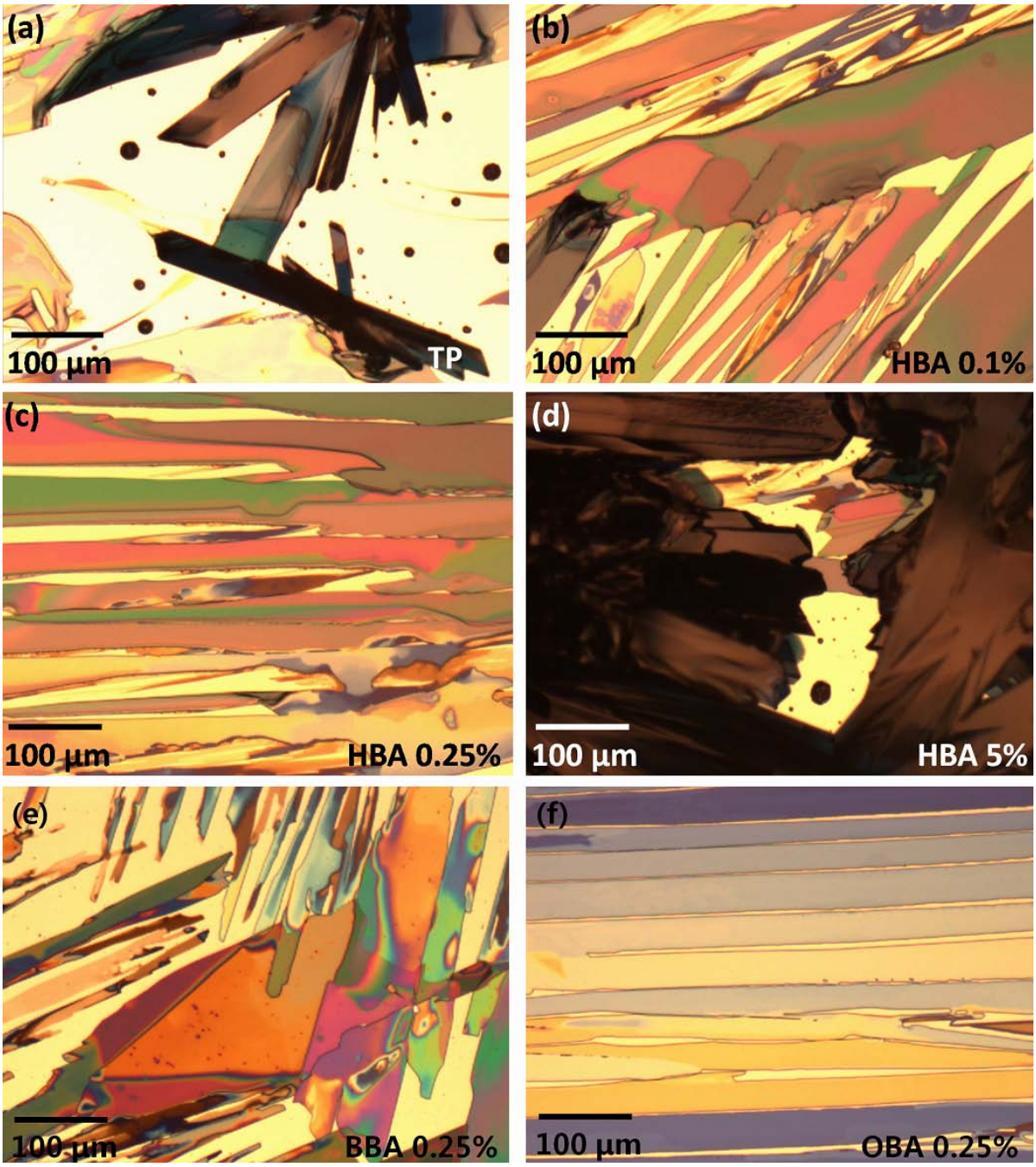

Figure 5.2. Optical micrographs of (a) pristine TIPS pentacene film, and TIPS pentacene/HBA blend film with varied content of HBA loading at (b) 0.1%, (c) 0.25%, and (d) 5%, respectively. (e) TIPS pentacene/BBA blend film with optimal loading at 0.25%. (f) TIPS pentacene/OBA blend film with optimal loading of 0.25%.

To investigate the effect of hydrophobic tail length on the thin film morphology, BBA and OBA were used to blend with TIPS pentacene at the optimal weight ratio of 0.25%, corresponding to 0.9% and 0.69% in molar fraction, respectively. The optical micrographs are presented in Figure 5.2(e) and (f), respectively. The addition of BBA with the shortest hydrophobic tail only moderately diminishes the crystal gaps, but crystal misorientation still exists. The addition of OBA with the longest hydrophobic tail demonstrates the most significant improvement in film morphology, that is, the smallest crystal gaps and the least crystal misorientation. Therefore, the enhancement of TIPS pentacene crystal alignment and film coverage from addition of the small-molecules is strongly dependent on the length of hydrophobic tail of small molecules.

Figure 5.3 (a) and (b) show the typical output and transfer characteristics of the TC OTFTs based on the TIPS pentacene/small-molecule blend film with the optimal weight ratio of 0.25%. Field-effect mobility and threshold voltage (V_T) are determined from the fitted line in the square root plot of the transfer characteristic in the saturation region.

Figure 5.4 (a) compares the measured hole mobilities among TC OTFTs based on pure TIPS pentacene film, TIPS pentacene/BBA, TIPS pentacene/HBA, and TIPS pentacene/OBA blend films at the optimal weight ratio of 0.25%, respectively. The field-effect mobilities of pure TIPS pentacene OTFTs vary by four orders of magnitude (8.2×10^{-2} $cm^2V^{-1}s^{-1}$ to 2.7×10^{-5} $cm^2V^{-1}s^{-1}$), while OTFTs based on TIPS pentacene/BBA, TIPS pentacene/HBA, and TIPS pentacene/OBA blend films demonstrate field-effect mobilities of 9.3×10^{-2} $cm^2V^{-1}s^{-1}$ to 2.3×10^{-3} $cm^2V^{-1}s^{-1}$, 1.6×10^{-1} $cm^2V^{-1}s^{-1}$ to 8.7×10^{-2} $cm^2V^{-1}s^{-1}$, and 1.8×10^{-1} $cm^2V^{-1}s^{-1}$ to 1.1×10^{-1} $cm^2V^{-1}s^{-1}$, respectively. These results indicate that the addition of small-molecule additives generally

reduces the variation of field-effect mobilities because of improved crystal orientation and film coverage.

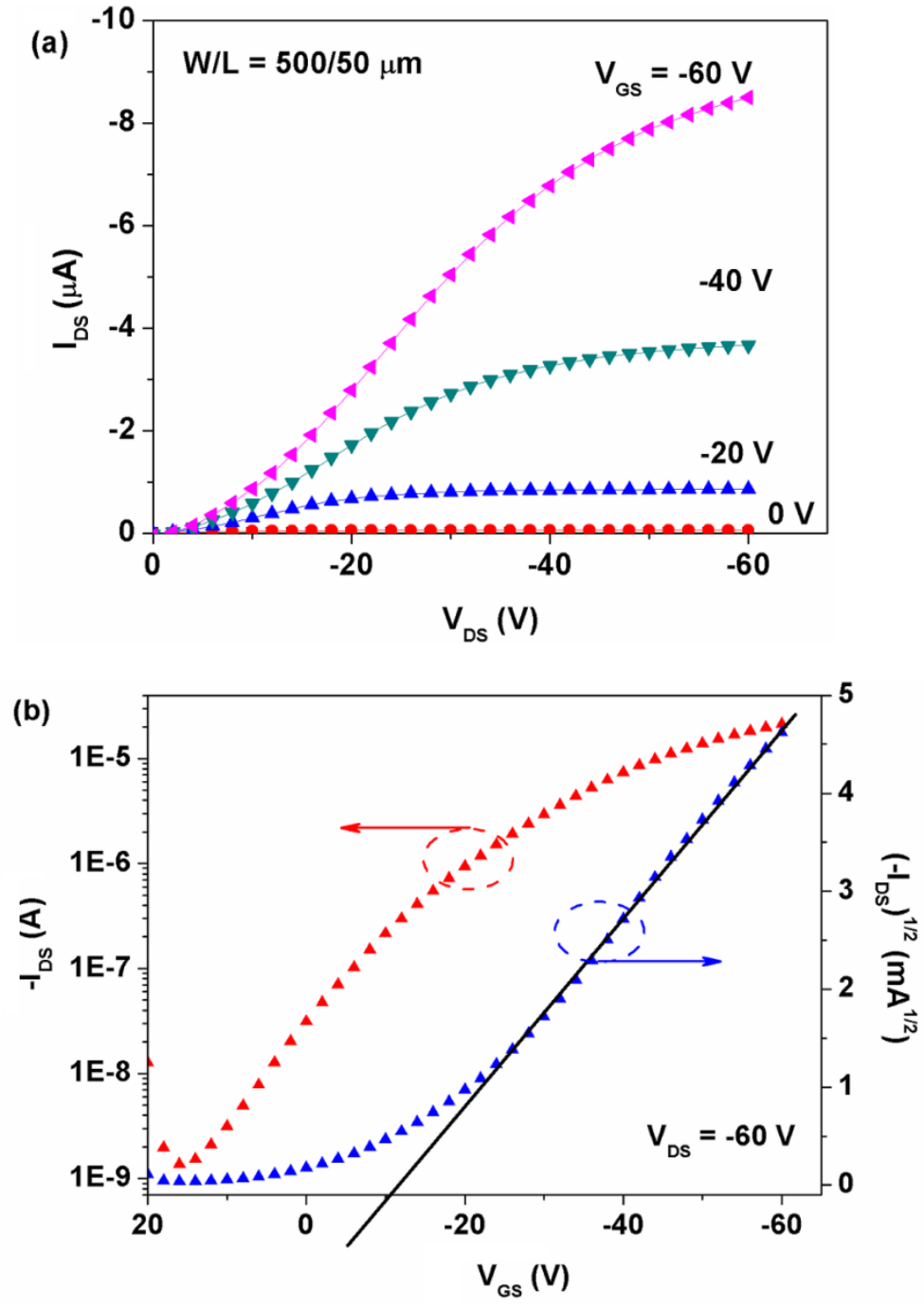

Figure 5.3. Typical (a) output and (b) transfer characteristics of bottom-gate, top-contact OTFTs based on TIPS pentacene/small molecule blend film.

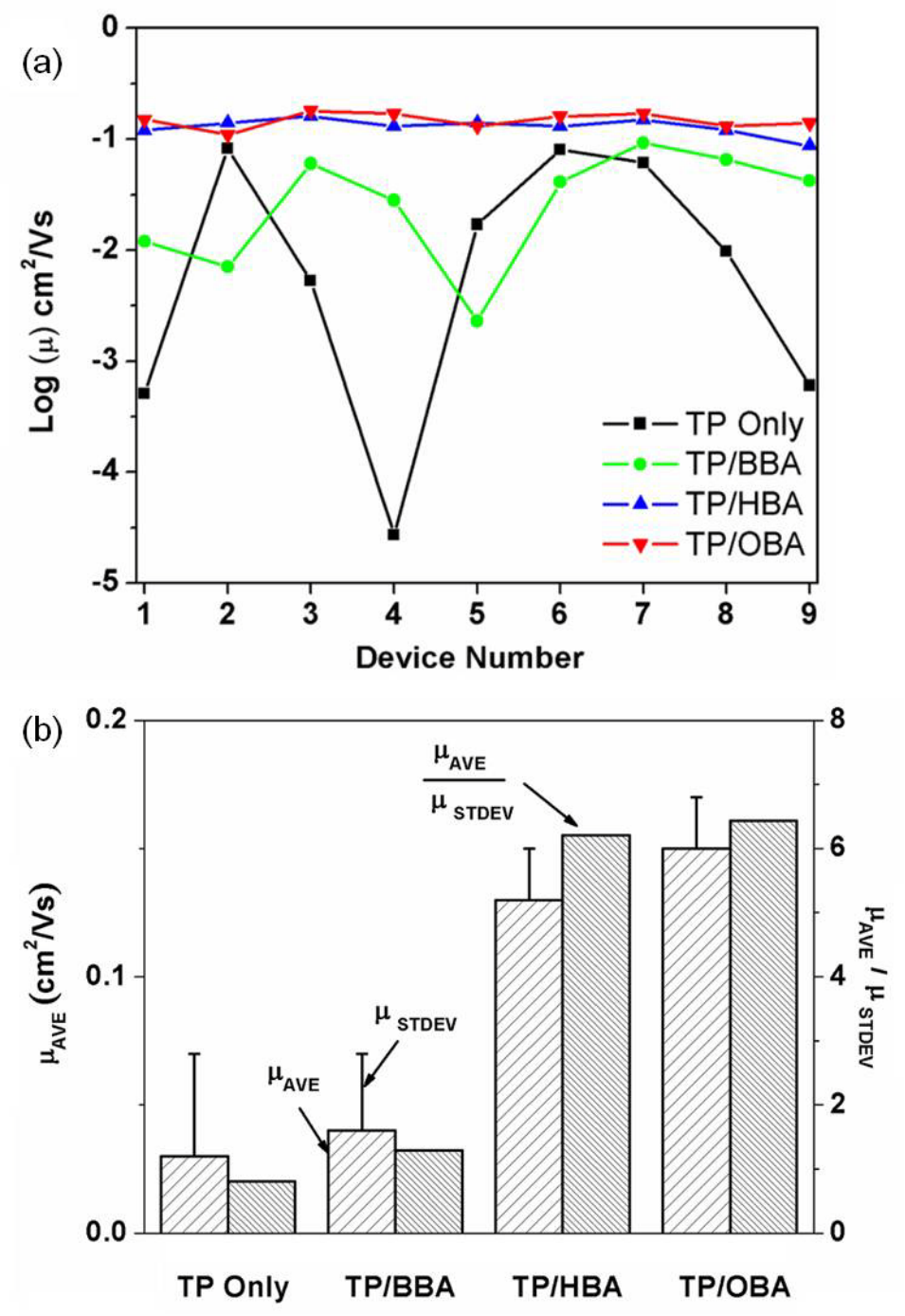

Figure 5.4. (a) Comparison of average mobilities of pristine TIPS pentacene film and TIPS pentacene/small-molecule blend films. (b) Comparison of performance consistency of OTFTs, as indicated by the ratio of average mobility to standard deviation (μ_{Ave}/μ_{Stdev}). All small molecules are loaded into TIPS pentacene solution at 0.25% weight ratio.

Figure 5.4 (b) shows a comparison of the average field-effect mobilities with standard deviation. Standard deviation is calculated based on 9 devices for each type of OTFTs. Pristine TIPS pentacene based OTFTs show an average field-effect mobility of 0.03±0.04 $cm^2V^{-1}s^{-1}$, while with the addition of BBA, HBA, and OBA, the average mobility increases to 0.04±0.03 $cm^2V^{-1}s^{-1}$, 0.13±0.02 $cm^2V^{-1}s^{-1}$, and 0.15±0.02 $cm^2V^{-1}s^{-1}$, respectively. Particularly, OTFTs based on TIPS pentacene/OBA blend film demonstrate a five-fold enhancement in average field-effect mobilities. In addition, the ratio of average mobilities (μ_{Ave}) to standard deviation of mobilities (μ_{Stdev}) is used as a metric to evaluate the performance consistency of OTFTs. Pristine TIPS pentacene OTFTs show a μ_{Ave}/μ_{Stdev} ratio of 0.81, while OTFTs based on TIPS pentacene/BBA, TIPS pentacene/HBA and TIPS pentacene/OBA blend films demonstrate μ_{Ave}/μ_{Stdev} ratios of 1.29, 6.21 and 6.43, respectively, indicating the addition of small-molecule additives also improves performance consistency. Specially, the addition of OBA leads to an eight-fold enhancement of performance consistency of OTFTs, when compared to the pristine TIPS pentacene OTFTs.

Figure 5.5(a) shows the X-ray diffraction results of the pure TIPS pentacene film and TIPS pentacene/small-molecule blend films. To clearly illustrate the peak intensities of each type of film, the XRD spectra were vertically shifted. All of the films demonstrate typical (*00l)* type of reflections, which are consistent with previously published results, indicating the same edge-on orientation and unit cell structure.[46] To better present the change of peak intensities with the addition of small-molecule additives, the values of the peak intensities in Figure 5.5(a) were extracted and plotted as a function of each type of film as shown in Figure 5.5(b). It is noted that when compared to the pure TIPS pentacene film, all types of blend films demonstrate enhanced peak intensities. Specially, TIPS pentacene/OBA blend film exhibits the highest peak intensities,

which results from a combination of the best crystal alignment, the highest film coverage, and the most improved π-π stacking of TIPS pentacene on the hydrophobic self-assembled interfacial layer.

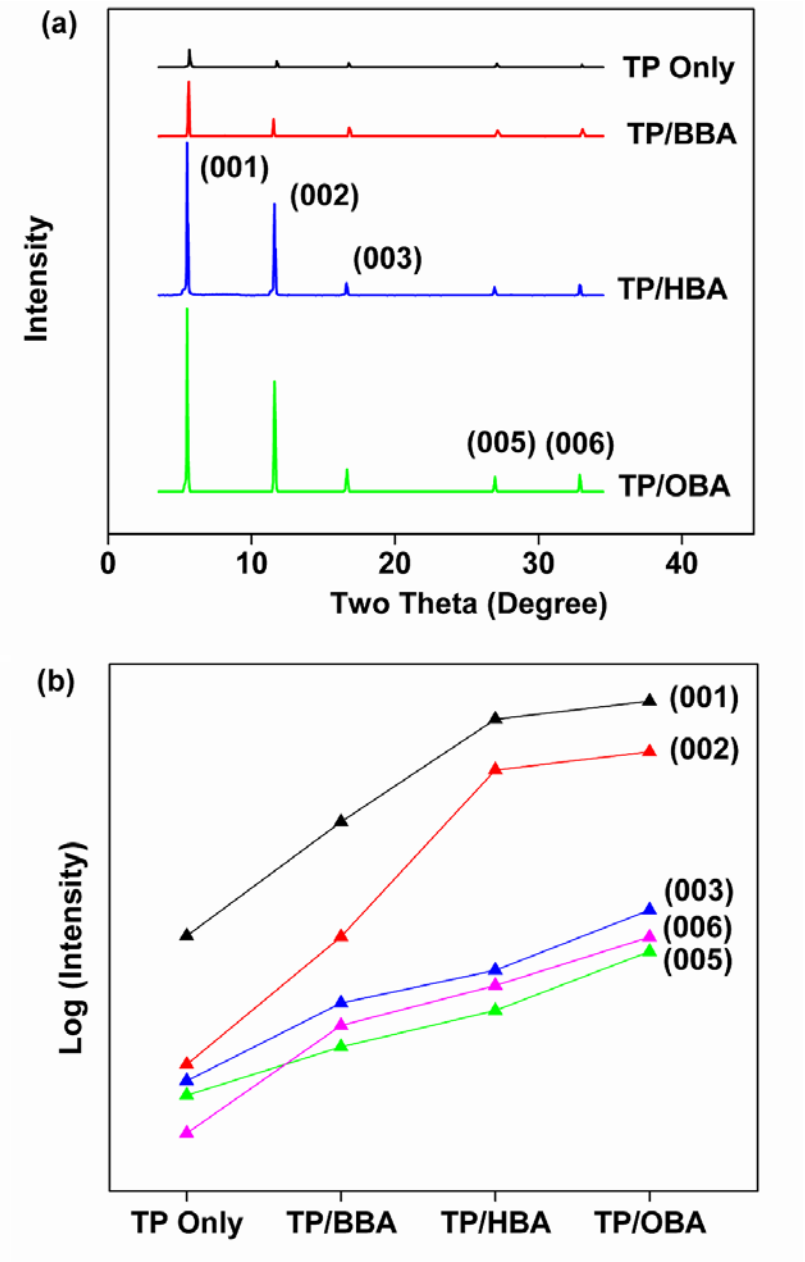

Figure 5.5. (a) XRD spectra for pure TIPS pentacene film and TIPS pentacene/small-molecule blend films. (b) Plot of peak intensities of (*00l)* type reflections as a function of each type of film.

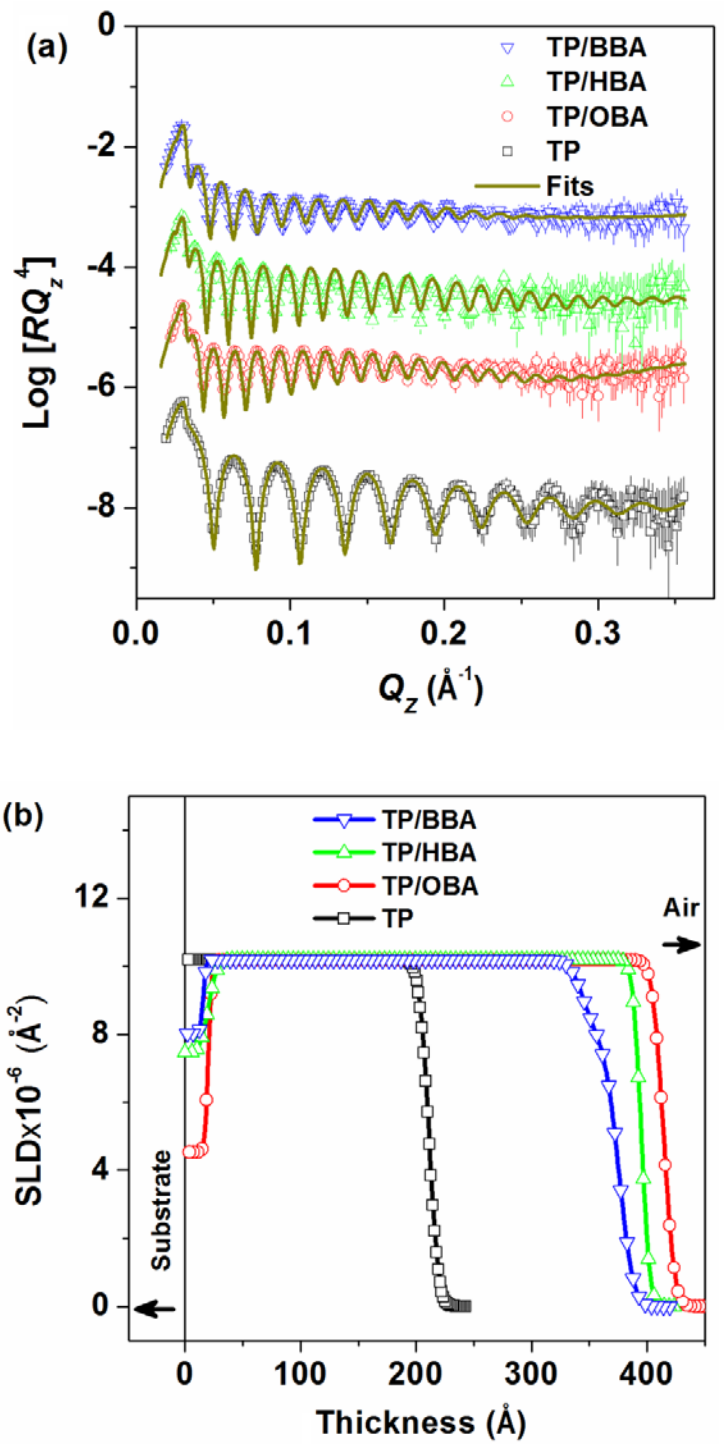

Figure 5.6. (a) X-ray reflectivity (XRR) data and fitting for pristine TIPS pentacene, and its blends with BBA, HBA, and OBA, respectively. (b) The scattering length density (SLD) profiles.

Figure 5.6(a) shows X-ray reflectivity data for pristine TIPS pentacene, and its blends with BBA, HBA and OBA, respectively. The XRR data were fitted using Parratt formalism [108] and the scattering length density (SLD) profiles are shown in Figure 5.6(b). For the pristine TIPS pentacene film, the single layer model gave rise to a goodness of fit where the X-ray SLD of TIPS pentacene calculated from the mass density (1.10 g/cm^3) [109] was 10.2×10^{-6} Å^{-2}. Adding 3 wt% of BBA, HBA or OBA to TIPS pentacene induced the formation of additional layer(s) with different SLDs, implying that the added materials are not mixed homogeneously with TIPS pentacene but segregated with different composition along the direction normal to the substrate. It can be seen from Figure 5.6(b) that adding HBA or OBA results in a separate layer adjacent to the semiconductor/substrate interface in TIPS pentacene/HBA and TIPS pentacene/OBA film, respectively, while the addition of BBA leads to two additional layers adjacent to both semiconductor/substrate and semiconductor/air interfaces. Two mechanisms are considered to impact the distribution of the small-molecule additives in the film. One is the interaction between the small molecules and the silanol groups on the hydrophilic SiO_2 substrate, which attracts the small molecules to form self-assembled interfacial layers on the substrate surface, whereas the other is related to the small molecule weight. In particular, the formation of HBA or OBA layer at the semiconductor/substrate interface began with the self-assembly process followed by the deposition of the residual molecules since both HBA and OBA have relatively large molecular weight. On the other hand, although the formation of BBA layer also initiated with the self-assembly process at the semiconductor/substrate interface, it was followed by the segregation of the residual BBA molecules to the semiconductor/air interface since BBA has the smallest molecular weight among these three small molecules. The smallest molecular weight facilitates part of the BBA additive to segregate to the semiconductor/air interface.

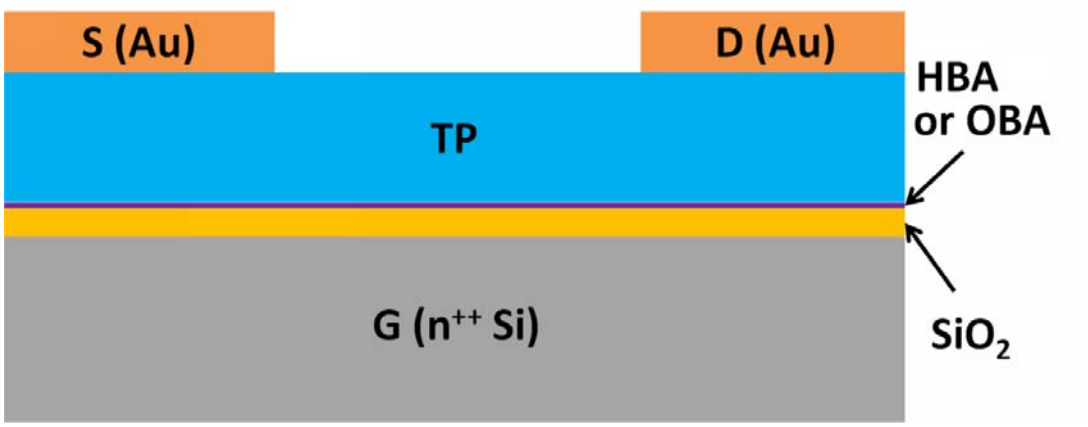

Figure 5.7. A cartoon illustration of TC OTFT configuration with small-molecule interfacial layer at the bottom and TIPS pentacene-rich layer on the top in the active layer.

Since the small-molecule HBA and OBA additives exhibit more pronounced effect than the BBA additive on enhancement of crystal orientation and film coverage, bottom-gate, top-contact OTFTs, with TIPS pentacene as the top active layer and HBA or OBA as the bottom interfacial layer, were fabricated and represented in Figure 5.7. The vertically layered structure due to the addition of small-molecule HBA or OBA contributes to the morphology improvement in the TIPS pentacene/small molecule blend films. The hydrophilic head of the small-molecule HBA or OBA additive is preferentially attracted by the silanol groups on the oxide substrate and self-assembles on the surface, forming an interfacial layer. Simultaneously, the hydrophobic tail of the small-molecule HBA or OBA is pushed away from the substrate and interacts with the alkyl groups of TIPS pentacene due to van der Waals force. These interactions from both hydrophilic head and hydrophobic tail of HBA or OBA result in uniform deposition of TIPS pentacene crystal seeds on the self-assembled interfacial layer, which contributes to improved π-π stacking and crystal coverage. The small molecules with longer hydrophobic tail are expected to have more orderly molecular packing,[110] thereby causing more uniform deposition of TIPS pentacene seeds on the top of the interfacial layer. As TIPS pentacene crystals grow along a

slightly tilted substrate, a TIPS pentacene film with enhanced crystal orientation and film coverage was achieved. The reduction of TIPS pentacene crystal misorientation and crystal gaps, along with the improved π-π stacking of TIPS pentacene, leads to an enhanced charge transport and performance consistency of OTFTs.

5.4. Conclusions

In summary, we demonstrated that the small-molecule additives are able to effectively reduce TIPS pentacene crystal misorientation and enhance film coverage. This effect is dependent on the length of hydrophobic side group of the small molecules. XRR measurement reveals that the TIPS pentacene/small-molecule blend films exhibit a vertically layered structure. Both HBA and OBA additives segregate only to the semiconductor/substrate interface, while the BBA additive segregates to both the semiconductor/substrate interface and semiconductor/air interface. Top-contact OTFTs based on TIPS pentacene/small-molecule blend films demonstrate an enhancement in both average mobilities and performance consistency. Particularly, OTFTs based on TIPS pentacene/OBA, which has the longest hydrophobic tail of eight carbon atoms, exhibit approximately five-fold increase in average hole mobilities and eight-fold increase in performance consistency when compared to pure TIPS pentacene OTFTs.

CHAPTER 6

CONCLUSIONS AND FUTURE WORK

6.1. Conclusions

This dissertation demonstrates four different approaches to address the problems of crystal misorientation of TIPS pentacene film and correspondingly the device performance variations of TIPS pentacene based OTFTs. These approaches include the utilization of silicon dioxide nanoparticles (SiO_2 NPs), air flow navigation, the addition of polyacrylate polymers, and the loading of small-molecule additives.

Chapter 2 introduces the utilization of SiO_2 NPs to address the problems mentioned above. SiO_2 NPs are blended with TIPS pentacene in solution at different weight ratios, and the effect of SiO_2 NPs to on the TIPS pentacene film morphology at each varied content has been characterized by using optical microscopy, semiconductor parameter analyzer, X-ray diffraction (XRD), scanning electron microscope (SEM), and transmission electron microscope (TEM). The results from optical microscopy and electrical characterization indicate that while pure TIPS pentacene film exhibits essential crystal misorientation and poor film coverage, the loading of SiO_2 NPs at the optimum weight ratio of 10% effectively improves both crystal orientation and enhances film coverage, which consequently leads to an improved average mobilities and performance consistency of TIPS pentacene/SiO_2 NPs blend OTFTs. TEM results show that

most of the SiO_2 NPs aggregate at the grain boundaries of TIPS pentacene crystals, effectively facilitating TIPS pentacene to form well-aligned crystal with improved orientation. SEM was utilized to investigate the vertical distribution of SiO_2 NPs across the bulk TIPS pentacene active layer. SEM results show that a very small portion of SiO_2 NPs locate at the semiconductor/insulator interface while most SiO_2 NPs are in the regions away from the interface, demonstrating the addition of SiO_2 NPs does not significantly affect charge transport at semiconductor/insulator interface.

Chapter 3 describes the use of air flow to navigate the crystal growth of TIPS pentacene. Air flow was applied at different flow speeds in order to investigate the optimum flow speed, at which the TIPS pentacene film shall exhibit both improved crystal orientation and film coverage. Results from optical microscopy indicate that the film morphology strongly depend on the applied flow speed. At a lower flow speed, the air flow is not able to counteract various factors that cause "coffee ring effect" and still results in the aggregation of TIPS pentacene crystals, while at a higher flow speed, it excessively facilitates solvent evaporation and reduces thin film crystallinity. Therefore, only at an optimum speed can air flow effectively reduce the coffee ring effect, improve film uniformity, and enhance crystal orientation. As a result, OTFTs based on TIPS pentacene crystals grown with air flow navigation at the optimized flow speed, show four-times increase in average mobility and an eleven-fold enhancement of performance consistency. Such improvement can be reasonably explained by a balance of crystal orientation, crystallinity, and film connectivity achieved at this optimal flow speed.

Chapter 4 demonstrates a novel method to improve the TIPS pentacene crystal orientation and film uniformity simply by switching between lateral and vertical phase separation in

semiconducting TIPS pentacene/polymer blend films by simply varying the alkyl length of the polyacrylate polymer component. In order to demonstrate different phase separation modes, a series of polyacrylate polymers are used in this chapter: poly(ethyl acrylate) (PEA), poly(butylacrylate) (PBA), and poly(2-ethylhexyl acrylate) (P2EHA), respectively. PEA, PBA and P2EHA share similar molecular structures but have different length of hydrophobic side group, from two carbon atoms of PEA, to four of PBA, and to eight of P2EHA. The hydrophobicity of a polymer is proportional to the length of its hydrophobic side chain. P2EHA is most hydrophobic, PEA is the least hydrophobic, and PBA is between P2EHA and PEA. The phase separation modes strongly correlate with the hydrophobicity of a polymer and with intermolecular interactions between small molecule TIPS pentacene and a polymer additive. Results from TEM, SEM and water contact angle measurement show that the addition of a polymer additive with a shorter hydrophobic side chain, such as PEA, leads to lateral phase separation between TIPS pentacene and the polymer, providing only limited confinement of crystal growth. On the other hand, the addition of a polymer additive with a longer hydrophobic side chain, such as P2EAH, demonstrates vertical phase separation between TIPS pentacene and the polymer, providing effective alignment of TIPS pentacene crystals and resulting in a TIPS pentacene film with greatly enhanced crystal orientation and film coverage. Electrical characterization also indicate that TIPS pentacene/P2EHA OTFTs demonstrate the highest average hole mobilities and least performance variations.

Chapter 5 describes blending TIPS pentacene with a series of small-molecule additives, 4-butylbenzoic acid (BBA), 4-hexylbenzoic acid (HBA) and 4-octylbenzoic acid (OBA), to improve both charge transport and performance consistency in the TIPS pentacene/small-molecule additive blend OTFTs. The series of small-molecule additives share similar structure of

a benzoic acid moiety but have different length of hydrophobic tails. In particular, BBA has the smallest number of carbon atoms as its hydrophobic tail, OBA has the largest number of carbon atoms as its hydrophobic tail, and HBA lies in between. When blended with TIPS pentacene, the hydrophobic tails of small-molecule additives would self-assemble to the surface of gate oxide, forming a very thin interficial layer at the semiconductor/dieletric interface and facilitating TIPS pentacene crystal seeds to more uniformly deposit onto the small-molecule additive layer. X-ray reflectivity results demonstrate that both HBA and OBA additives segregate to the semiconductor/dieletric interface, while BBA additive segregates to both semiconductor/air and semiconductor/dieletric interface. As a result, TIPS pentacene crystallize and grow along the tilted orientation of substrate, forming a film of enhanced crystal orientation and film coverage. Electrical characterization demonstrate that the TIPS pentacene/small-molecule additive blend OTFTs show improved average hole mobility and performance consistency, an effect strongly correlated with the length of hydrophobic side group of small molecules. Specially, the addition of OBA, which has the longest hydrophobic tail of eight carbon atoms, leads to the most enhancement of both average hole mobility and performance consistency of TIPS pentacene/OBA blend OTFTs.

The average mobility and highest mobility corresponding to each approach as mentioned above are summarized in Figure 6.1. Particularly, TIPS pentacene OTFTs with the addition of SiO_2 NPs at 10% show an improved average mobility of 0.13±0.04 cm^2/Vs with the highest mobility of 0.21 cm^2/Vs. Air flow navigation at 2 L/min results in an average mobility of 0.11±0.01 cm^2/Vs with the highest mobility of 0.12 cm^2/Vs of TIPS pentacene OTFTs. TIPS pentacene/P2EHA OTFTs demonstrate an average mobility of 0.35±0.06 cm^2/Vs with the

highest mobility of 0.43 cm^2/Vs. TIPS pentacene/OBA OTFTs exhibit an average mobility of 0.15±0.02 cm^2/Vs with the highest mobility of 0.18 cm^2/Vs.

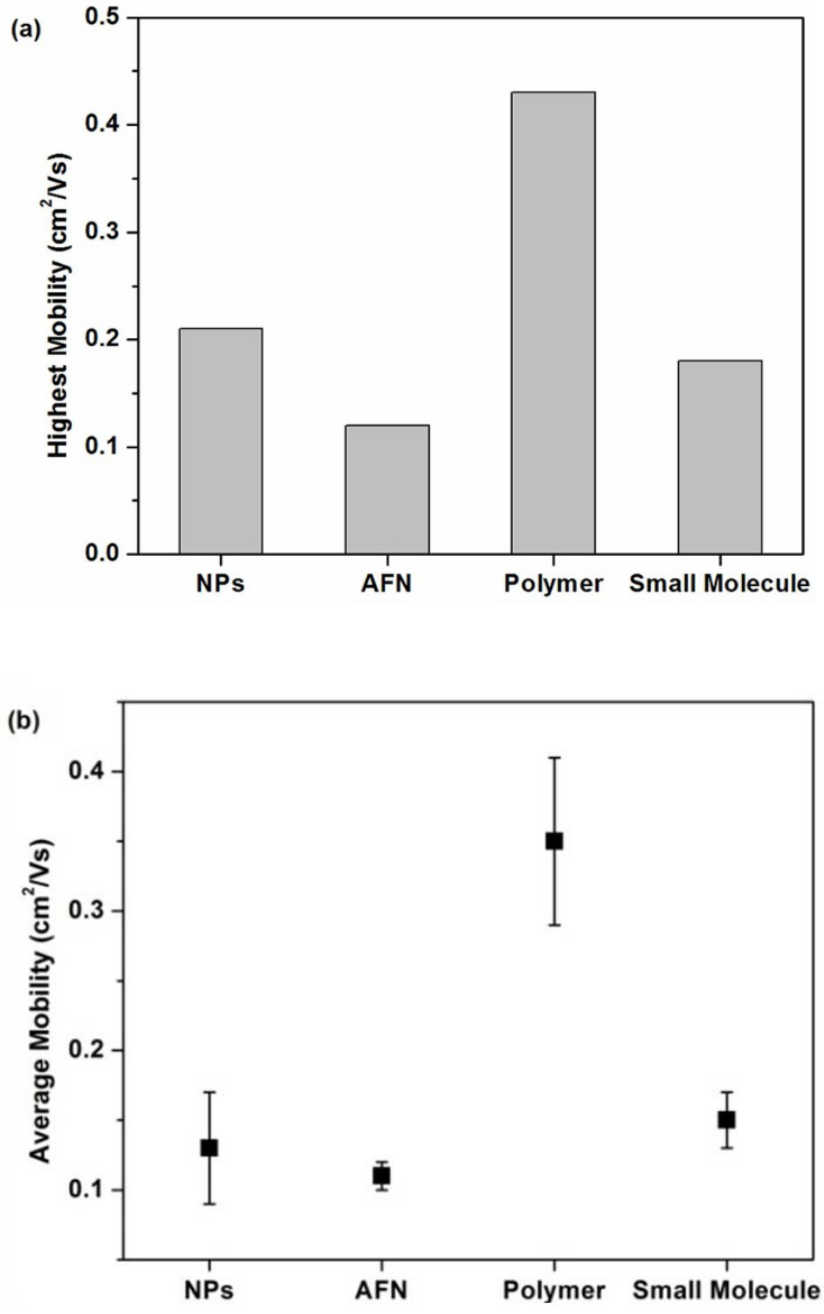

Figure 6.1. The average mobility and highest mobility of TIPS pentacene based OTFTs corresponding to each of the four approaches: the addition of SiO_2 NPs, air flow navigation, polymer blend and small-molecule additive as self-assembled interfacial layer, respectively.

It is noted that TIPS pentacene OTFTs with P2EHA additive demonstrates the highest average mobility of 0.35±0.06 cm^2/Vs among these four approaches. This can be reasonably explained by the fact that the bottom-gate, bottom-contact device configuration utilized for the TIPS pentacene/polyacrylate blend OTFTs was optimized with surface treatment, including HMDS treatment and PFBT treatment. HMDS treatment turned the hydrophilic SiO_2 surface into a hydrophobic surface, which leads to improved π-π stacking and facilitates charge transport. Besides, PFBT treatment was carried out to tune the energy level of the Au contact electrodes, which lowers the energy level for charge injection. As a result, the surface treatments have effectively facilitated charge transport and enhanced the average mobility for the TIPS pentacene OTFTs with P2EHA additive.

6.2. Future Work

Future work can be done about measuring the air stability of the TIPS pentacene/small molecule blend films in Chapter 5. Upon the completion of the first-time electrical characterization, the devices can be left in air and then measured after certain period of time. In addition to air stability, the TIPS pentacene/small molecule blend devices are also expected to demonstrate enhanced stability to humidity. To characterize the effect of humidity on the device performances of the TIPS pentacene/small molecule blend OTFTs, the devices can be placed in a glove box filled with nitrogen. The humidity in the glove box can be adjusted simply by tuning the nitrogen content. The more nitrogen filling the glove box, the lower humidity level it leads to. Electrical characterization of both TIPS pentacene/small molecule blend OTFTs and pure TIPS pentacene OTFTs can be done at different humidity levels over different period of time, allowing a plot of degradation of device performances over time. From the comparison of the device

performances of the OTFTs, it can be known how the addition of each of small molecule affects the air stability of each type of TIPS pentacene/small molecule blend OTFTs.

Also, these small-molecule additives can be used to disperse the single crystals of TIPS pentacene. The study of single crytals provides an ideal case to investigate the possible highest hole mobility of the *p*-type semiconductor TIPS pentacene. Single crystals can be obtained via solvent exchange method.[90] However, these single crystals typically exhibit severe aggregations, making it difficult for device fabrication as well as electrical characterization. Apart from serving as an interfacial layer to improve the crystal orientation and film coverage of TIPS pentacene film, these small-molecule additives can be further utilized to disperse the crystal aggregations of TIPS pentacene single crystals.

REFERENCES

[1] Y. M. Sun, Y. Q. Liu, and D. B. Zhu, Journal of Materials Chemistry **15**, 53 (2005).

[2] S. R. Forrest, Nature **428**, 911 (2004).

[3] T. Sekitani, M. Takamiya, Y. Noguchi, S. Nakano, Y. Kato, T. Sakurai, and T. Someya, Nature Materials **6**, 413 (2007).

[4] C. D. Sheraw, L. Zhou, J. R. Huang, D. J. Gundlach, T. N. Jackson, M. G. Kane, I. G. Hill, M. S. Hammond, J. Campi, B. K. Greening, J. Francl, and J. West, Applied Physics Letters **80**, 1088 (2002).

[5] C. R. Kagan, D. B. Mitzi, and C. D. Dimitrakopoulos, Science **286**, 945 (1999).

[6] Q. Cao, H. S. Kim, N. Pimparkar, J. P. Kulkarni, C. J. Wang, M. Shim, K. Roy, M. A. Alam, and J. A. Rogers, Nature **454**, 495 (2008).

[7] M. Halik, H. Klauk, U. Zschieschang, G. Schmid, C. Dehm, M. Schutz, S. Maisch, F. Effenberger, M. Brunnbauer, and F. Stellacci, Nature **431**, 963 (2004).

[8] J. H. Chen, C. K. Tee, M. Shtein, D. C. Martin, and J. Anthony, Organic Electronics **10**, 696 (2009).

[9] R. H. Bube, Photoelectronic Properties of Semiconductors (Cambridge Univ. Press) (1992).

[10] Z. R. He, K. Xiao, W. Durant, D. K. Hensley, J. E. Anthony, K. L. Hong, S. M. Kilbey, J. H. Chen, and D. W. Li, Advanced Functional Materials **21**, 3617 (2011).

[11] C. E. Swenberg M. Pope, Electronic Processes in Organic Crystals (Clarendon Press, Oxford) (1982).

[12] J. E. Anthony, J. S. Brooks, D. L. Eaton, and S. R. Parkin, Journal of the American Chemical Society **123**, 9482 (2001).

[13] Y. Y. Lin, D. J. Gundlach, S. F. Nelson, and T. N. Jackson, Ieee Electron Device Letters **18**, 606 (1997).

[14] H. Klauk, M. Halik, U. Zschieschang, G. Schmid, W. Radlik, and W. Weber, Journal of Applied Physics **92**, 5259 (2002).

[15] F. Eder, H. Klauk, M. Halik, U. Zschieschang, G. Schmid, and C. Dehm, Applied Physics Letters **84**, 2673 (2004).

[16] Fjmz Heringdorf, M. C. Reuter, and R. M. Tromp, Nature **412**, 517 (2001).

[17] O. D. Jurchescu, J. Baas, and T. T. M. Palstra, Applied Physics Letters **84**, 3061 (2004).

[18] P. F. Baude, D. A. Ender, M. A. Haase, T. W. Kelley, D. V. Muyres, and S. D. Theiss, Applied Physics Letters **82**, 3964 (2003).

[19] S. F. Nelson, Y. Y. Lin, D. J. Gundlach, and T. N. Jackson, Applied Physics Letters **72**, 1854 (1998).

[20] A. Afzali, C. D. Dimitrakopoulos, and T. L. Breen, Journal of the American Chemical Society **124**, 8812 (2002).

[21] D. J. Gundlach, T. N. Jackson, D. G. Schlom, and S. F. Nelson, Applied Physics Letters **74**, 3302 (1999).

[22] C. D. Sheraw, T. N. Jackson, D. L. Eaton, and J. E. Anthony, Advanced Materials **15**, 2009 (2003).

[23] M. H. Choi and J. Jang, Current Applied Physics **12**, E6 (2012).

[24] M. H. Choi, B. S. Kim, and J. Jang, Ieee Electron Device Letters **33**, 1571 (2012).

[25] R. Saive, L. Mueller, E. Mankel, W. Kowalsky, and M. Kroeger, Organic Electronics **14**, 1570 (2013).

[26] E. Lim, D. Taguchi, and M. Iwamoto, Org. Electron. **14**, 1903 (2013).

[27] S. Y. Cho, J. M. Ko, J. Y. Jung, J. Y. Lee, D. H. Choi, and C. Lee, Organic Electronics **13**, 1329 (2012).

[28] M. W. Lee, G. S. Ryu, Y. U. Lee, C. Pearson, M. C. Petty, and C. K. Song, Microelectronic Engineering **95**, 1 (2012).

[29] G. S. Ryu, M. W. Lee, S. H. Jeong, and C. K. Song, Japanese Journal of Applied Physics **51** (2012).

[30] K. Sakamoto, J. Ueno, K. Bulgarevich, and K. Miki, Applied Physics Letters **100** (2012).

[31] S. H. Kim, H. R. Hwang, H. J. Kwon, and J. Jang, Applied Physics Letters **100** (2012).

[32] D. K. Hwang, C. Fuentes-Hernandez, J. D. Berrigan, Y. N. Fang, J. Kim, W. J. Potscavage, H. Cheun, K. H. Sandhage, and B. Kippelen, Journal of Materials Chemistry **22**, 5531 (2012).

[33] R. Kamiya, T. Hosokai, T. Watanabe, T. Koganezawa, M. Kikuchi, and N. Yoshimoto, Molecular Crystals and Liquid Crystals **568**, 134 (2012).

[34] C. Ramanan, A. L. Smeigh, J. E. Anthony, T. J. Marks, and M. R. Wasielewski, Journal of the American Chemical Society **134**, 386 (2012).

[35] J. H. Chen, S. Subramanian, S. R. Parkin, M. Siegler, K. Gallup, C. Haughn, D. C. Martin, and J. E. Anthony, Journal of Materials Chemistry **18**, 1961 (2008).

[36] H. B. Akkerman, H. Y. Li, and Z. N. Bao, Organic Electronics **13**, 2056 (2012).

[37] Y. Nicolas, F. Castet, M. Devynck, P. Tardy, L. Hirsch, C. Labrugere, H. Allouchi, and T. Toupance, Organic Electronics **13**, 1392 (2012).

[38] D. Choi, B. Ahn, S. H. Kim, K. Hong, M. Ree, and C. E. Park, Acs Applied Materials & Interfaces **4**, 117 (2012).

[39] P. G. Schroeder, C. B. France, J. B. Park, and B. A. Parkinson, Journal of Physical Chemistry B **107**, 2253 (2003).

[40] J. H. Kang and X. Y. Zhu, Applied Physics Letters **82**, 3248 (2003).

[41] K. S. Lee, T. J. Smith, K. C. Dickey, J. E. Yoo, K. J. Stevenson, and Y. L. Loo, Advanced Functional Materials **16**, 2409 (2006).

[42] J. P. Hong, A. Y. Park, S. Lee, J. Kang, N. Shin, and D. Y. Yoon, Applied Physics Letters **92** (2008).

[43] C. Tanase, E. J. Meijer, P. W. M. Blom, and D. M. de Leeuw, Organic Electronics **4**, 33 (2003).

[44] L. Torsi A. Dodabalapur, H. E. Katz, Science **268**, 2 (1995).

[45] J. H. Chen, D. C. Martin, and J. E. Anthony, Journal of Materials Research **22**, 1701 (2007).

[46] Z. R. He, J. H. Chen, Z. Z. Sun, G. Szulczewski, and D. W. Li, Organic Electronics **13**, 1819 (2012).

[47] P. A. Smith, C. D. Nordquist, T. N. Jackson, T. S. Mayer, B. R. Martin, J. Mbindyo, and T. E. Mallouk, Applied Physics Letters **77**, 1399 (2000).

[48] Y. G. Zhang, A. L. Chang, J. Cao, Q. Wang, W. Kim, Y. M. Li, N. Morris, E. Yenilmez, J. Kong, and H. J. Dai, Applied Physics Letters **79**, 3155 (2001).

[49] A. Ural, Y. M. Li, and H. J. Dai, Applied Physics Letters **81**, 3464 (2002).

[50] T. Xu, Y. Q. Zhu, S. P. Gido, and T. P. Russell, Macromolecules **37**, 2625 (2004).

[51] T. Prasse, J. Y. Cavaille, and W. Bauhofer, Composites Science and Technology **63**, 1835 (2003).

[52] T. Hashimoto, J. Bodycomb, Y. Funaki, and K. Kimishima, Macromolecules **32**, 952 (1999).

[53] T. Ohe, M. Kuribayashi, A. Tsuboi, K. Satori, M. Itabashi, and K. Nomoto, Applied Physics Express **2** (2009).

[54] T. Ohe, M. Kuribayashi, R. Yasuda, A. Tsuboi, K. Nomoto, K. Satori, M. Itabashi, and J. Kasahara, Appl. Phys. Lett. **93**, 053303 (2008).

[55] H. Sirringhaus, Advanced Materials **17**, 2411 (2005).

[56] G. H. Gelinck, H. E. A. Huitema, E. Van Veenendaal, E. Cantatore, L. Schrijnemakers, Jbph Van der Putten, T. C. T. Geuns, M. Beenhakkers, J. B. Giesbers, B. H. Huisman, E. J. Meijer, E. M. Benito, F. J. Touwslager, A. W. Marsman, B. J. E. Van Rens, and D. M. De Leeuw, Nature Materials **3**, 106 (2004).

[57] E. J. Meijer, D. M. De Leeuw, S. Setayesh, E. Van Veenendaal, B. H. Huisman, P. W. M. Blom, J. C. Hummelen, U. Scherf, and T. M. Klapwijk, Nature Materials **2**, 678 (2003).

[58] D. W. Li and L. J. Guo, Appl. Phys. Lett. **88**, 063513 (2006).

[59] D. W. Li and L. J. Guo, J. Phys. D-Appl. Phys. **41**, 105115 (2008).

[60] S. K. Park, D. A. Mourey, J. I. Han, J. E. Anthony, and T. N. Jackson, Organic Electronics **10**, 486 (2009).

[61] X. R. Li, B. K. C. Kjellander, J. E. Anthony, C. W. M. Bastiaansen, D. J. Broer, and G. H. Gelinck, Advanced Functional Materials **19**, 3610 (2009).

[62] C. W. Sele, B. K. C. Kjellander, B. Niesen, M. J. Thornton, Jbph van der Putten, K. Myny, H. J. Wondergem, A. Moser, R. Resel, Ajjm van Breemen, N. van Aerle, P. Heremans, J. E. Anthony, and G. H. Gelinck, Advanced Materials **21**, 4926 (2009).

[63] S. K. Park, T. N. Jackson, J. E. Anthony, and D. A. Mourey, Applied Physics Letters **91** (2007).

[64] R. L. Headrick, S. Wo, F. Sansoz, and J. E. Anthony, Applied Physics Letters **92**, 3 (2008).

[65] J. Kang, N. Shin, D. Y. Jang, V. M. Prabhu, and D. Y. Yoon, J. Am. Chem. Soc. **130**, 12273 (2008).

[66] J. Smith, R. Hamilton, I. McCulloch, M. Heeney, J. E. Anthony, D. D. C. Bradley, and T. D. Anthopoulos, Synthetic Metals **159**, 2365 (2009).

[67] R. Hamilton, J. Smith, S. Ogier, M. Heeney, J. E. Anthony, I. McCulloch, J. Veres, D. D. C. Bradley, and T. D. Anthopoulos, Advanced Materials **21**, 1166 (2009).

[68] J. Smith, R. Hamilton, I. McCulloch, N. Stingelin-Stutzmann, M. Heeney, D. D. C. Bradley, and T. D. Anthopoulos, J. Mater. Chem. **20**, 2562 (2010).

[69] G. B. Appetecchi F. Croce, L. Persi, B. Scrosati, Nature **394**, 3 (1998).

[70] M. B. Madec, D. Crouch, G. R. Llorente, T. J. Whittle, M. Geoghegan, and S. G. Yeates, Journal of Materials Chemistry **18**, 3230 (2008).

[71] J. H. Chen, J. Anthony, and D. C. Martin, Journal of Physical Chemistry B **110**, 16397 (2006).

[72] J. H. Chen, C. K. Tee, J. Y. Yang, C. Shaw, M. Shtein, J. Anthony, and D. C. Martin, Journal of Polymer Science Part B-Polymer Physics **44**, 3631 (2006).

[73] J. H. Chen, C. K. Tee, J. Y. Yang, C. Shaw, M. Shtein, D. C. Martin, and J. Anthony, Journal of Polymer Science Part B-Polymer Physics **46**, 1878 (2008).

[74] J. E. Anthony, D. L. Eaton, and S. R. Parkin, Organic Letters **4**, 15 (2002).

[75] J. H. Kwon, S. I. Shin, K. H. Kim, M. J. Cho, K. N. Kim, D. H. Choi, and B. K. Ju, Applied Physics Letters **94**, 3 (2009).

[76] G. Giri, E. Verploegen, S. C. B. Mannsfeld, S. Atahan-Evrenk, D. H. Kim, S. Y. Lee, H. A. Becerril, A. Aspuru-Guzik, M. F. Toney, and Z. A. Bao, Nature **480**, 504 (2011).

[77] R. Z. Rogowski, A. Dzwilewski, M. Kemerink, and A. A. Darhuber, J. Phys. Chem. C **115**, 11758 (2011).

[78] J. A. Lim, W. H. Lee, H. S. Lee, J. H. Lee, Y. D. Park, and K. Cho, Advanced Functional Materials **18**, 229 (2008).

[79] G. F. Li, K. Graf, E. Bonaccurso, D. S. Golovko, A. Best, and H. J. Butt, Macromolecular Chemistry and Physics **208**, 2134 (2007).

[80] A. P. Sommer and N. Rozlosnik, Crystal Growth & Design **5**, 551 (2005).

[81] E. Bonaccurso, H. J. Butt, B. Hankeln, B. Niesenhaus, and K. Graf, Applied Physics Letters **86** (2005).

[82] R. D. Deegan, O. Bakajin, T. F. Dupont, G. Huber, S. R. Nagel, and T. A. Witten, Physical Review E **62**, 756 (2000).

[83] R. D. Deegan, O. Bakajin, T. F. Dupont, G. Huber, S. R. Nagel, and T. A. Witten, Nature **389**, 827 (1997).

[84] J. B. Kim, C. Fuentes-Hernandez, D. K. Hwang, S. P. Tiwari, W. J. Potscavage, and B. Kippelen, Organic Electronics **12**, 1132 (2011).

[85] J. Smith, W. M. Zhang, R. Sougrat, K. Zhao, R. P. Li, D. K. Cha, A. Amassian, M. Heeney, I. McCulloch, and T. D. Anthopoulos, Advanced Materials **24**, 2441 (2012).

[86] W. H. Lee, D. Kwak, J. E. Anthony, H. S. Lee, H. H. Choi, D. H. Kim, S. G. Lee, and K. Cho, Advanced Functional Materials **22**, 267 (2012).

[87] W. H. Lee, J. A. Lim, D. Kwak, J. H. Cho, H. S. Lee, H. H. Choi, and K. Cho, Advanced Materials **21**, 4243 (2009).

[88] N. Shin, J. Kang, L. J. Richter, V. M. Prabhu, R. J. Kline, D. A. Fischer, D. M. DeLongchamp, M. F. Toney, S. K. Satija, D. J. Gundlach, B. Purushothaman, J. E. Anthony, and D. Y. Yoon, Advanced Functional Materials **23**, 366 (2013).

[89] H. J. Jung, Y. J. Shin, Y. J. Park, S. C. Yoon, D. H. Choi, and C. Park, Advanced Functional Materials **20**, 2903 (2010).

[90] D. H. Kim, D. Y. Lee, H. S. Lee, W. H. Lee, Y. H. Kim, J. I. Han, and K. Cho, Advanced Materials **19**, 678 (2007).

[91] I. Bae, S. J. Kang, Y. J. Shin, Y. J. Park, R. H. Kim, F. Mathevet, and C. Park, Advanced Materials **23**, 3398 (2011).

[92] S. C. B. Mannsfeld, M. L. Tang, and Z. A. Bao, Advanced Materials **23**, 127 (2011).

[93] B. K. C. Kjellander, W. T. T. Smaal, J. E. Anthony, and G. H. Gelinck, Advanced Materials **22**, 4612 (2010).

[94] L. F. Drummy, R. J. Davis, D. L. Moore, M. Durstock, R. A. Vaia, and J. W. P. Hsu, Chemistry of Materials **23**, 907 (2011).

[95] J. H. Chen, X. Yu, K. L. Hong, J. M. Messman, D. L. Pickel, K. Xiao, M. D. Dadmun, J. W. Mays, A. J. Rondinone, B. G. Sumpter, and S. M. Kilbey, Journal of Materials Chemistry **22**, 13013 (2012).

[96] P. J. Flory, Discuss. Faraday Soc. **49**, 7 (1970).

[97] C. M. Gomez, E. Verdejo, J. E. Figueruelo, A. Campos, and V. Soria, Polymer **36**, 1487 (1995).

[98] Zhengran He, Dawen Li, Dale K Hensley, Adam J Rondinone, and Jihua Chen, Appl. Phys. Lett. **103**, 113301 (2013).

[99] L. Jiang, J. Zhang, D. Gamota, and C. G. Takoudis, Organic Electronics **11**, 344 (2010).

[100] J. B. Koo, S. H. Kim, J. H. Lee, C. H. Ku, S. C. Lim, and T. Zyung, Synthetic Metals **156**, 99 (2006).

[101] D. Kumaki, S. Ando, S. Shimono, Y. Yamashita, T. Umeda, and S. Tokito, Appl. Phys. Lett. **90**, 063514 (2007).

[102] Y. H. Kim, J. E. Anthony, and S. K. Park, Organic Electronics **13**, 1152 (2012).

[103] L. Miozzo, A. Yassar, and G. Horowitz, Journal of Materials Chemistry **20**, 2513 (2010).

[104] T. Kato, C. Jin, F. Kaneuchi, and T. Uryu, Bulletin of the Chemical Society of Japan **66**, 3581 (1993).

[105] E. Kim, S. Paliwal, and C. S. Wilcox, Journal of the American Chemical Society **120**, 11192 (1998).

[106] J. A. Lim, W. H. Lee, D. Kwak, and K. Cho, Langmuir **25**, 5404 (2009).

[107] W. H. Lee, D. H. Kim, Y. Jang, J. H. Cho, M. Hwang, Y. D. Park, Y. H. Kim, J. I. Han, and K. Cho, Appl. Phys. Lett. **90**, 132106 (2007).

[108] L. G. Parratt, Phys. Rev. **95**, 359 (1954).

[109] O. R. L. Griffith, Ph. D. Thesis, The University of Arizona (2010).

[110] D. M. Spori, N. V. Venkataraman, S. G. P. Tosatti, F. Durmaz, N. D. Spencer, and S. Zurcher, Langmuir **23**, 8053 (2007).

APPENDIX

LIST OF PUBLICATIONS AND PRESENTATIONS

Journal Publications

1. **Z. He**, J. Chen, J. K. Keum, G. Szulczewski, and D. Li*, "Improving Performance of TIPS Pentacene-Based Organic Thin Film Transistors with Small-Molecule Additives", ***Organic Electronics***, 15, (2014).

2. **Z. He**, D. Li*, D. K. Hensley, A. J. Rondinone, and J. Chen*, "Switching Phase Separation Mode by Varying the Hydrophobicity of Polymer Additives in Solution-Processed Semiconducting Small-Molecule/Polymer Blends", ***Applied Physics Letter***, 103, (2013).

3. J. Chen*, M. Shao, K. Xiao, **Z. He**, D. Li, B. S. Lokitz, D. Hensley, S. M. Kilbey, J. E. Anthony, J. K. Keum, A. J. Rondinone, W. Lee, S. Hong, and Z. Bao*, "Conjugated Polymer-Mediated Polymorphism of High Performance, Small-Molecule Organic Semiconductor with Tuned Intermolecular Interactions, Enhanced Long-Range Order and Charge Transport", ***Chemistry of Materials***, 25, (2013).

4. **Z. He**, J. Chen, Z. Sun, G. Szulczewski, and D. Li*, "Air-Flow Navigated Crystal Growth for TIPS Pentacene-Based Organic Thin-Film Transistors", ***Organic Electronics***, 13, (2012).

5. **Z. He**, K. Xiao, W. Durant, D. K. Hensley, J. E. Anthony, K. Hong, S. M. Kilbey, J. Chen*, and D. Li*, "Enhanced Performance Consistency in Nanoparticle/TIPS Pentacene-Based Organic Thin Film Transistors", ***Advanced Functional Materials***, 21, (2011).

6. **Z. He**, S. Shaik, and D. Li*, "High-Performance Air-Stable Solution Processed n-Type Organic Thin Film Transistors with Polymer Binders", paper in preparation, (2014).

7. **Z. He,** Xiaoliu Chi, and D. Li*, "Solution-Processed Tetrachlorotetracene Based Organic Thin Film Transistors with Double Solvents", paper in preparation, (2014).

8. **Z. He**, K. A. Yeboah, and D. Li*, "TIPS Pentacene Growth for High Performance Solution-Processed Organic Thin Film Transistors", paper in preparation, (2014).

Conference Presentations

1. **Z. He** and D. Li*, "Crystal Alignment for Solution Processed TIPS Pentacene-Based Organic Thin Film Transistors", ECE Seminar, The University of Alabama, Tuscaloosa, AL (2014).

2. **Z. He**, J. Chen, G. Szulczewski, and D. Li*, "High-Performance TIPS Pentacene-Based Organic Thin Film Transistors with Small-Molecule Additives", MRS Fall Meeting, Boston, MA (2013).

3. **Z. He** and D. Li*, "Self-Assembled Liquid Crystal Interfacial Layers for Enhanced Charge Transport in Organic Thin Film Transistors", MINT Review, The University of Alabama, Tuscaloosa, AL (2013).

4. **Z. He**, G. Szulczewski, and D. Li*, "High-Performance Solution-Processed Thin Film Transistors with Liquid Crystal Self-Assembled Monolayers", Science and Technology Open House, Montgomery, AL (2013).

5. **Z. He**, J. Chen, Z. Sun, and D. Li*, “Study of Crystal Growth by Air-Flow Navigation for TIPS Pentacene-Based Organic Thin-Film Transistors”, MRS Spring Meeting, San Francisco, CA (2012).

6. **Z. He**, J. Chen, G. Szulczewski, and D. Li*, “Controlled Solvent Evaporation Towards Fabrication of High Performance Small Molecule-Based Organic Thin-Film Transistors”, MINT Review, The University of Alabama, Tuscaloosa, AL (2011).

7. **Z. He**, W. Durant, K. Xiao, J. E. Anthony, J. Chen, and D. Li*, “Polymer and Nanoparticle Mediated TIPS-Pentacene Crystallization: Towards Enhanced Performance Consistency in Small Molecule-Based Organic Thin-Film Transistors”, MRS Fall Meeting, Boston, MA (2010).